All-Optical Switching Using Semiconductor Amplifiers Biased at Transparency

by

Bryan S. Robinson

Submitted to the Department of Electrical Engineering and Computer Science
in partial fulfillment of the requirements for the degree of

Master of Engineering in Electrical Engineering and Computer Science

at the

MASSACHUSETTS INSTITUTE OF TECHNOLOGY

June 1998

Author .....
Department of Electrical Engineering and Computer Science
May 13, 1998

Certified by .....
Hermann A. Haus
Institute Professor
Thesis Supervisor

Accepted by .....
Arthur C. Smith
Chairman, Department Committee on Graduate Students

All-Optical Switching Using Semiconductor Amplifiers Biased at Transparency

by

Bryan S. Robinson

Submitted to the Department of Electrical Engineering and Computer Science
on May 13, 1998, in partial fulfillment of the
requirements for the degree of
Master of Engineering in Electrical Engineering and Computer Science

Abstract

In this thesis, we discuss how the nonlinear refractive index, linear and nonlinear loss, and dispersion of a waveguide affect interferometric all-optical switching devices. We perform simulations to demonstrate the detrimental effects of long-lived gain and refractive index changes in interferometric switches. The effects of long-lived index changes are reduced in a single arm interferometer, such as the ultrafast nonlinear interferometer. However, the effects of long-lived gain changes remain a problem. We suggest the use of semiconductor optical amplifiers biased at the transparency point as a means of reducing the long-lived effects of carrier population dynamics in semiconductor waveguides.

We demonstrate a spectral interferometric technique for measuring the nonlinear phase shift in optical pulses due to self-phase modulation in a nonlinear material. This technique, which has previously been used for dispersion measurements, is based on observation of the spectral interference of two temporally separated pulses before and after propagation through the nonlinear material. Using this technique, we measure the nonlinear phase shift induced in optical pulses propagating through semiconductor optical aplifiers biased at transparency. Our results suggest that switching at the transparency point is possible.

We use semiconductor optical amplifiers biased at the transparency point in various switching demonstrations. We show the effects of long-lived gain changes associated with carrier populations dynamics in the absorption and gain regime of a semiconductor waveguide. We show amplitude modulation in the output pulses of a switch arising from gain saturation. We demonstrate 10 Gbits/s all-optical switching using a semiconductor optical amplifier biased at the transparency current.

Research Supervisor: K. L. Hall
Title: Senior Staff, Lincoln Laboratory

Thesis Supervisor: Hermann A. Haus
Title: Institute Professor

Acknowledgments

It has been a great privilege to have Professor Haus as my thesis and academic advisor. His enthusiastic lectures in 6.013 are largely responsible for my decision to pursue a degree in electrical engineering. As an academic advisor, Professor Haus has shown a genuine interest in my success at MIT. In spite of his busy schedule, Professor Haus always made time for me when I needed it (usually on short notice).

I have really enjoyed working with Katie Hall at Lincoln Laboratory. I especially thank Katie for giving me the opportunity to work in her lab, despite my inexperience. She has been a great resource. Her technical knowledge is remarkable and her skills in the lab are unmatched. Whenever I was stumped, I knew she had a solution. I look forward to doing more work with Katie during the coming years.

I thank all the Lincoln staff members who generously offered advice and equipment for my research: Steve Chinn, Joe Donnelly, Jeff Korn, John Moores, Kristin Rauschenbach. Many students in the Advanced Networks group have made my experiences at Lincoln enjoyable: Victor Lum, Naimish Patel, Serena Chan, Tengo Saengudomlert, Dedric Carter, David Jones, and Erik Thoen. I am especially grateful for Claudia Fennelly and Kirk VanBrocklyn for keeping the labs organized and running smoothly, in spite of my best efforts.

Many friends at MIT have contributed to my success. Sara Ransom has been a constant source of support and motivation. I thank my roommate, Cayce Ramey, for his encouragement over the past four years. Thanks also to my friend, Jonathan Goldman, for general technical support and LaTeX advice. I am grateful for all my friends on the squash team and in the United Christian Fellowship for helping me keep my sanity throughout my time at MIT.

I have been blessed with a trully wonderful family. Thanks to Mom, Dad, Tom, Arnette for all the love and support. I hope you guys can share the joy that I have in finishing this work.

Finally, I thank God for changing my perspective at MIT and making this all possible.

Contents

1 Introduction **11**

2 All-Optical Switching Background **15**

2.1 Third-Order Nonlinearities 15

2.2 Nonlinear Mach-Zehnder Interferometer 18

2.3 Mach-Zehnder Interferometer Problems 21

2.4 Ultrafast Nonlinear Interferometer 22

2.5 Material Properties 26

2.5.1 Nonlinearity 26

2.5.2 Loss 27

2.5.3 Dispersion 30

2.5.4 Birefringence 34

3 Semiconductor Devices **38**

3.1 Semiconductor Waveguides 38

3.2 Carrier Population Dynamics 40

3.3 Nonlinear Gain Mechanisms 48

3.4 Refractive Index 51

3.5 Dispersion 55

3.6 Discussion 56

3.6.1 Passive Devices 57

3.6.2 Transparency Point 58

4 Device Characterization **61**

4.1 Measurement of Transparency Current 62

4.2 Spectral Interferometry 64

4.3 Pulse Source 65

4.4 Nonlinear Refractive Index 68

4.4.1 Other Effects 74

4.5 Other Measurements 80

5 Switching Experiments **82**

5.1 Experimental Setup 82

5.2 Pulse Sources 84

5.2.1 Gain-switched Laser 84

5.2.2 PriTel Soliton Source 85

5.2.3 Soliton Compression Source 86

5.3 Switching Results 87

5.3.1 Interband Effects 87

5.3.2 Patterning in Gain Regime 90

5.3.3 Transparency 91

5.4 Discussion 93

6 Conclusions **95**

6.1 Future Work 96

Bibliography **99**

List of Figures

2-1 A Nonlinear Mach-Zehnder Interferometer 19

2-2 Output intensity versus total phase difference between the arms of a nonlinear Mach-Zehnder interferometer. 20

2-3 Simulation of effects of long-lived index changes in an unbalanced interferometric all-optical switch. 22

2-4 Block diagram of a single-arm interferometer. 23

2-5 Ultrafast-nonlinear interferometer implementation. 23

2-6 Simulation of effects of long-lived index changes in an ultrafast nonlinear interferometer. 24

2-7 Simulation of the effects of long-lived gain changes on the output pulses from the UNI. Here, the output is shown for the signal and control inputs shown in Figure 2-6 with carrier recovery times of 2.5 ps, 25 ps, 250 ps, and 2.5 ns. 25

2-8 Intensity required to achieve a π phase shift as a function of the figure-of-merit, T. 30

2-9 Dispersion-induced broadening of a Gaussian pulse. 33

2-10 Inverse contrast ratio, $R = E_{\text{off}}/E_{\text{on}}$ of the UNI as a function of timing offset of the two signal pulses normalized by the pulse width. 36

2-11 Interference of two Gaussian pulses for various values of $L/L_D = \Delta\beta_2 L/T_0^2$ where $\Delta\beta_2 = \beta_{2x} - \beta_{2y}$. Initial Gaussian pulse width is T_0. Initial intensitiy is I_0. 37

2-12 Inverse contrast ratio of the UNI as a function of the difference in dispersion, $\Delta L/L_D = \Delta\beta_2 L/T_0^2$ where $\Delta\beta_2 = \beta_{2x} - \beta_{2y}$. 37

3-1 An index-guided semiconductor optical amplifier. 39
3-2 Dispersion relationship for a direct bandgap semiconductor. 40
3-3 The Fermi-Dirac distribution fuction for various temperatures. 42
3-4 Quasi-Fermi energies as a function of the injected carrier density, N. The dashed line is the quasi-Fermi energy for electrons in the conduction band. The dot-dashed line is the quasi-Fermi energy for holes in the valence band. 44
3-5 Schematic of absorption process for a photon with energy $h\nu$ 46
3-6 Gain coefficient, g, as a function of the excess photon energy, $E - E_g$. 48
3-7 Gain coefficient as a function of excess photon energy for various carrier densities, N. The carrier densities are $N \times 10^{18}\text{cm}^{-3} = 0.7, 1.8$, and 3.0. 49
3-8 Gain coefficient as a function of excess photon energy for various carrier temperatures. Here, the carrier temperature for the valence band is fixed at 300 K. The gain coefficient is shown for conduction carrier temperatures of 300 K (solid), 310 K (dashed), 320 K (dotted). . . . 50
3-9 Changes in gain and refractive index due to carrier population density changes. These changes correspond to carrier population changes of $\Delta N(\times 10^{18}) = 0.02, 0, -0.02, -0.05, -0.07$ around $N = 1.8 \times 10^{18}\text{cm}^{-3}$. 53
3-10 Changes in refractive index for various gain changes, $\Delta g(E)$, for carrier temperature changes of 0K, +10K, +20K, +40K around 300K. 54
3-11 Transparency wavelength as a function of the injected carrier population density. 59

4-1 Experimental apparatus for measuring transparency current in a semicondcutor laser amplifier. 62
4-2 Measured differential voltage due to stimulated absorption and emission in a semiconductor optical amplifier as a function of the bias current in the amplifier. 63
4-3 Generic Mach-Zehnder Interferometer. 64
4-4 Stretched-pulse laser used in spectral interferometry experiments. . . 66

4-5 Spectrum from output port of stretched pulse laser. The solid line is the unfiltered output spectrum. The dashed line is the output spectrum when a 4.93 nm filter is used. 67
4-6 Autocorrelation of a 640 fs pulse from the stretched-pulse laser with a 4.93 nm filter at the output. 68
4-7 Method for measuring the nonlinear refractive index of a material using spectral interferometry. 69
4-8 Frequency domain interference for two Gaussian pulses. The FWHM for these pulses is 1 ps. The temporal spacing between the pulses is $T = 5$ ps. The scaling factor is $\alpha = 0.25$. 70
4-9 Frequency domain interference for two Gaussian pulses. The FWHM for these pulses is 1 ps. The temporal spacing between the pulses is $T = 5$ ps. The scaling factor is $\alpha = 0.25$. The pump pulse has acquired a uniform phase shift of π relative to the reference pulse. 72
4-10 Setup for creating two temporally separated pulses used in spectral interferometry experiments. 73
4-11 Spectral interference and autocorrelation of two pulses used in experiment. 75
4-12 Measurements of phase shift in frequency domain versus average power from pulse source 76
4-13 Spectral broadening due to self-phase modulation in a Gaussian pulse. 76
4-14 Spectral broadening due to self-phase modulation in a Gaussian pulse. Here, the nonlinear refractive index change is assumed to have a recovery time of 600 fs 77
4-15 Simulation of interference of two Gaussian pulses. The pulse width is 1ps and the temporal separation is 5 ps. The scaling factor is $\alpha = 0.1$. Interference patterns are plotted for peak phase shifts of 0, $pi/2$, and π. 78
4-16 Simulation of observed phase shift in spectral modulation versus peak phase shift due to self-phase modulation for two 1 ps Gaussian pulses. The pulses are separated by 5 ps and have scaling factor, $\alpha = 0.1$. . . 79

4-17 Michelson interferometer used for directly observing the propagation constant, $\beta(\omega)$ in a semiconductor optical amplifier. 81

5-1 Experimental setup for switching demonstrations. Optical paths are indicated by solid lines. Electrical paths are indicated by dashed lines. 83

5-2 Autocorrelation of pulse from DFB laser modulated at 10 GHz before and after compression in 400 m of dispersion compensating fiber. The FWHM is 32 ps before compression and 10 ps after compression . . . 85

5-3 Autocorrelation of 3.6 ps pulse from PriTel Soliton source operating at 12.5 GHz. 86

5-4 Soliton compression source schematic. 87

5-5 Autocorrelation of a 2 ps pulse from the 100 GHz soliton compression source. 88

5-6 Switching demonstration showing effects of carrier population changes in various operation regimes. 89

5-7 Amplitude modulation in the output signal due to gain suppression. . 90

5-8 Switching demonstration at transparency point. 92

List of Tables

3.1 Energy bandgap, and effective carrier masses for lattice-matched InGaAsP/InP. m_0 is the effective mass of an electron in free space. . . . 42

3.2 Group velocity dispersion measurements in InGaAsP semiconductor amplifiers as reported by [1]. 56

Chapter 1

Introduction

In recent years, much research effort has been directed toward fully utilizing the information transmission capacity of optical fibers. Optical fibers transmit with low loss over a bandwidth of more than 200 nm. This corresponds to more than 25 THz of usable bandwidth for information transmission[2]. Taking advantage of this enormous capacity requires high-speed processing in network receivers and transmitters. For these types of simple processing applications, all-optical switches have a number of advantages over their electronic counterparts. For example, all-optical switches based on ultrafast nonlinearities can be used for switching at rates beyond 100 Gbits/s. All-optical switches also have the advantage that signals may be propagated from one switch to another without opto-electronic conversion.

Ultrafast all-optical switches have many applications in the development of ultra-high speed multi-access time-division multiplexing (TDM) networks. For instance, bitwise logic is required in receivers in the network for tasks such as address recognition, rate conversion, and demultiplexing [3]. All-optical switches can also be used for specific applications such as ultrafast data-encryption [4], analog-to-digital conversion [5], and wavelength conversion [6].

To date, many different switch designs have been proposed (for example, see [7]). These switches are often based on an interferometric design employing an intensity-dependent refractive index in a waveguide. A key design issue in an optical switch is the choice of nonlinear material. Numerous nonlinear materials have been employed

in optical switches to date.

The nonlinearities in optical fiber have been used in many all-optical switches [2]. The nonlinear response of optical fiber is composed primarily of bound-electron processes. The response time of these processes is virtually instantaneous with relaxation times that are typically less than 100 fs. This allows for switching at very high data rates. A nonlinear optical loop mirror using nonlinearities in fiber has been demonstrated for demultiplexing at rates up to 160 Gbits/s [8]. The main disadvantage of using optical fiber is that the nonlinear refractive index is very small. Thus, switching using fibers requires long interaction lengths (on the order of hundreds of meters) or high pulse intensities. Because very low loss fibers are available, these demands are not unreasonable. However, when using such long lengths of fiber, the accumulated effects of self-phase modulation and group velocity dispersion can lead to pulse distortion [9, 10]. Pulse walk-through due to group-velocity dispersion can also reduce the effective length over which a signal pulse is affected by the fiber nonlinearity. In addition, long lengths of fiber make switches using optical fiber nonlinearities bulky and difficult to package.

As a result, semiconductor waveguides have become a very popular choice for nonlinear materials in all-optical switches. Semiconductors typically have a nonlinear refractive index that is more than four orders of magnitude larger than that of optical fibers. Hence, interaction lengths on the order of millimeters are suitable for obtaining a desirable phase shift. Semiconductors can also be reliably manufactured and easily integrated into a compact switch.

Logic gates employing nonlinearities in active semiconductors such as semiconductor optical amplifiers (SOA) have been demonstrated at rates up to 100 Gbits/s [11]. The SOA's in these switches are biased in the gain regime. Pulses propagating through these devices affect the carrier distributions within the semiconductor. The duration of these effects is governed by the carrier lifetimes of the device (typically > 100 ps). Consequently, gain saturation is observable at high data rates. The resulting amplitude modulation in the output signal inhibits switching at higher rates and makes cascading difficult.

There are several alternatives to gain-biased SOA's which may avoid these complications without sacrificing the convenience of using semiconductor waveguides for the nonlinear material. For instance, one may bias the semiconductor amplifier at the transparency point. At this point, net changes in the carrier populations of the device due to an incident optical pulse are eliminated. Thus, the nonlinear response of this material is potentially quite fast [12]. Recently, a low repetition rate, 2-ps switching window, was demonstrated in a switch using an amplifier biased at transparency [13].

Another approach is to use passive semiconductor waveguides. These waveguides are fabricated to have a bandgap energy slightly higher than the energies of the optical switching pulses. For these devices, at low optical pulse intensities, carrier populations remain relatively unchanged. Therefore, one expects a fast nonlinear response. Four wave mixing experiments in passive InGaAsP/InP semiconductors have confirmed the existence of a fast, relatively large, nonlinear refractive index in these devices [14].

In this thesis, we discuss methods for characterizing various nonlinear waveguides to determine their suitability for use in all-optical switches. A spectral interferometric technique is used to characterize the nonlinear refractive index in the devices. Suitable devices are demonstrated in all-optical switching experiments.

Chapter 2 presents background material on all-optical switching. We describe the operation of a nonlinear Mach-Zehnder interferometer, a common switch design used today. We discuss how third-order nonlinearities in optical materials can lead to a phase shift in an optical pulse traveling through the material. We describe the ultrafast nonlinear interferometer, the single-arm interferometer used for experiments in this thesis. We discuss the effects of non-instantaneous gain and index changes, loss, birefringence, and dispersion on all-optical switching in the UNI.

Chapter 3 contains a description of the semiconductor waveguides used in this thesis. We begin with a discussion of the structure of active and passive semiconductor waveguides. A brief description of the carrier population dynamics of semiconductors is followed by a discussion of the third order nonlinearities of these devices. Results of recent pump-probe studies of the nonlinear refractive index and dispersion

in semiconductors are presented. We discuss how passive waveguides and SOA biased at transparency may be used to reduce the effects of long-lived gain changes in all-optical switches.

Chapter 4 describes the methods used for characterizing the nonlinearities in the semiconductor waveguides studied in this thesis. We show how observations of the interference between two optical pulses in the frequency domain allows direct observation of the phase shift due to the nonlinear refractive index in a material. We use this spectral interferometric (SI) technique to measure the nonlinear refractive index in SOA biased at the transparency point. We discuss how SI may be used to measure dispersion and birefringence in waveguides.

Chapter 5 presents the results of various switching experiments performed using SOA's biased at transparency. We show the long-lived effects of gain changes in SOA's biased in the absorption and gain regimes. We demonstrate an all-optical AND gate operating at the transparency point. This is the first demonstration of ultrahigh speed all-optical switching in semiconductors biased at transparency.

Chapter 6 summarizes the results presented in this thesis. Suggestions for further study are presented.

Chapter 2

All-Optical Switching Background

In this section, I will present background material on the operation of all-optical switches. Most practical all-optical switches rely on a nonlinear phase shift accumulating in a signal pulse as it propagates through a nonlinear material. I will begin by discussing how such a phase shift arises due to third-order nonlinearities. Then, I will describe the basic operating principles of an interferometric switch. This is followed by a brief discussion of the ultrafast nonlinear interferometer (UNI), the all-optical switch used in this thesis. The chapter is concluded with remarks on how various material properities such as nonlinearity, loss, dispersion, and birefringence affect the operation of the UNI.

2.1 Third-Order Nonlinearities

Third-order nonlinearities in an optical material can lead to an intensity dependent refractive index in the material. This nonlinear refractive index allows one to control the phase of a signal pulse using an intense control pulse. To better understand this interaction, we must consider the interaction of the two electric fields in the nonlinear material [15]. We write the signal pulse field as:

$$\mathbf{E_S}(t) = \hat{\mathbf{e}}_\mathbf{S}(\frac{1}{2}E_S(t)e^{-j\omega_S t} + c.c.), \tag{2.1}$$

where $\hat{\mathbf{e}}_\mathbf{S}$ is the carrier frequency of the pulse and $E_S(t)$ is the slowly-varying pulse envelope. For simplicity, we have assumed that the field is linearly polarized in the $\hat{\mathbf{e}}_\mathbf{S}$ direction. Similarly, we write the field of the control pulse as:

$$\mathbf{E_C}(t) = \hat{\mathbf{e}}_\mathbf{C}(\frac{1}{2}E_C(t)e^{-j\omega_C t} + c.c.). \tag{2.2}$$

The total field in the nonlinear material, $\mathbf{E}$, is given by the sum of the signal and control fields.

In a third-order nonlinear material, a nonlinear polarization arises due to the interaction of the electric fields and the third-order nonlinear susceptibility tensor, $\chi^{(3)}$:

$$\mathbf{P_{NL}^{(3)}} = \epsilon_0 \chi^{(3)} \vdots \mathbf{EEE}. \tag{2.3}$$

Since the nonlinear susceptibility tensor is generally not instantaneous, the nonlinear polarization may be calculated by convolving the material impulse response, $\chi^{(3)}(t_1, t_2, t_3)$ with the input field:

$$\mathbf{P_{NL}^{(3)}}(t) = \epsilon_0 \int\int\int_{-\infty}^{\infty} \chi^{(3)}(t-t_1, t-t_2, t-t_3) \vdots \mathbf{E}(t_1)\mathbf{E}(t_2)\mathbf{E}(t_3) dt_1 dt_2 dt_3. \tag{2.4}$$

As a simple first approximation, let us assume that the signal and control pulses are copolarized in the $\hat{\mathbf{x}}$ direction. Additionally, we shall assume that the nonlinear response of the material is instantaneous, $\chi^{(3)}(t_1, t_2, t_3) = \chi^{(3)}\delta(t_1, t_2, t_3)$. The electric field in the material may be written as:

$$\mathbf{E}(t) = \frac{1}{2}\hat{\mathbf{x}}[(E_S(t)e^{-j\omega_S t} + E_C(t)e^{-j\omega_C t}) + c.c.]. \tag{2.5}$$

Substituting into equation 2.4 gives the nonlinear polarization [15]:

$$\begin{aligned}\mathbf{P_{NL}^{(3)}}(t) = \frac{1}{2}\hat{\mathbf{x}}\{&P_{NL}(\omega_S)e^{-j\omega_S t} + P_{NL}(\omega_C)e^{-j\omega_C t} \\ &+ P_{NL}(2\omega_S - \omega_C)e^{-j(2\omega_S-\omega_C)t} \\ &+ P_{NL}(2\omega_C - \omega_S)e^{-j(2\omega_C-\omega_S)t}\} + c.c.,\end{aligned} \tag{2.6}$$

where

$$P_{NL}(\omega_S) = \chi_{\text{eff}}(|E_S|^2 + 2|E_C|^2)E_S, \tag{2.7}$$

$$P_{NL}(\omega_C) = \chi_{\text{eff}}(|E_C|^2 + 2|E_S|^2)E_C, \tag{2.8}$$

$$P_{NL}(2\omega_S - \omega_C) = \chi_{\text{eff}}E_S^2E_C^*, \tag{2.9}$$

$$P_{NL}(2\omega_C - \omega_S) = \chi_{\text{eff}}E_C^2E_S^*, \tag{2.10}$$

and the effective third order nonlinearity, $\chi_{\text{eff}} = \frac{3\epsilon_0}{4}\chi^{(3)}_{xxxx}$.

We are interested in the change in the signal field due to the presence of the control field, so the relevant nonlinear polarization for our purposes is $P_{NL}(\omega_S)$. We may rewrite the nonlinear contribution to the polarization as:

$$\mathbf{P_{NL}}(\omega_S) = \epsilon_0\epsilon_{NL}\mathbf{E_S} \tag{2.11}$$

where $\epsilon_{NL} = \chi_{\text{eff}}(|E_S|^2 + 2|E_C|^2)$. Thus, the total dielectric permittivity for the material is given by the sum of the linear and nonlinear parts[15]:

$$\epsilon = \epsilon_L + \epsilon_{NL} = (n_L + \Delta n)^2 \tag{2.12}$$

where n_L is the linear refractive index and Δn is the nonlinear contribution to the refractive index. If we assume $\Delta n << n_L$ we find:

$$\Delta n \approx n_2(|E_S|^2 + 2|E_C|^2) \tag{2.13}$$

where,

$$n_2 = \frac{3}{8n}\mathrm{Re}(\chi^{(3)}_{xxxx}). \tag{2.14}$$

Here, n_2 is the so-called nonlinear refractive index coefficient. It is commonly used to characterize the instantaneous nonlinear refractive index of a material.

From equation 2.13, we see that the index of refraction seen by the signal pulse is affected by both the intensity of the signal pulse and the intensity of the control pulse. The signal pulse therefore acquires a differential nonlinear phase shift as it propagates through a differential length dL:

$$d\Phi_{\mathrm{nl}} = \frac{2\pi}{\lambda} n_2 \{|E_S|^2 + 2|E_C|^2\} dL \tag{2.15}$$

The contribution to the nonlinear phase shift from the signal pulse itself is known as self-phase modulation (SPM). The effects of SPM are discussed in more detail in Chapter 4. The contribution from the control pulse is known as cross-phase modulation (XPM). We shall show in the next section, (XPM) may be used in a nonlinear Mach-Zehnder interferometer to achieve all-optical switching.

2.2 Nonlinear Mach-Zehnder Interferometer

Many all-optical switch designs studied today are based on an interferometric architecture. A simple implementation of this design is the nonlinear Mach-Zehnder interferometer shown in Figure 2-1. Signal pulses with intensity I_{in} entering on the left are split into two pulses of equal intensity via a 50/50 beam splitter at the input. Pulses in the lower arm travel through a linear material with refractive index $n = n_0^l$. Since the velocity of light traveling through this material is given by $v_l = c/n$, the phase change accumulated by the pulse while travelling through this material is given by:

$$\Phi_{\mathrm{linear}} = \int_0^{L_l} \frac{2\pi}{\lambda} n_0^l dz = \frac{2\pi}{\lambda} n_0^l L_l, \tag{2.16}$$

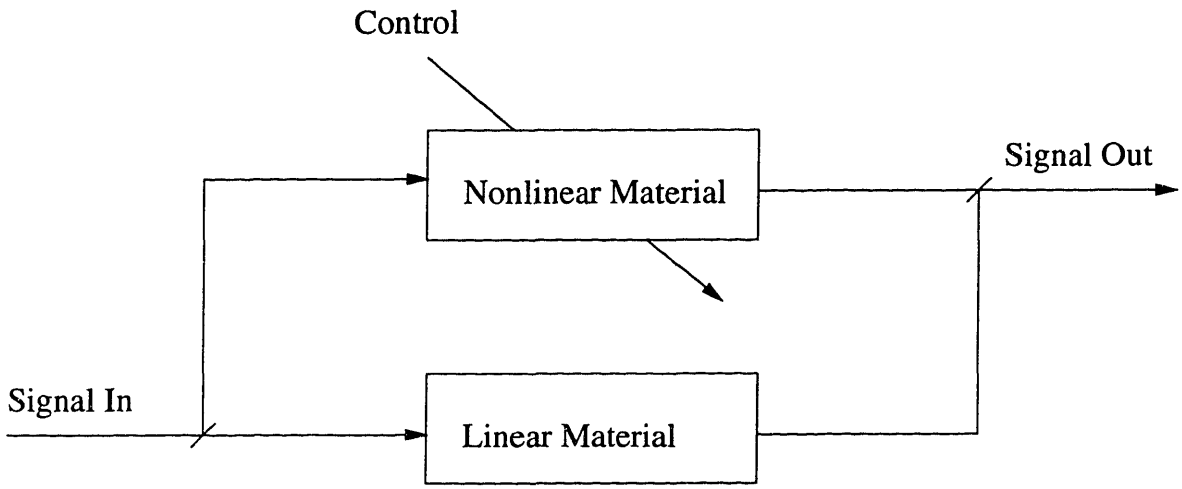

Figure 2-1: A Nonlinear Mach-Zehnder Interferometer

where λ is the freespace center wavelength of the optical pulse and L_l is the length of the linear material.

Pulses in the upper arm travel through a nonlinear material. This material has an refractive index that is intensity dependent. That is, in the presence of an intense control pulse, the refractive index is given by: $n = n_0^{nl} + n_2 I_C$. The phase accumulated by the pulse as it propagates through this arm is given by:

$$\Phi_{\text{nonlinear}} = \int_0^{L_{nl}} \frac{2\pi}{\lambda}(n_0^{nl} + n_2 I_C)dz = \frac{2\pi}{\lambda}(n_0^{nl} + n_2 I_C)L_{nl} \tag{2.17}$$

where L_{nl} is the length of the nonlinear device.

When the two pulses are interfered at the output, the output intensity is proportional to the relative phase shift in the two arms:

$$\begin{aligned} I_{\text{out}} &\propto I_{\text{in}}|1 + e^{j(\Phi_{\text{linear}} - \Phi_{\text{nonlinear}})}|^2 \\ &= I_{\text{in}} \cos^2\left(\frac{\Phi_{\text{linear}} - \Phi_{\text{nonlinear}}}{2}\right) \\ &= I_{\text{in}} \cos^2\left(\frac{\Phi_{\text{bias}} - \Phi_{\text{nl}}}{2}\right) \end{aligned} \tag{2.18}$$

Here, we have defined the bias phase shift, $\Phi_{\text{bias}} = \frac{2\pi}{\lambda}(n_0^l L_l - n_0^{nl} L_{nl} + \Delta L)$, where ΔL is the difference in the freespace path lengths of the two arms. The bias phase accounts for phase differences between the two arms owing to differences in the path

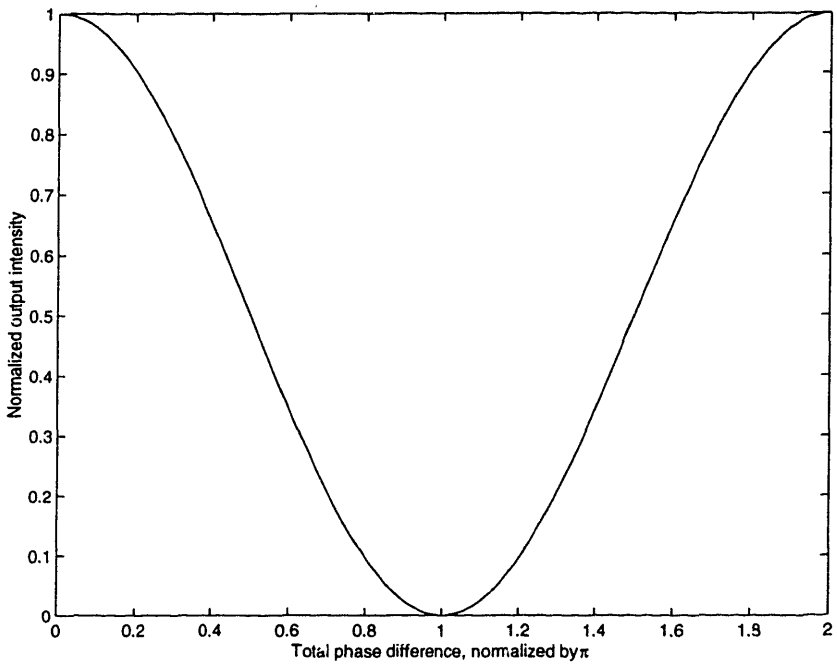

Figure 2-2: Output intensity versus total phase difference between the arms of a nonlinear Mach-Zehnder interferometer.

lengths and linear refractive indices in the arms. Since the nonlinear phase shift term,

$$\Phi_{\text{nl}} = \frac{2\pi}{\lambda} n_2 I_C L_{nl}, \tag{2.19}$$

is directly related to the intensity of the control pulse, we can control the output intensity of the signal pulses by adjusting the intensities of the control pulses. A plot of the output intensity as a function of the total phase difference between the arms is shown in Figure 2-2.

By appropriately setting the bias phase, we can switch the signal pulses ON or OFF using the control pulses. For instance, suppose that there is no bias phase, $\Phi_{\text{bias}} = 0$. Then, in the absence of a control pulse ($I_C = 0$), the signal pulse intensity at the output is equal to the signal pulse intensity at the input (neglecting losses in the system). If we introduce a control pulse into the second arm with sufficient intensity such that $\Phi_{\text{nonlinear}} = \pi$, the output signal pulses are completely switched OFF ($I_{\text{out}} = 0$). In this case, the pulse energy has been redirected to the unused port on the output beam splitter. Alternatively, we can set the bias phase to π and use

the presence of a control pulse to switch the signal pulses ON, performing a logical AND function between the two pulse streams.

2.3 Mach-Zehnder Interferometer Problems

The nonlinear Mach-Zehnder interferometer described above, while attractive for its simplicity, is not a very practical design for an all-optical switch. Because signal pulses travel through separate paths in the interferometer, the switch may be imbalanced by thermal or acoustic variation between the two arms. These variations may affect the relative path lengths through which the signal pulses travel causing unintentional changes in the bias phase of the interferometer, Φ_{bias}. This leads to unpredictable behavior from the switch. These problems can be reduced by using active path length stabilization. However, such a solution is generally difficult and unsatisfactory.

An additional problem with the nonlinear Mach-Zehnder interferometer arises when one considers that the response of the nonlinear material may not be instantaneous. For example, semiconductor materials used in this thesis have nonlinear responses which have been observed to be well modeled by a sum of exponential decays with time responses ranging from a few femtoseconds to several nanoseconds [12]. If the refractive index changes from a single control pulse last more than one bit period, subsequent signal pulses may receive a nonlinear phase shift and be at least partially switched by the interferometer, even in the absence of a control pulse. These effects lead to undesirable patterning on the output pulses from the switch.

N. S. Patel has done simulations to demonstrate the effect of a long-lived nonlinear response in an unbalanced interferometer configured as an AND gate [16, 17]. In these simulations, the nonlinear phase response was assumed to have an instantaneous component, an ultrafast component with a relaxation time of 600 fs, and a long-lived component due to carrier with a relaxation time of 100 ps. The results of these simulations on a 40Gbps data stream are shown in Figure 2-3. The bits at the output suffer from amplitude modulation due to long-lived index changes. More significantly, output pulses are appearing in slots that should be zero. This reduces the contrast

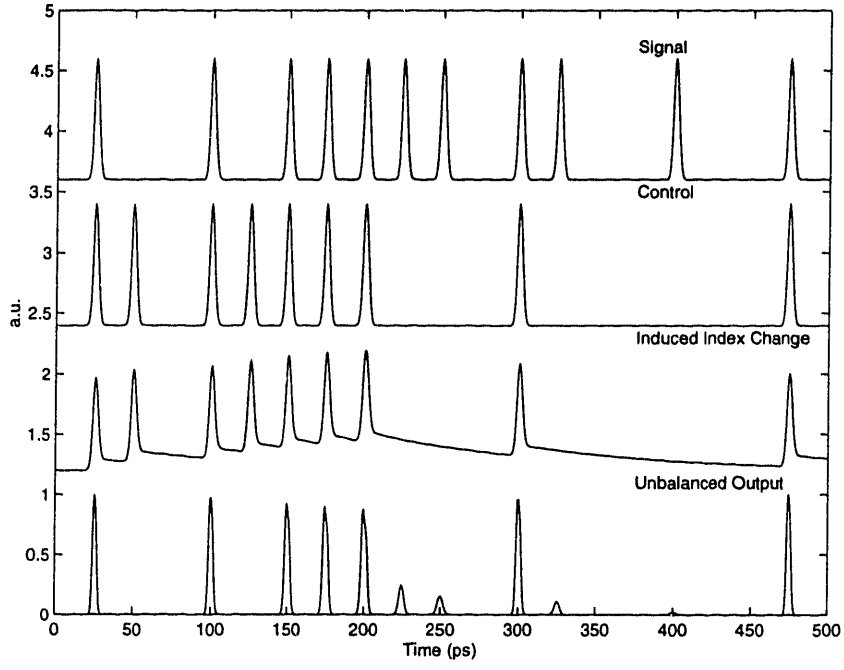

Figure 2-3: Simulation of effects of long-lived index changes in an unbalanced interferometric all-optical switch.

ratio of the switch considerably.

2.4 Ultrafast Nonlinear Interferometer

Many of these problems can be remedied using a single-arm interferometer (SAI) switch design [18, 20]. The SAI works on the same principles as the nonlinear Mach-Zehnder interferometer, only signal pulses are separated temporally in a single arm. A block diagram of the SAI is shown in Figure 2-4. Signal pulses entering on the left are split into two equal-power, orthogonally-polarized pulses by a polarization sensitive delay (PSD). These pulses are separated by at least one pulse width. A copropagating control pulse is introduced after the PSD. This pulse is timed to overlap with precisely one of the signal pulses. All three pulses then travel through the nonlinear material (NLM). Third order nonlinearities in the material cause a differential nonlinear phase shift in the overlapping signal pulse when a control pulse is present. The two signal pulses are then recombined temporally in a second PSD. Finally, the signal pulses are interfered in a polarizer and the control pulse is filtered out to give the output pulse.

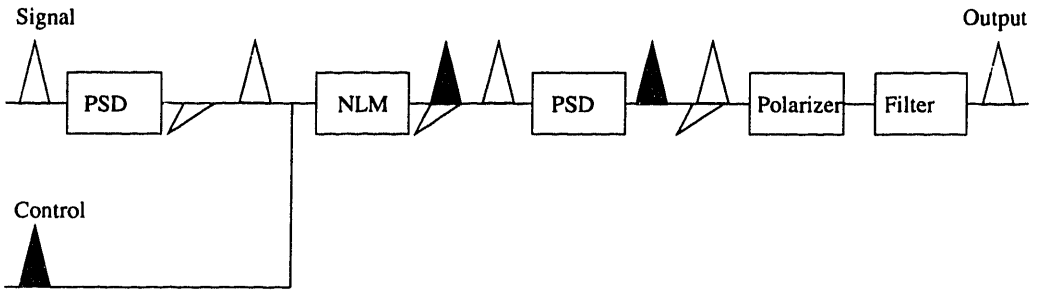

Figure 2-4: Block diagram of a single-arm interferometer.

The ultrafast-nonlinear interferometer (UNI), shown in Figure 2-5, is a fiber implementation of the SAI. Entering signal pulses travel through a polarization sensitive isolator (PSI). At the output of the PSI, the signal pulses are linearly polarized at 45 degrees with respect to the fast and slow axes of a length of birefringent fiber (BRF) which acts as a polarization sensitive delay. After traversing the BRF, signal pulses pass through a 50/50 coupler where the control pulse is introduced. These pulses then travel through the nonlinear material (NLM). Signal pulses are temporally recombined in a second length of BRF. The orthogonally polarized signal pulses are then interfered in a second PSI. Polarization paddles before the PSI allow adjustment of the bias phase of the interferometer. Finally, control pulses are filtered out using a fiber-coupled band-pass filter leaving the output signal pulse.

The UNI is a balanced interferometer. Both signal pulses in the UNI travel along the same path. So the problems encountered in the nonlinear Mach-Zehnder interferometer due to thermal and acoustic variations between the two arms are eliminated. The UNI has been demonstrated at rates up to 100Gbps [11] with no active bias stabilization.

The balanced interferometer design of the UNI also reduces the effects of long-

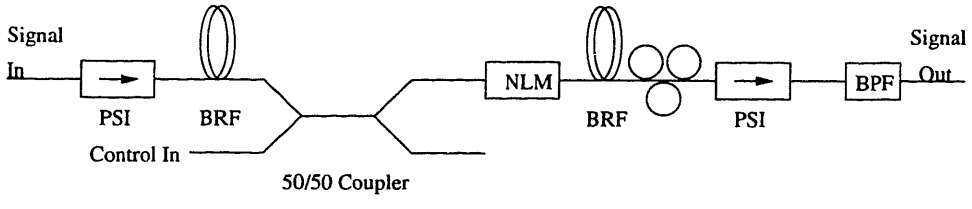

Figure 2-5: Ultrafast-nonlinear interferometer implementation.

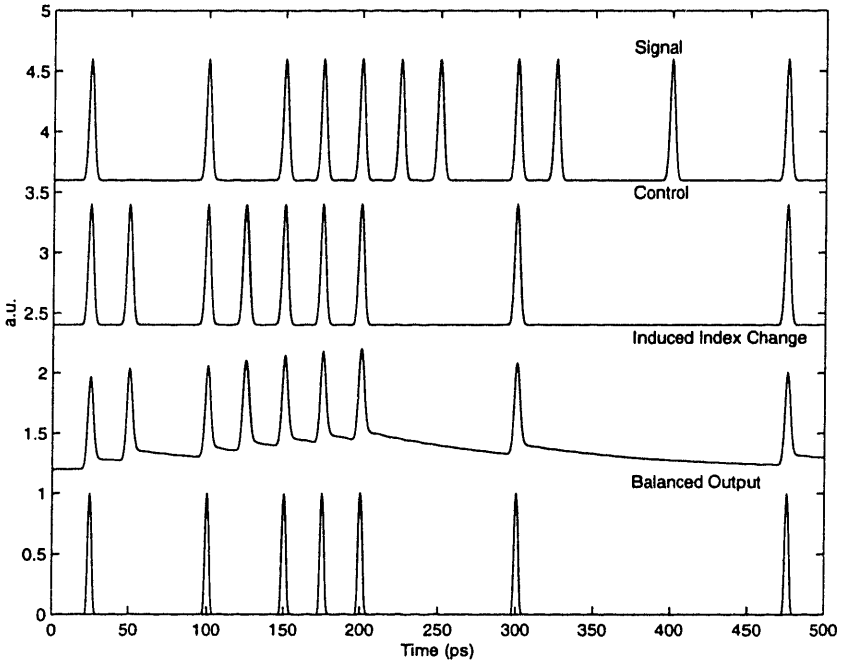

Figure 2-6: Simulation of effects of long-lived index changes in an ultrafast nonlinear interferometer.

lived index changes. For example, if a control pulse induces a long-lived nonlinear refractive index change, subsequent signal pulse pairs sense these lingering changes equally and are not switched by the interferometer. Therefore, the UNI is insensitive to these long-lived index changes. Only ultrafast refractive index changes induced by a control pulse, introducing differential phase shifts between the two signal pulses, can cause the UNI to switch. N. S. Patel has performed other simulations of the effects of long-lived index changes in the UNI [16, 17]. The results of one these simulations are shown in Figure 2-6. This simulation used the same impulse response as the simulation of the unbalanced interferometer shown in Figure 2-3. The pulses in the UNI were temporally separated by 12.5ps. The effects of the long-lived index changes are negligible.

One reason the simulated results are so uniform is that they only take into account changes in the refractive index. There are also corresponding changes in the gain of the material. These gain changes may be related to the index changes through the Kramers-Kronig relations. In the UNI, gain changes that last more than one half of the bit period will be experienced by both signal pulses. We have performed

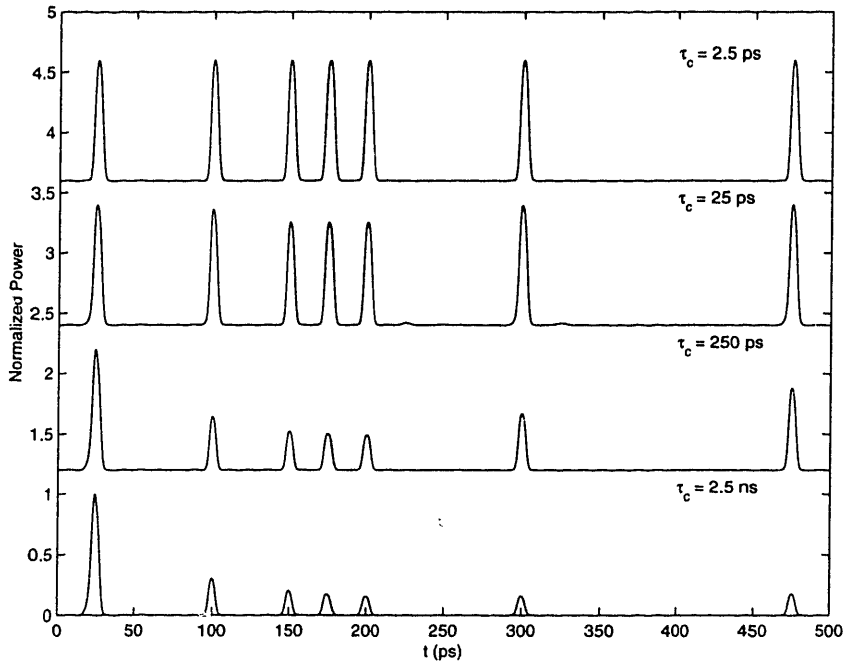

Figure 2-7: Simulation of the effects of long-lived gain changes on the output pulses from the UNI. Here, the output is shown for the signal and control inputs shown in Figure 2-6 with carrier recovery times of 2.5 ps, 25 ps, 250 ps, and 2.5 ns.

simulations to show the effects of gain changes on signal pulses in the UNI using the analytical method described in [21]. For these simulations, we have used the same 40 GHz signal and control pulse patterns shown in Figure 2-6. We have assumed the energy in a single control pulse is 10 percent of the saturation energy for the nonlinear material and that the effects of the signal pulses are negligible compared to the effects of the high intensity control pulses. The small signal gain is assumed to be 20 dB. To isolate the gain effects, we have assumed that a uniform phase shift of π is obtained between the two orthogonal signal pulses when a control pulse is present. We have plotted the resulting output pulse stream for various values of the gain recovery time, τ_c, in Figure 2-7. As is evident in the plot, when the gain recovery time becomes much longer than the bit period, significant patterning is observed on the output bits. This patterning limits achievable switching rates and prevents cascading of multiple switches.

2.5 Material Properties

In choosing a nonlinear material for use in the UNI, several characteristics of the material must be considered. The material must have a large, fast nonlinear response, low loss, small dispersion, and low birefringence. In this section, we discuss each of these properties and describe how they affect the operation of the UNI.

2.5.1 Nonlinearity

The ideal nonlinear material for an interferometric optical switch will have a very large third-order nonlinearity. As seen in Equation 2.19, the nonlinear phase shift induced in a signal pulse is directly related to the nonlinear refractive index, the intensity of the control pulse, and the length of the device. If n_2 is small, large control pulse intensities or device lengths are required to achieve a π phase shift. For example, optical fiber, a popular switching material has a relatively small nonlinearity ($|n_2| \approx 3 \times 10^{-16}$ cm^2/W). Optical switches have been demonstrated using fiber nonlinearities, but have required long lengths of fiber (100's of meters) to achieve reasonable switching intensities. Typically, one kilometer of fiber is needed to induce a π phase shift with peak pulse powers of 1 W. The third-order nonlinearity in semiconductor waveguides is typically 3-4 orders of magnitude larger than that of optical fiber. Additionally, because of the higher refractive index of semiconductors, the effective area of the guiding region in a single-mode semiconductor waveguide is typically smaller than the effective area of the core in an optical fiber. Thus, for the same optical power, optical intensities in a semiconductor waveguide are typically higher than they are in optical fibers. Hence, semiconductor device lengths on the order of a millimeter can be used for switching with reasonable signal intensities.

As we have already discussed, a fast third-order nonlinearity is desirable in materials used in all-optical switches. However, many semiconductor materials have a non-instantaneous third-order nonlinearity. The balanced interferometric design of the UNI reduces the effects of long-lived refractive index changes, but long-lived gain effects are still a problem. This is especially true in active semiconductor devices

where intense control pulses cause significant changes in the carrier populations. For example, when the device is biased for gain, above-band control pulses stimulate electron transitions from the conduction band into the valence band. These carrier-induced changes in the gain and refractive index may persist for tens of picoseconds to a few nanoseconds. Therefore, at high bit rates (> 10 Gbits/s) it takes several bit periods for these carriers to recover to their equilibrium state. This increases the linear loss of subsequent signal pulses and leads to undesirable amplitude modulation on the output.

In the past, most switching experiments using nonlinearities in semiconductors have been done with active devices biased in the gain regime (for example, [11, 22]). The problems with amplitude modulation were apparent in these demonstrations. Alternatively, one can use semiconductor optical amplifiers (SOA) biased at the transparency point or passive semiconductor waveguides. In SOA biased at transparency, the probability of a signal photon stimulating emission is equal to the probability of the photon stimulating absorption (see Chapter 3 for a more detailed discussion of transparency). A signal pulse travelling through the device causes no net changes in carrier populations. Thus, slow recovery times and gain dynamics are avoided. In passive waveguides, the signal and control wavelengths are below the bandgap of the material. Hence, linear absorption processes are nonexistent and carrier populations may remain relatively unchanged by low-power optical pulses propagating through the device. In both of these cases, however, ultrafast nonlinearities due to carrier heating, carrier scattering, and bound-electronic effects remain and may be utilized for all-optical switching. In this thesis, we will explore the properties of these devices in detail and determine their suitability for all-optical switching.

2.5.2 Loss

Consideration of waveguide losses is important since switching in the UNI is based on intensity dependent refractive index changes. In this section, we shall show that waveguide losses decrease the effective interaction length for signal and control pulses in the nonlinear material. This loss reduces the nonlinear phase shift accrued by the

signal pulses. As a result, higher control pulse intensities are required in waveguides with higher losses to achieve the desired phase shift. This necessitates the use of optical amplifiers and makes cascading of switches difficult.

The effect of losses on the pulse intensity, $I(z)$, may be quantified as

$$\frac{\partial I}{\partial z} = -\alpha I - \beta I^2 + \ldots. \tag{2.20}$$

The linear loss coefficient, α, accounts for linear material losses, and linear absorption in materials. The nonlinear loss coefficient, β, accounts for nonlinear losses such as two-photon absorption. In most cases β is quite small (on the order of 10 cm/GW in semiconductors), but its effects can become significant at high optical intensities. Third-order and higher terms may be neglected for most practical applications. Equation 2.20 may be integrated to find the pulse intensity at a position z:

$$I(z) = \frac{I_0 \exp(-\alpha z)}{1 + \beta I_0 [1 - \exp(-\alpha z)]/\alpha}, \tag{2.21}$$

where I_0 is the intensity at $z = 0$.

In the limit of low nonlinear losses ($\beta \to 0$), we have

$$I(z) = I_0 \exp(-\alpha z) \tag{2.22}$$

Using this intensity profile, we find that the nonlinear phase shift induced in a signal pulse of wavelength λ after propagating through a waveguide of length L with nonlinear refractive index n_2 may be expressed as a function of the control pulse intensity, I:

$$\begin{aligned} \Phi_{\text{nl}} &= \int_0^L \frac{2\pi}{\lambda} n_2 I(z) dz \\ &= \frac{2\pi}{\lambda} n_2 I_0 \left(\frac{1 - \exp(-\alpha L)}{\alpha} \right). \end{aligned} \tag{2.23}$$

Note that this equation is identical to equation 2.19 if we define the effective interaction length $L_{\text{eff}} = [1 - \exp(-\alpha L)]/\alpha$. As α becomes larger, the effective interaction

length approaches $1/\alpha$ asymptotically. However, in this case, the losses are so large that switching is impractical.

Nonlinear losses also affect switching requirements. Including the effects of β, we find that the nonlinear phase shift accrued over a length L is:

$$\Phi_{\rm nl} = \frac{2\pi}{\lambda} n_2 \frac{1}{\beta} \ln\left[1 + \frac{I_0\beta}{\alpha}(1 - \exp(-\alpha L))\right] \tag{2.24}$$

To explore the individual effects of β, set $\alpha = 0$. Then, the nonlinear phase shift is

$$\Phi_{\rm nl} = \frac{2\pi}{\lambda} n_2 \frac{1}{\beta} \ln\left[1 + I_0\beta L\right]. \tag{2.25}$$

We see that the initial intensity required to achieve a phase shift of π is

$$I_\pi = \frac{1}{\beta L}\left[\exp\left(\frac{\beta\lambda}{2n_2}\right) - 1\right]. \tag{2.26}$$

In the absence of nonlinear losses ($\beta = 0$),

$$I_\pi^0 = \frac{\lambda}{2n_2 L}. \tag{2.27}$$

Now, we find from equation 2.26,

$$\frac{I_\pi}{I_\pi^0} = \frac{\exp(T) - 1}{T}, \tag{2.28}$$

where

$$T = \frac{\beta\lambda}{2n_2}. \tag{2.29}$$

The parameter T has been suggested as a figure of merit for switching using materials with nonlinear losses [23, 24]. Figure 2-8 shows the relationship between I_π/I_π^0 and T. As T increases, the required control pulse intensities increase dramatically. To achieve switching with minimal nonlinear losses, we must have $T < 1$.

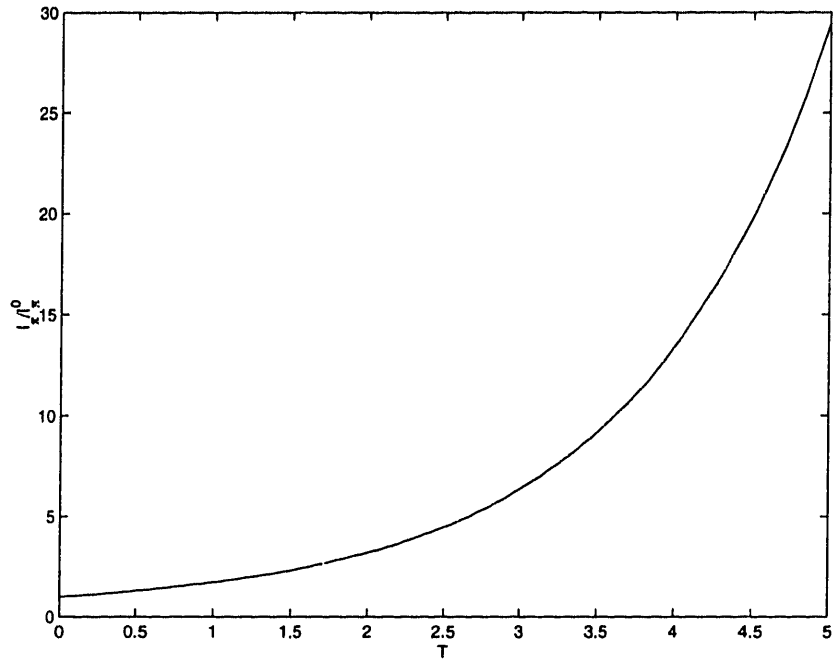

Figure 2-8: Intensity required to achieve a π phase shift as a function of the figure-of-merit, T.

2.5.3 Dispersion

Dispersion in the nonlinear material also affects the operation of the UNI. In a dispersive material, the propagation constant, β, is a function of the frequency of light. A short optical pulse contains many optical frequencies. In a dispersive waveguide, some of these frequencies propagate faster than others. This leads to pulse distortion as the faster frequencies move ahead of the slower frequencies.

Let us consider the effect of dispersion on a Gaussian pulse as an example. We write the propagation constant in the dispersive medium around a frequency ω_0 as

$$\beta(\omega) = \beta_0 + \beta_1(\omega - \omega_0) + \frac{1}{2}\beta_2(\omega - \omega_0)^2 + \ldots, \tag{2.30}$$

where $\beta_n = \frac{\partial^n \beta}{\partial \omega^n}|_{\omega=\omega_0}$ [25]. Now consider an initially unchirped Gaussian pulse with center frequency ω_0 propagating in the z direction in the medium. We write the

electric field for the pulse at $z = 0$ as:

$$E(z=0,t) = E_0 \exp\left(-\frac{t^2}{2T_0^2}\right) \exp(j\omega_0 t) \tag{2.31}$$

This pulse has a full-width at half-maximum (FWHM) of:

$$T_{\text{FWHM}} = 2(\ln 2)^{1/2} T_0 \tag{2.32}$$

The frequency content of the pulse is found by computing the Fourier transform of $E(z=0,t)$:

$$\begin{aligned} E(z=0,\omega) &= \frac{1}{2\pi}\int_{-\infty}^{\infty} E(z=0,t)\exp(-j\omega t)dt \\ &= \frac{E_0 T_0}{\sqrt{2\pi}} \exp\left(-\frac{(\omega-\omega_0)^2 T_0^2}{2}\right) \end{aligned} \tag{2.33}$$

Thus, the spectral content of the pulse is Gaussian, as well. The spectral FWHM is found to be:

$$\Delta\omega_{\text{FWHM}} = \frac{2(\ln 2)^{1/2}}{T_0}. \tag{2.34}$$

After propagating a distance L into the dispersive medium, the pulse spectrum becomes:

$$\begin{aligned} E(z=L,\omega) &= E(z=0,\omega)\exp\left(-j\beta(\omega)L\right) \\ &= \frac{E_0 T_0}{\sqrt{2\pi}} \exp\Bigg[-\left(\frac{T_0^2}{2} + \frac{j\beta_2 L}{2}\right)(\omega-\omega_0)^2 \\ &\qquad - j\beta_1 L(\omega-\omega_0) - j\beta_0 L\Bigg]. \end{aligned} \tag{2.35}$$

Note that the spectrum is still Gaussian with the same FWHM. However, there is now a frequency dependent phase shift in the spectrum, $\Phi(z=L,\omega) = \beta(\omega)L$. Taking the inverse Fourier transform of $E(z=L,\omega)$, we find the time-domain equation for

the pulse at $z = L$:

$$E(z = L, t) = \int_{-\infty}^{\infty} E(z = L, \omega) \exp(j\omega t) d\omega$$
$$= \frac{E_0}{\sqrt{1 + \frac{j\beta_2 L}{T_0^2}}} \exp\left[-j\beta_0 L - j\omega_0 t\right] \exp\left[-\frac{(t - \beta_1 L)}{2(T_0^2 + j\beta_2 L)}\right] \quad (2.36)$$

The pulse is still Gaussian, although its shape has changed slightly. At this point, it is useful to define a few terms related to the frequency dependent propagation constant. The phase velocity of the pulse, $v_\phi = \omega_0/\beta_0$, relates the speed at which the sinusoidal carrier frequency of the pulse is propagating through the material. Similarly, the group velocity, $v_g = 1/\beta_1$, is the speed at which the pulse envelope is propagating through the material. Finally, β_2 is the group velocity dispersion which relates to the rate at which the pulse is broadening in the dispersive medium. Defining the dispersion length, $L_D = T_0^2/|\beta_2|$, the pulse width at $z = L$ is found to be [15]:

$$T_{\text{FWHM}}(z = L) = 2(\ln 2)^{1/2} T_0 \sqrt{1 + (L/L_D)^2}. \quad (2.37)$$

The peak intensity is similarly found to be:

$$P_{\text{peak}} = \frac{E_0^2}{1 + (L/L_D)^2} \quad (2.38)$$

Figure 2-9 shows the dispersion of a Gaussian pulse for various values of L/L_D.

This pulse distortion in the nonlinear material has important consequences for all-optical switching in the UNI. For materials with fast nonlinearities, the effect of the nonlinearity is reduced as the instantaneous peak intensity of the pulse lessens due to dispersion. The dispersion-induced reduction in peak intensity reduces the effective length of the nonlinear interaction between signal and control pulses. For slower nonlinear responses, this reduction in the peak intensity of the pulse is less of an issue as the effect of the nonlinearity is integrated over the entire pulse. That is, the nonlinearity is proportional to the pulse energy rather than the peak power.

Additional problems arise as a result of the pulse broadening. The SAI requires

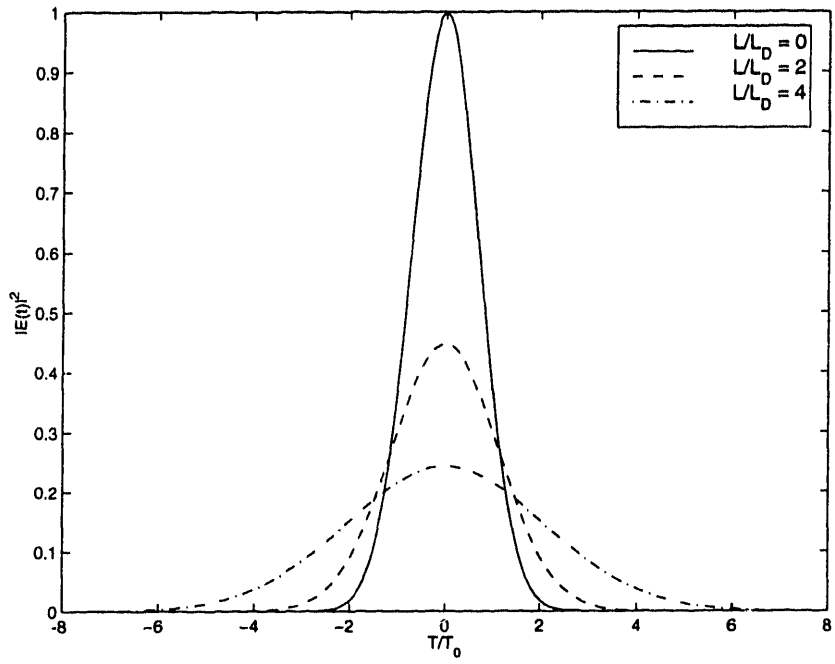

Figure 2-9: Dispersion-induced broadening of a Gaussian pulse.

that the signal pulses be separated temporally to isolate the nonlinear effects of the control pulse within the interferometer. If the control pulses become very wide, they may overlap both of the temporally separated signal pulses, reducing the differential effects of the nonlinearity in the interferometer and making switching difficult. Signal pulses are also affected by dispersion. In the extreme case, signal pulses may become so broad that they interfere with neighboring pulses. While this problem may not arise in a single switch, it may become a significant issue when cascading of multiple switches is considered. Hence, choosing a material with a small group velocity dispersion, β_2, relative to the length of the device is important.

The problems associated with dispersion are a primary reason for using semiconductor waveguides for the nonlinear material in all-optical switches instead of optical fiber. Long lengths of fiber are required to achieve a π phase shift with reasonable pulse energies. This means that dispersion is a significant issue when fiber is used. Indeed, in these lengths of fiber, other issues such as pulse walk-through due to the different group velocities of signal and control pulses arise. Since semiconductor waveguides can achieve the same phase shift in a device that is less than a millimeter

in length, the effects of dispersion are reduced.

2.5.4 Birefringence

Birefringence occurs when the propagation constant for a material, $\beta(\omega)$ is polarization dependent. In ordinary optical fiber and bulk semiconductor waveguides, this effect is typically negligible. Some of the semiconductors tested in this thesis contain quantum wells, however. In these quantum wells, the lattice structure of the semiconductor is strained, inducing birefringence in the device. This birefringence affects the operation of the UNI since the two signal pulses propagating through the nonlinear material have orthogonal polarizations. Different propagation constants between the two polarizations will affect the interference of the pulses at the output.

Suppose that the propagation constant for the x polarization is $\beta_x(\omega)$ and the propagation constant for the y polarization is $\beta_y(\omega)$. Then, define the difference between these two propagation constants

$$\begin{aligned} \Delta\beta(\omega) &= \beta_x(\omega) - \beta_y(\omega) \\ &= \Delta\beta_0 + \Delta\beta_1(\omega - \omega_0) + \Delta\beta_2(\omega - \omega_0)^2 + \ldots. \end{aligned} \tag{2.39}$$

Each of the constants, $\Delta\beta_0$, $\Delta\beta_1$, and $\Delta\beta_2$, has a different affect on the operation of the UNI which must be considered.

The modal birefringence, $\Delta\beta_0$, relates the difference in the phase velocities of the two polarizations. From equation 2.36, we see that this difference results in an overall phase difference between the two pulses. This phase contributes to the bias phase of the interferometer. The initial phase bias of the UNI is important because it determines its logical operation. However, the changes in bias phase due to modal birefringence can be easily compensated by adjusting the polarization paddles prior to the polarizer at the output of the switch.

A more serious problem arises when there is a difference in group velocities, $\Delta\beta_1$. This is also referred to as the polarization mode dispersion (PMD). Birefringent fiber, for instance, typically has a PMD of ~ 1.5 ps/m [26]. When PMD exists in the UNI,

the two orthogonally polarized signal pulse envelopes propagate at different speeds. After propagating through a device of length L, the two envelopes will be offset by a time $\tau = \Delta\beta_1 L$. Hence, they may not overlap at the output. This reduced overlap may affect the contrast ratio of the switch. To observe this effect, consider a Gaussian pulse at the input of the UNI,

$$E(t) = E_0 \exp\left[-\frac{t^2}{2T_0^2}\right] \exp(-j\omega_0 t). \tag{2.40}$$

Suppose the UNI imparts a uniform π phase shift on one of the signal pulses in the nonlinear material. Additionally, suppose that the difference in the group velocities of the pulses in the material delays one of the signal pulse envelopes by time τ. Then, the intensity of the pulse at the output of the interferometer will be:

$$I_{\text{out}}(t) \propto \left|\frac{E(t)}{\sqrt{2}} - \frac{E(t-\tau)}{\sqrt{2}}\right|^2 \tag{2.41}$$

Integrating this intensity with respect to time gives the energy of the pulse. Figure 2-10 shows the inverse contrast ratio of the UNI, defined as the energy of the switched OFF pulse divided by the energy of the switched ON pulse, as a function of τ/T_0. Note that a small inverse contrast ratio is desired for optimum switching performance. As the inverse contrast ratio approaches 1, it becomes more difficult to distinguish the ON pulse from the OFF pulses. As τ increases, we observe that the ability of the UNI to switch OFF pulses lessens. Differences in the group velocities of the signal pulses may be compensated for by adjusting the length of the polarization sensitive delays (PSD) in the UNI. However, this would only fix the problem for a single nonlinear material with signals at a particular wavelength. If the material or signal wavelength were changed later, one would have to recalibrate the length of the PSD accordingly. Clearly this is not a very desirable solution.

Differences in the group velocity dispersions of the two polarizations, $\Delta\beta_2$ also affect the operation of the UNI. Such a difference leads to the signal pulses having different widths and intensities when they are interfered at the output of the UNI. This

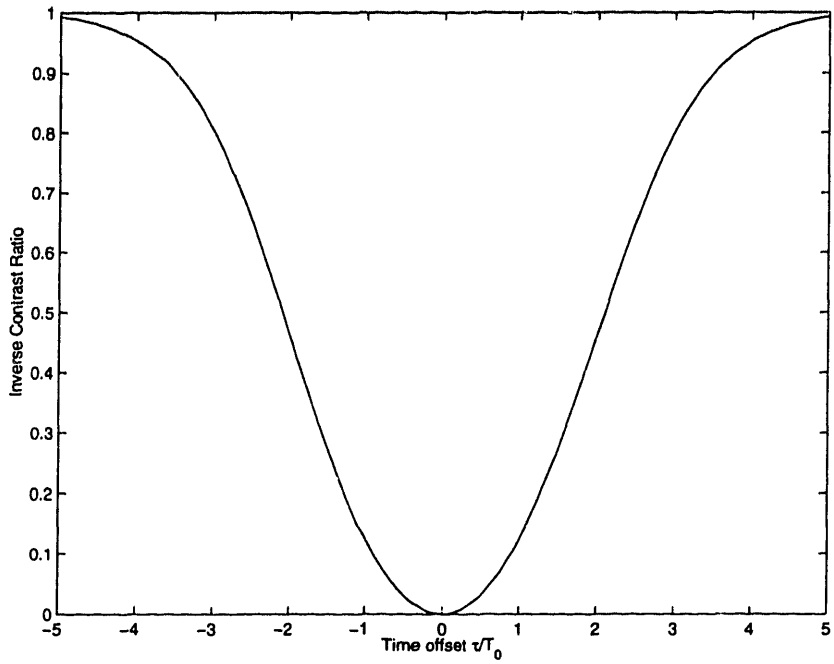

Figure 2-10: Inverse contrast ratio, $R = E_{\text{off}}/E_{\text{on}}$ of the UNI as a function of timing offset of the two signal pulses normalized by the pulse width.

leads to nonuniform interference at the output. Figure 2-11 illustrates the effect of nonuniform interference on the output pulse shape. Here, one of the pulses experiences no dispersion and propagates through the device undistorted. The second pulse has a uniform π phase shift relative to the first pulse and experiences dispersion as it propagates through the device. The figure shows the interference of the two pulses for various dispersion lengths, L/L_D. When no dispersion occurs ($L/L_D = 0$), the output pulse is completely switched OFF, as expected. As the dispersion increases, the output is no longer completely switched OFF. When $L/L_D = 4$, the peak output pulse intensity is almost half of the original pulse intensity. Figure 2-12 shows a the inverse contrast ratio of the UNI as a function of the difference in GVD for the two polarizations.

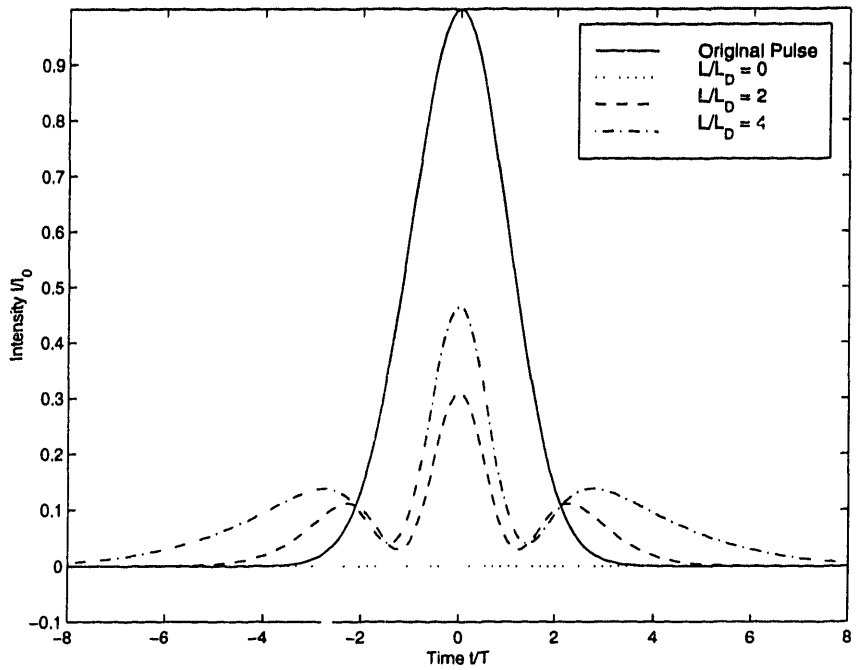

Figure 2-11: Interference of two Gaussian pulses for various values of $L/L_D = \Delta\beta_2 L/T_0^2$ where $\Delta\beta_2 = \beta_{2x} - \beta_{2y}$. Initial Gaussian pulse width is T_0. Initial intensitiy is I_0.

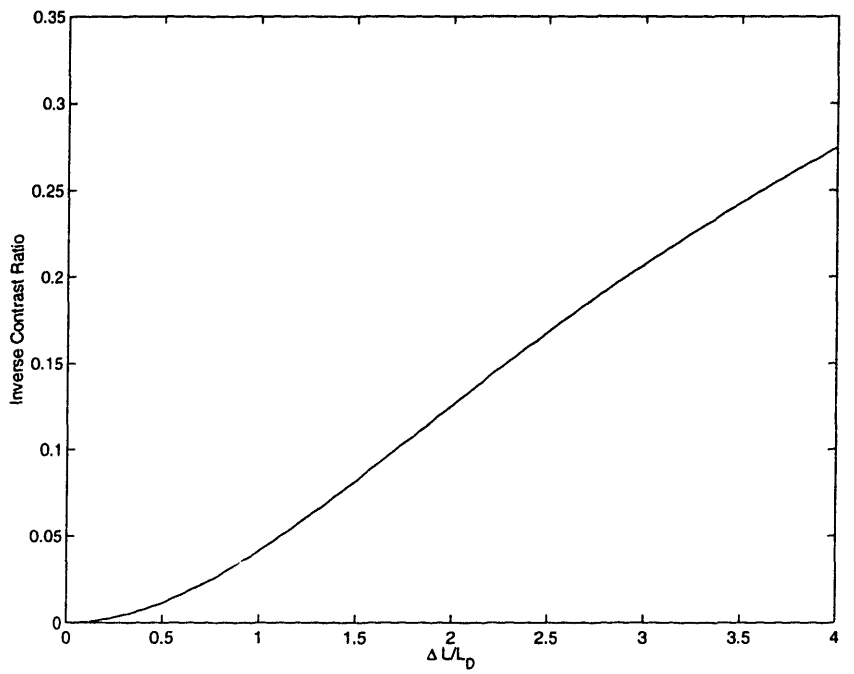

Figure 2-12: Inverse contrast ratio of the UNI as a function of the difference in dispersion, $\Delta L/L_D = \Delta\beta_2 L/T_0^2$ where $\Delta\beta_2 = \beta_{2x} - \beta_{2y}$.

Chapter 3

Semiconductor Devices

In this chapter, we will describe the semiconductor waveguides used in this thesis. We begin with a description of a typical semiconductor waveguide. This is followed by a discussion of the carrier population dynamics in semiconductors. We describe how these interactions lead to linear gain. Then, we present the various mechanisms which cause nonlinear gain changes in semiconductor waveguides. Next, we show how the nonlinear gain changes of a semiconductor relate to nonlinear refractive index changes through a Kramers-Kronig transformation. Then, we discuss measurements of dispersion in semiconductor waveguides. Finally, we discuss the use of semiconductors in all-optical switching.

3.1 Semiconductor Waveguides

A typical index-guided semiconductor waveguide like those studied in this thesis is shown in Figure 3-1 [27]. The device is a dielectric waveguide consisting of a layer of InGaAsP (the active region) between two layers of InP (the cladding regions). The higher refractive index of the InGaAsP region confines light in the vertical direction. The ridge etched in the top layer of InP provides an effective index change which confines light in the horizontal direction.

The device pictured is a diode, or p-n junction. When the diode is forward biased, carriers are injected into the active region of the waveguide. The bandgap of the

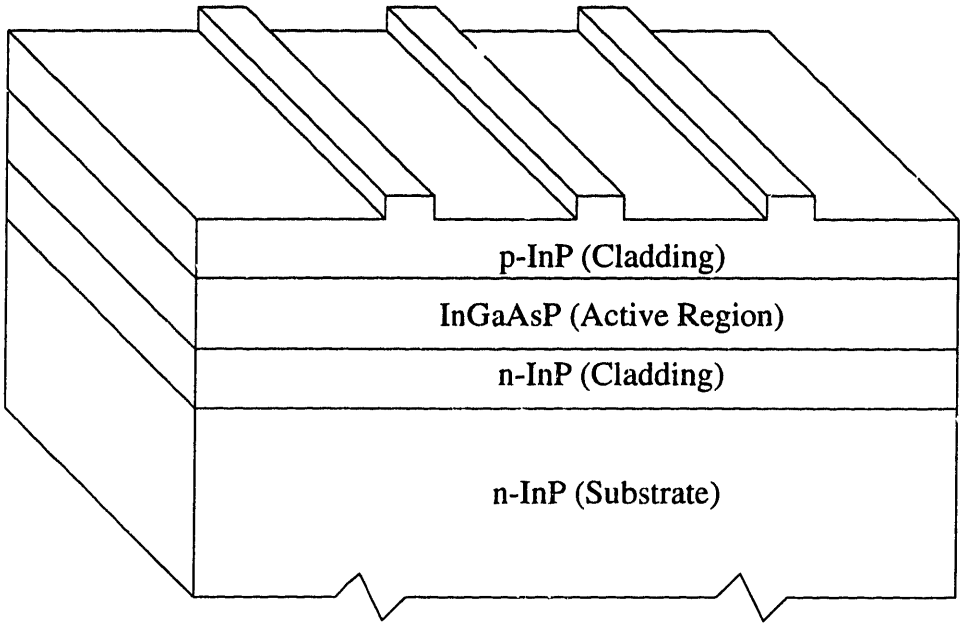

Figure 3-1: An index-guided semiconductor optical amplifier.

InGaAsP layer is engineered to be less than that of the surrounding InP laters. This potential barrier created by the layers serves to confine the injected carriers to the active region where most optical interactions occur. Such as device is commonly referred to as "active." A passive waveguide has a similar structure, only the cladding regions are not necesarily doped to create a p-n junction, and carriers are not injected electrically into the material.

The facets of the semiconductor waveguide are typically cleaved normal to the waveguide. However, since the refractive index of the semiconductor is relatively large, the reflectivity of these facets is quite high (typically ~ 0.3). This large reflectivity of the end facets causes coupling losses and creates Fabry-Perot cavity effects. For example, in an active device, these mirrors provide feedback and may enable laser activity. To reduce these effects, the facets may be cleaved at an angle or anti-reflection (AR) coated. In this case, the waveguide provides gain, but lasing is not achieved. Such a device is called a semiconductor optical amplifier (SOA).

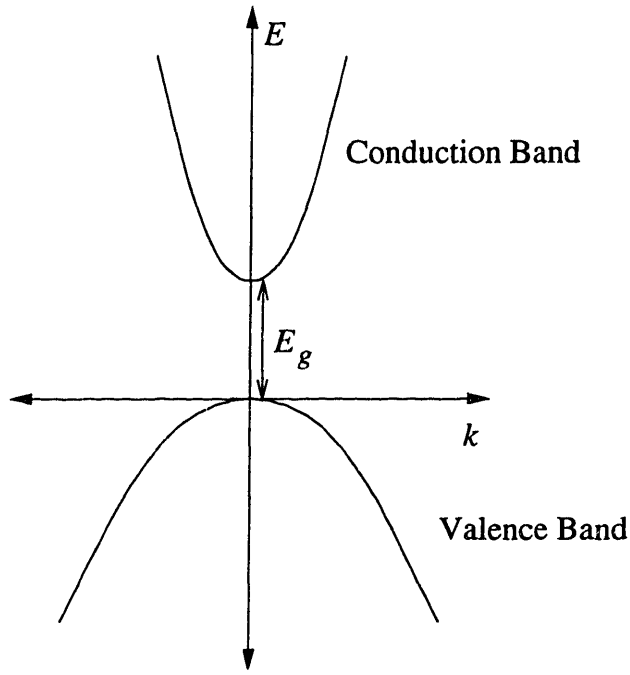

Figure 3-2: Dispersion relationship for a direct bandgap semiconductor.

3.2 Carrier Population Dynamics

Optical interactions with semiconductors are strongly influenced by carrier population dynamics within the semiconductor. Electrons in a semiconductor are distributed among the avaliable energy levels of the semiconductor. The highest filled energy level in a direct bandgap semiconductor at 0K is known as the *valence band.* The *conduction band* is separated from the valence band by an energy bandgap, E_g. No electrons reside in the energy levels between the valence and conduction bands. In semiconductors, E_g is on the order of a few eV. Electrons in the valence band may be excited into the conduction band. These, excited electrons, known as *free carriers*, fill the bottom of the conduction band, leaving behind holes in the top of the valence band.

Near the bottom of the conduction band, the band structure of a typical semiconductor is well approximated by a parabola [28]. If we define the top of the valence band as having 0 energy, the energy in the conduction band as a function of the wave

vector $\mathbf{k}$ is given by:

$$E_c(\mathbf{k}) = E_g + \frac{\hbar^2 k^2}{2m_e}. \tag{3.1}$$

Here, m_e is the effective mass of electrons in the conduction band and k is the magnitude of $\mathbf{k}$. Similarly, the energy structure in the valence band may be written as:

$$E_v(\mathbf{k}) = -\frac{\hbar^2 k^2}{2m_h} \tag{3.2}$$

where m_h is the effective hole mass in the valence band. Figure 3-2 shows an example dispersion relation for electrons in a direct bandgap semiconductor. It is interesting to note the similarity between these dispersion equations and the dispersion relationship for a free electron. Indeed, negative-charged electrons in the conduction band and positive-charged holes in the valence act much like free carriers with masses m_e and m_h, respectively. Their movement in response to an applied voltage gives rise to current.

The devices studied in this thesis are fabricated using the quaternary semiconductor $In_{1-x}Ga_xAs_yP_{1-y}$. The InGaAsP is grown on an InP substrate. In order to ensure that these two semiconductors are lattice matched, we must have $x = 0.4526y/(1 - 0.031y)$ [29]. The energy bandgap and effective masses for electrons in the conduction band and holes in the valence band in lattice-matched InGaAsP/InP are given in Table 3.1 Note that the bandgap can be varied between 0.75eV and 1.35eV ($0.92\mu m < \lambda_G < 1.65\mu m$). This region of energies overlaps with the low loss energies in optical fiber, making InGaAsP devices very practical choices for integration in fiber-optic data networks.

Electrons in a semiconductor are subject to the Pauli-exclusion principle. This dictates that at most two electrons (with opposite spin states) can occupy the same energy state simultaneously. The distribution of electrons among the available energy states at thermal equilibrium is thus described by Fermi-Dirac statistics. The probability that an electron occupies a state with energy E is given by the Fermi-Dirac

Parameter	Value
Energy bandgap	$E_g = 1.35 - 0.72y + 0.12y^2$
Eff. electron mass	$m_e/m_0 = 0.080 - 0.039y$
Eff. hole mass	$m_h/m_0 = (1-y)[0.79x + 0.45(1-x)] + y[0.45x + 0.4(1-x)]$

Table 3.1: Energy bandgap, and effective carrier masses for lattice-matched InGaAsP/InP. m_0 is the effective mass of an electron in free space.

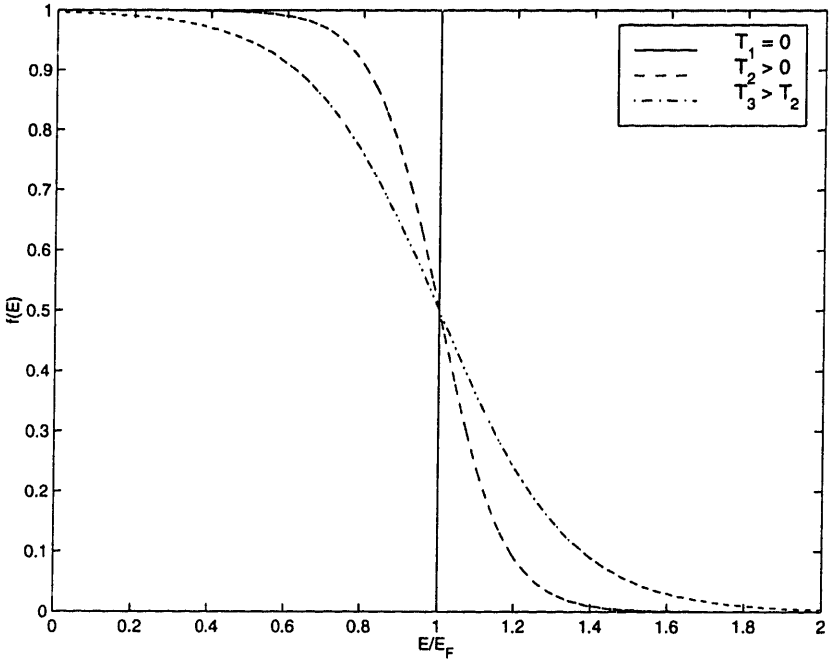

Figure 3-3: The Fermi-Dirac distribution fuction for various temperatures.

distribution function:

$$f_e(E) = \frac{1}{e^{(E-E_F)/k_BT} + 1} \tag{3.3}$$

Here, T is temperature and k_B is Boltzmann's constant. The energy E_F is known as the Fermi energy. At the Fermi energy, the probability of occupation is precisely 1/2. The Fermi-Dirac distribution fuction is plotted in Figure 3-3 for several temperatures. When $T = 0$ the distribution is simply a step function with all states below the Fermi energy filled. As T increases, thermal energy excites electrons into higher energy states, smearing out the distribution and filling the conduction band.

When the semiconductor is not in thermal equilibrium, the distribution of elec-

trons in the valence band and the conduction band cannot be written in terms of a single Fermi energy. Minority carrier injection into the bands is one way that the thermal equilibrium may be disturbed. If the number of injected carriers is small, the distribution of electrons within a particular band may remain in equilibrium among themselves. In this case, the quasi-Fermi energies for the valence and conduction bands are distinct. We write these energies as E_{Fc} and E_{Fv}, respectively. The distribution of electrons is then:

$$f_c(E) = \frac{1}{e^{(E-E_{Fc})/k_BT} + 1} \tag{3.4}$$

in the conduction band, and

$$f_v(E) = \frac{1}{e^{(E-E_{Fv})/k_BT} + 1} \tag{3.5}$$

in the valence band.

The density of states in the valence band, $\rho_v(E)$, is defined so that $\rho_v(E)dE$ quantifies the number of available energy states in the range $(E, E + dE)$ for a semiconductor[28]. The number of states in a region of **k**-space enclosed by a spherical shell of thickness dk is:

$$n_k = \frac{1}{(2\pi)^3} 4\pi k^2 dk. \tag{3.6}$$

Now, if we use the parabolic approximation for the dispersion relation between E and k, we find for the valence band,

$$\rho_v(E) = \frac{1}{2\pi^2} \left\{ \frac{2m_h}{\hbar} \right\}^{3/2} (-E)^{1/2}. \tag{3.7}$$

Similarly we find that the density of states in the conduction band is given by

$$\rho_v(E) = \frac{1}{2\pi^2} \left\{ \frac{2m_e}{\hbar} \right\}^{3/2} (E - E_g)^{1/2}. \tag{3.8}$$

Note that we have added a factor of two in the above equations to account for the

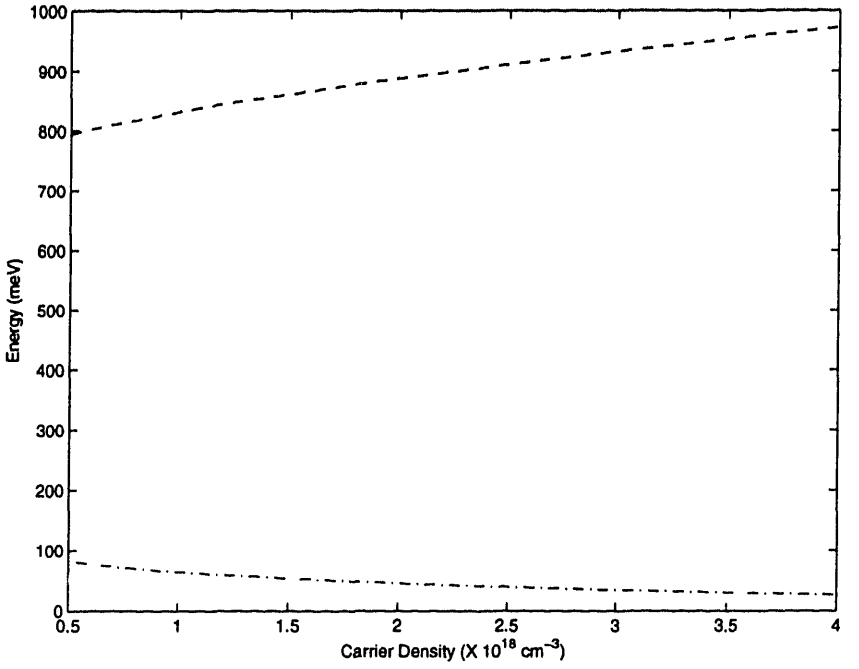

Figure 3-4: Quasi-Fermi energies as a function of the injected carrier density, N. The dashed line is the quasi-Fermi energy for electrons in the conduction band. The dot-dashed line is the quasi-Fermi energy for holes in the valence band.

fact that two electrons with opposite spin states may occupy the same energy state.

The total carrier density in the conduction band is then given by

$$N = \int \rho_c(E) f_c(E) dE. \tag{3.9}$$

Similarly, the density of holes in the valence band may be expressed as

$$P = \int \rho_v(E)(1 - f_v(E)) dE. \tag{3.10}$$

Since $f_v(E)$ and $f_c(E)$ are determined using the quasi-Fermi energies, E_{Fv} and E_{Fc}, we can numerically solve for the quasi-Fermi energies for a given injected carrier density, N. Figure 3-4 shows the relationship between the quasi-Fermi energies and the injected carrier density.

Carrier populations in a semiconductor interact with photons through the processes of radiative recombination, stimulated emission, and stimulated absorption.

Radiative recombination occurs when an electron in the conduction band recombines with a hole in the valence band, releasing energy in the form of a photon. When photons travelling through the device cause such recombinations, the process is referred to as stimulated emission. Alternatively, photons can excite an electron from the valence band into the conduction band through stimulated absorption.

The rates of these various processes are strongly dependent on the carrier population densities. However, for simplicity, we will start by considering these rates in a simple two level system. Consider the absorption transition diagrammed in Figure 3-5. Here, the absorption of a photon with energy $E = h\nu$ excites an electron with energy E_1 in the valence band into a conduction band energy state with energy $E_2 = E_1 + h\nu$. In order for this transition to occur, there must be an available electron with energy E_1 and an unoccupied state with energy E_2. For an incident spectral density of $P(E)$ we can quantify the rate of transitions from state E_1 to state E_2 due to absorption as:

$$r_{12} = B_{12}(E_2 - E_1)f_v(E_1)(1 - f_c(E_2))P(E_2 - E_1) \tag{3.11}$$

Here, B_{12} represents the transition probability, $f(E_1)$ is the probability that state E_1 is occupied, and $1 - f(E_2)$ is the probability that the state E_2 is unoccupied. Stimulated emission occurs through a similar process when a photon of energy $h\nu$ causes an electron with energy E_2 to recombine with a hole with energy E_1, releasing a second photon with energy $E = E_2 - E_1$. We can then write the rate of stimulated emission as

$$r_{21} = B_{21}(E_2 - E_1)(1 - f_v(E_1))f_c(E_2)P(E_2 - E_1) \tag{3.12}$$

By considering the rates of stimulated emission and absorption at equilibrium, we find[27]:

$$B_{12}(E) = B_{21}(E) = \frac{\pi q^2 \hbar}{m^2 \epsilon_0 n_g^2 E}|M|^2 \tag{3.13}$$

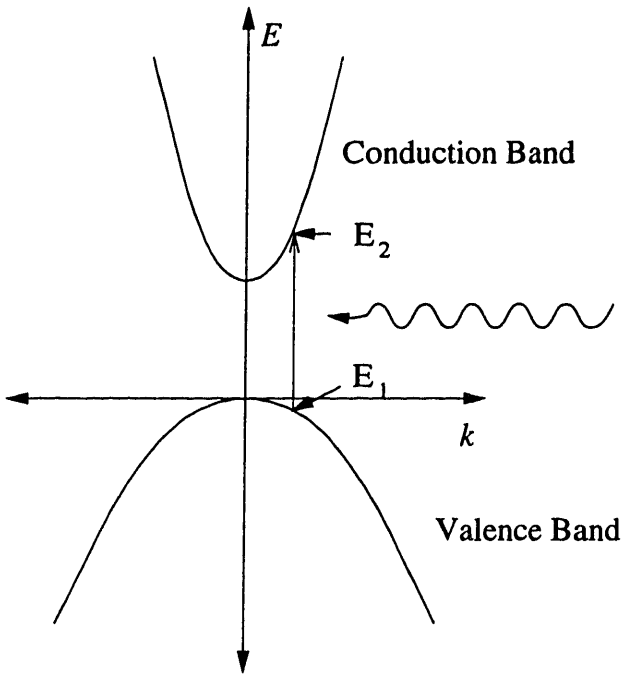

Figure 3-5: Schematic of absorption process for a photon with energy $h\nu$

where q is the charge of the electron, m is the mass of the electron, ϵ_0 is the permittivity of free space, n_g is the group index, and M is the matrix element of the momentum operator relating the upperstate wave-function to the lower state wave-function.

The net absorption rate is simply the difference between the rate of stimulated absorption and the rate of stimulated emission:

$$R_{12}(\text{net}) = r_{12} - r_{21} = B_{12}(f_v(E_1) - f_c(E_2))P(E_{12}) \tag{3.14}$$

Note that R_{12} is equivalent to the negative change in the incident spectral density at E_{12} over time, $-\partial P(E_{12})/\partial t$. Recall from Chapter 2 that we can write the linear absorption coefficient as:

$$\alpha = -\frac{\partial I/\partial z}{I}. \tag{3.15}$$

Here, I is the intensity of the incident light and we have neglected nonlinear losses. Now, since intensity is directly proportional to the spectral density, we can relate the

linear absorption coefficient to net absorption rate:

$$\alpha(E_{12}) = \frac{B_{12}(f_v(E_1) - f_c(E_2))}{v_g} \tag{3.16}$$

where $v_g = c/n_g$ is the group velocity.

The rate equations that we have discussed up to this point are only relevant for a simple two-level system. In a semiconductor, we must account for the density of states at a particular energy when calculating the rates of absorption and emission. For instance, the rate of absorption is proportional to the density of filled states in the valence band, $\rho_v(E_1)f_v(E_1)$, and the density of empty states in the conduction band, $\rho_c(E_2)(1 - f_c(E_2))$. Similar expressions may be written for the rate of stimulated emission. Additionally, in a semiconductor there are many possible transitions that are separated by a given energy E. So, to determine the absorption coefficient in a semiconductor, we must integrate over all possible energy transitions:

$$\alpha(E) = \frac{\pi q^2 \hbar}{m^2 \epsilon_0 c n_g} \int_{-\infty}^{\infty} |M|^2 \rho_v(E_1)\rho_c(E_1 + E)[f_v(E_1) - f_c(E_1 + E)]dE_1 \tag{3.17}$$

We can also define a gain coefficient $g(E) = -\alpha(E)$.

Figure 3-6 shows a sample gain curve a semiconductor. There are three regions of interest in this spectrum. In the gain regime, the gain coefficient is positive. Here, the rate of stimulated emission is greater than the rate of stimulated absorption and the incident light is amplified. This corresponds to the condition,

$$r_{21} > r_{12}. \tag{3.18}$$

Using equations 3.4, 3.5, 3.11, and 3.12, we find the equivalent relation:

$$E_{Fc} - E_{Fv} > E. \tag{3.19}$$

That is, in order for a signal to experience gain, the photon energy must be less

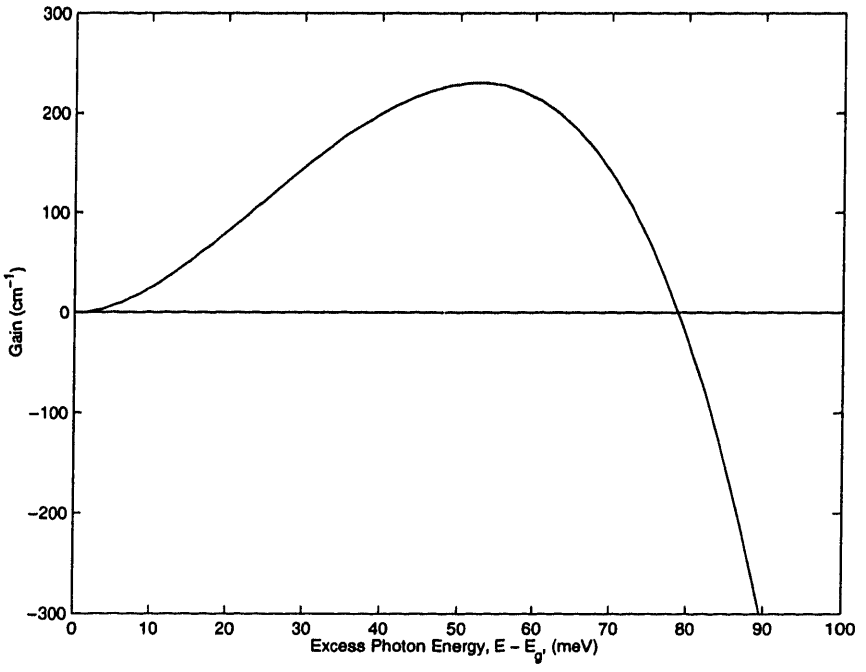

Figure 3-6: Gain coefficient, g, as a function of the excess photon energy, $E - E_g$.

than the difference of the quasi-Fermi energies. The photon energy that is equal to the difference in the quasi-Fermi energies is called the transparency point. Here, the rate of stimulated absorption is equal to the rate of stimulated emission and the gain coefficient is zero. For energies greater than the difference in the quasi-Fermi energies, the rate of absorption exceeds the rate of emission. This is referred to as the absorption regime. Incident light in this regime experiences losses due to stimulated absorption in the semiconductor.

3.3 Nonlinear Gain Mechanisms

There are a number of mechanisms which lead to nonlinear changes in the gain of a semiconductor. These mechanisms are discussed in detail in [30] and [31]. Here, we will give a brief review of the interband and intraband effects which lead to nonlinear gain changes.

Interband effects arise as a result of carrier population changes in the semiconductor. Figure 3-7 shows the gain spectrum for various carrier population densities, N.

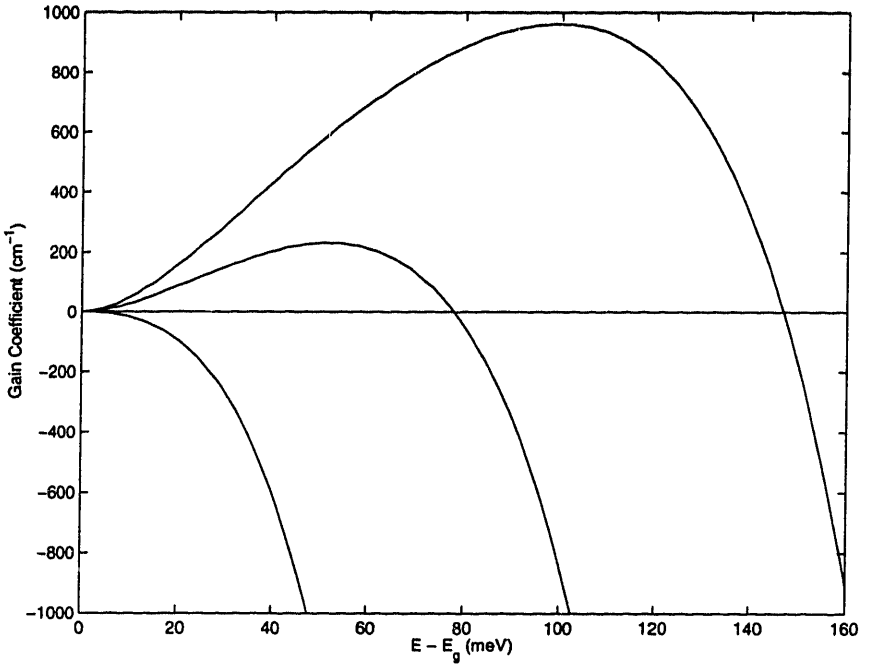

Figure 3-7: Gain coefficient as a function of excess photon energy for various carrier densities, N. The carrier densities are $N \times 10^{18}\text{cm}^{-3} = 0.7, 1.8$, and 3.0.

An incident photon energy in the gain regime or absorption regime of the semiconductor will lead to net changes in the carrier populations. These changes affect the gain spectrum of the semiconductor. For incident photons in the absorption regime, the gain is increased due to an increase in N from stimulated absorption. Similarly, in the gain regime, the gain is decreased. The recovery time for these changes depends on the carrier injection rate (from, say, a bias current in an SOA) and the carrier lifetime of the semiconductor. Typically, this recovery time is on the order of 100 ps to 1 ns [12].

Another nonlinear gain effect occurs due to the fact that certain photon energies only cause transitions in a narrow energy range of a semiconductor, rather than over the entire spectrum. This intraband effect distorts the Fermi distribution of the carriers and is known as spectral hole burning. As with the interband effects, spectral hole burning decreases the gain in the gain regime and increases the gain in the absorption regime. The duration of this effect is governed by the time required for carriers within the conduction band to redistribute via carrier-carrier scattering.

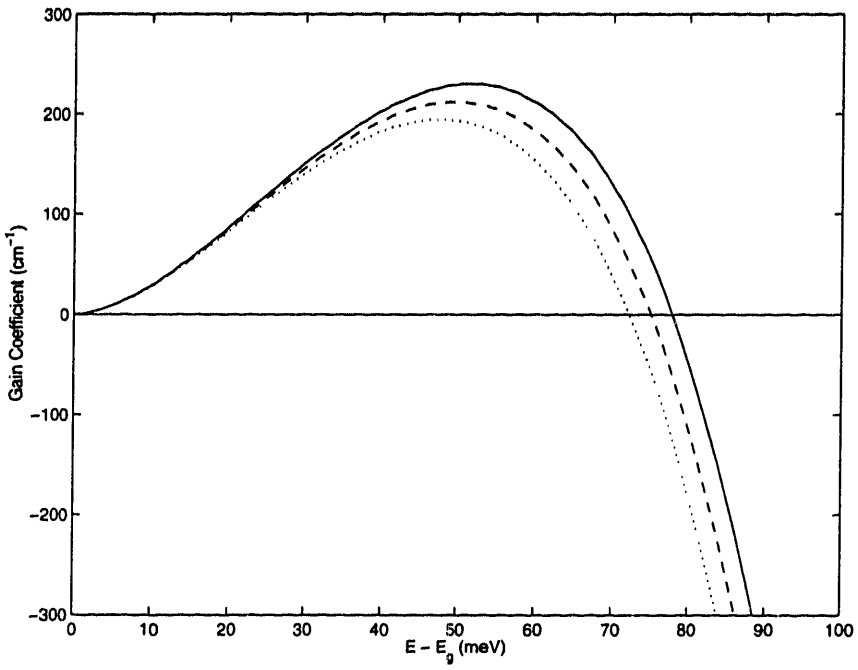

Figure 3-8: Gain coefficient as a function of excess photon energy for various carrier temperatures. Here, the carrier temperature for the valence band is fixed at 300 K. The gain coefficient is shown for conduction carrier temperatures of 300 K (solid), 310 K (dashed), 320 K (dotted).

Typically, this is on the order of 100 fs.

Carrier heating also affects the gain of the device. Mechanisms such as free-carrier absorption (FCA) can create highly energetic carriers. This excess energy increases the temperature of electrons in the conduction band and holes in the valence band. As seen in Figure 3-3, the increase in temperature smears out the Fermi distribution of the carriers. Figure 3-8 shows the gain spectrum for various carrier temperatures. We see that increases in carrier temperature lead to decreases in gain across the entire spectrum. These effects recover as the energetic carriers lose energy from carrier-carrier scattering and phonon emission [30]. Carrier heating effects recover on a time scale of about 600 fs [32].

3.4 Refractive Index

The refractive index of a semiconductor is closely related to the gain. This relationship is often presented in terms of the linewidth enhancement factor [33][34]:

$$\alpha = \frac{\Delta n_I}{\Delta n_R} \tag{3.20}$$

where n_R and n_I are the real and imaginary parts of the complex refractive index:

$$\tilde{n}(E) = n_R(E) + jn_I(E). \tag{3.21}$$

The real part of $\tilde{n}$, n_R, is the commonly used index of refraction, n. The imaginary part of $\tilde{n}$, n_I, describes the loss of the semiconductor. It may be related to the gain coefficient by

$$n_R(E) = \frac{g(E)c}{E} \tag{3.22}$$

The real and imaginary parts of $\tilde{n}$ are related by a Kramers-Kronig transformation [35]:

$$n_R = 1 + \frac{2}{\pi} P \int_0^\infty \frac{E' n_I(E')}{E'^2 - E^2} dE' \tag{3.23}$$

where P refers to the Cauchy principal value for the integral (which excludes the discontinuity at $E' = E$). Substituting equation 3.22, we find

$$n(E) = 1 - \frac{\hbar c}{\pi} P \int_0^\infty \frac{g(E')}{E'^2 - E^2} dE' \tag{3.24}$$

Thus, a small change in gain, Δg, leads to a change in index given by:

$$\Delta n(E) = -\frac{\hbar c}{\pi} P \int_0^\infty \frac{\Delta g(E')}{E'^2 - E^2} dE' \tag{3.25}$$

Therefore, the refractive index is affected by the same nonlinearities that affect the gain in semiconductors.

Figure 3-9 shows the change in the gain and refractive index for various population changes. Here, we see that an increase in the carrier population leads to an increase in gain for photon energies above the bandgap, as expected. Associated with this increase in gain is a decrease in the refractive index which peaks at an excess photon energy of around 150 meV. Note that the change in refractive index extends below the bandgap of the semiconductor. Similarly, we observe a decrease in gain associated with a reduction of the carrier population density. In this case, the refractive index increases across the entire spectrum shown.

Figure 3-10 illustrates the effect of carrier heating on the gain and refractive index of a semiconductor. Here, we see that an increase in the carrier temperature decreases the gain for the above band energies shown in the plot. Note, however, that the gain change is actually positive for higher energies as the increase in temperature extends the tail of the Fermi-distribution of carriers to higher energies. However, loss through the device for optical fields in this wavelength-range would be quite high. As a result, most experiments are conducted using optical pulses whose wavelengths are fairly close to the band edge. Associated with the decrease in gain is an increase in the refractive index for energies below and slightly above the band gap. The refractive index change peaks near 79 meV and changes sign around 190 meV.

K. L. Hall has done measurements of refractive index changes in InGaAsP diodes using a heterodyne pump-probe technique [36]. This technique uses a probe and reference pulse that differ in frequency. The beat frequency between these two pulses can be detected using a radio receiver. Pump-induced changes in the phase of the probe pulse can be measured using an FM receiver. These measurements reveal three contributions to the nonlinear index changes in a device biased in the gain regime. First, there is an instantaneous contribution that is attributed to a rapid electronic, or virtual process. The nonlinear refractive index for this process was measured as $n_2 = -3.2 \times 10^{-12}\text{cm}^2/\text{W}$ for a copolarized pump pulse. Long-lived index changes are related to the pump energy, rather than intensity. For instance,

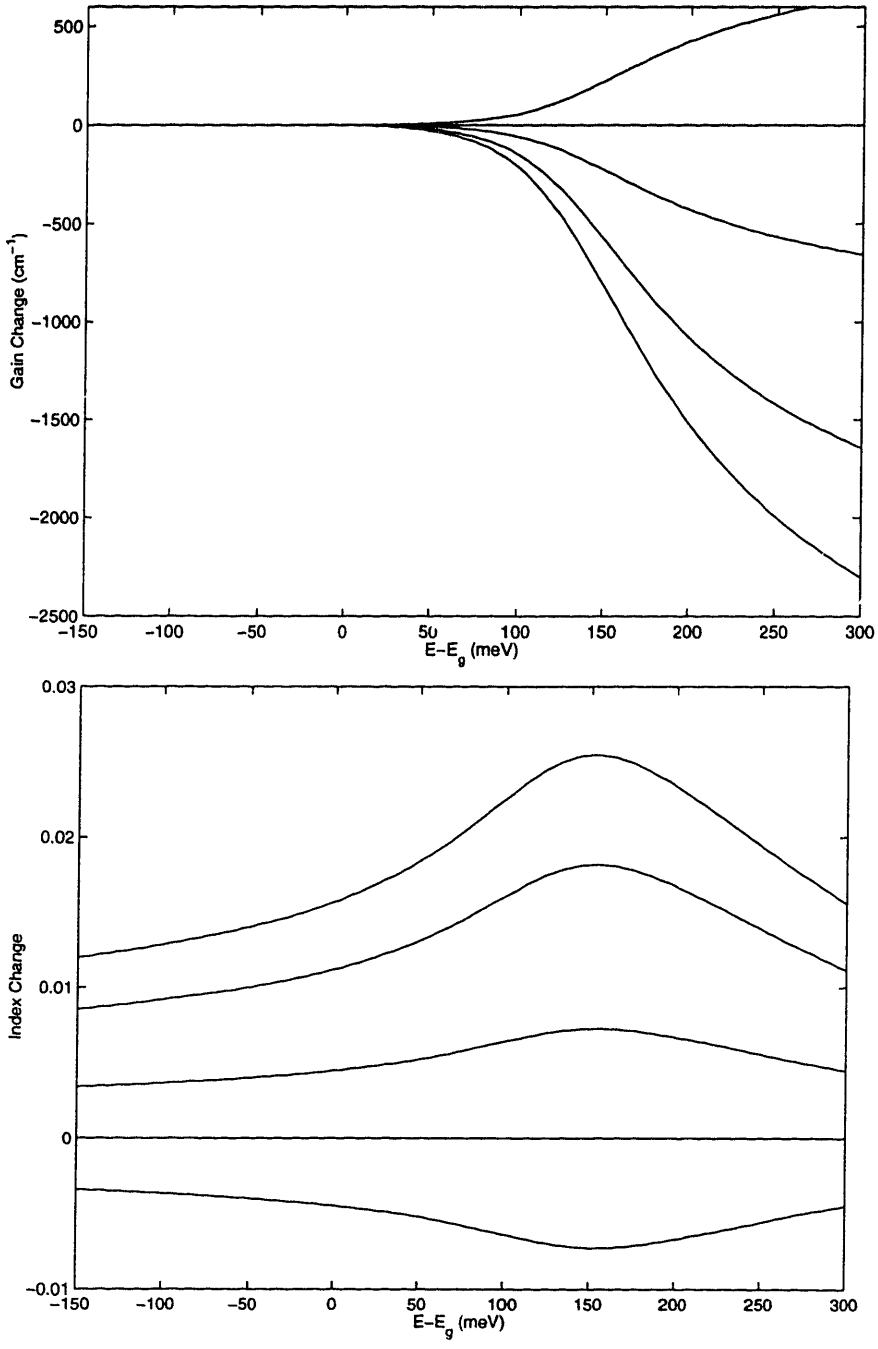

Figure 3-9: Changes in gain and refractive index due to carrier population density changes. These changes correspond to carrier population changes of $\Delta N(\times 10^{18}) = 0.02, 0, -0.02, -0.05, -0.07$ around $N = 1.8 \times 10^{18}\text{cm}^{-3}$.

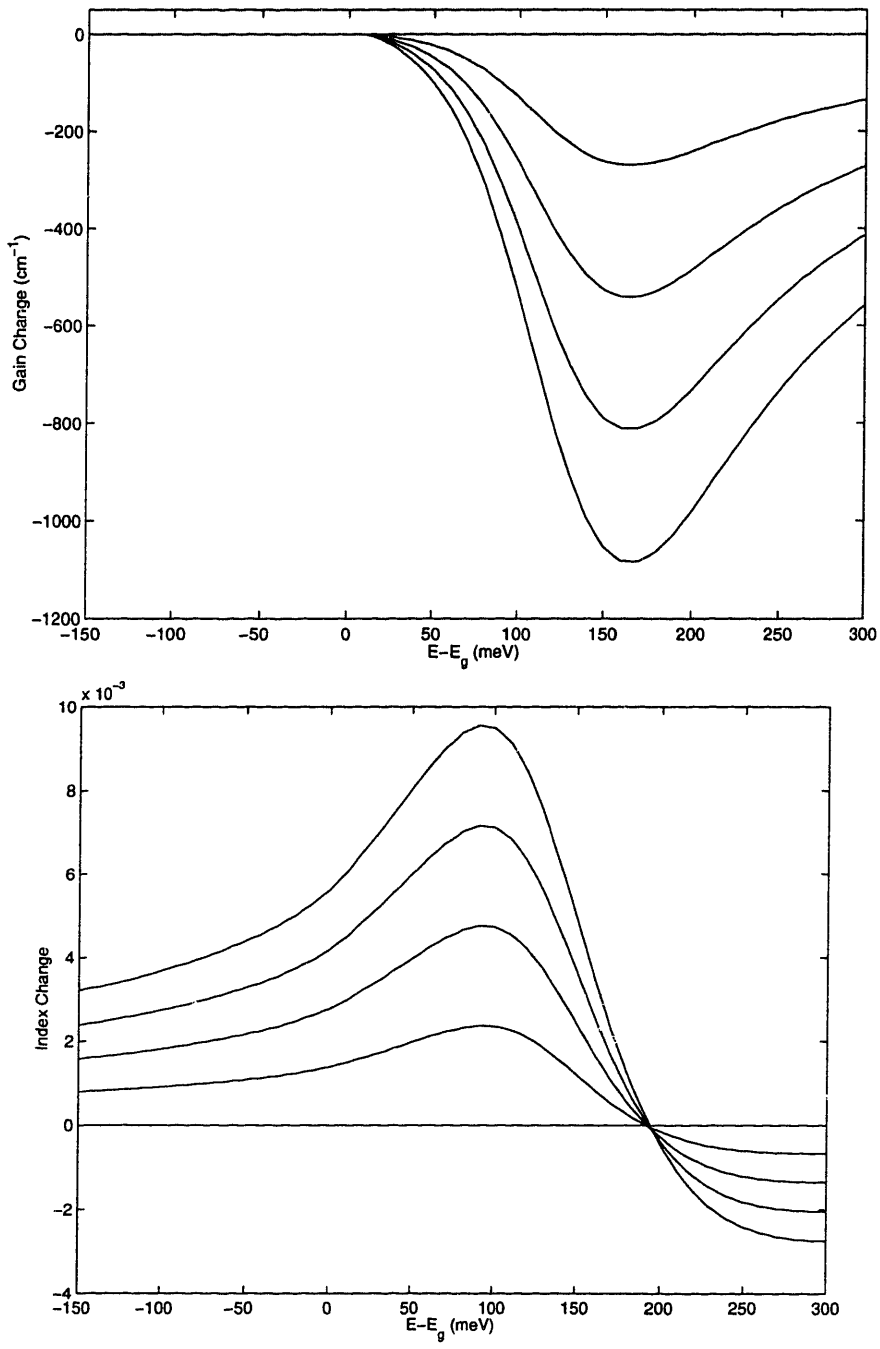

Figure 3-10: Changes in refractive index for various gain changes, $\Delta g(E)$, for carrier temperature changes of 0K, +10K, +20K, +40K around 300K.

there is an index change due carrier heating and two-photon absorption that recovers on a time scale of about 650 fs. This effect has an associated nonlinear index change of $\Delta n/E_p = 25\text{cm}^2/\text{J}$ for a copolarized pump pulse where E_p is the energy of the pump pulse. Finally, there is a long-lived index change owing to pump-induced changes in the carrier populations. These changes recover on a nanosecond time scale and are characterized by $\Delta n/E_p = 18\text{cm}^2/\text{J}$.

3.5 Dispersion

Dispersion in optical waveguides has been discussed in detail in [37]. There the group velocity dispersion is expressed in terms of four components:

$$\text{GVD}_{\text{total}} = \text{GVD}_{\text{mat}} + \text{GVD}_{\text{wg}} + \text{GVD}_{\text{cpd}} + \text{GVD}_{\text{r}} \tag{3.26}$$

The material term, GVD_{mat}, is a weighted average of the material dispersions of the waveguide core and cladding. The waveguide dispersion term, GVD_{wg}, contains contributions to the dispersion owing to the difference in refractive index between the core and the cladding. The composite profile dispersion term, GVD_{cpd}, relates to the index profile of the core and cladding regions of the semiconductor. The final term, GVD_{r}, is a remainder term composed of cross products that are not easily categorized in the above definitions.

Experimental measurements of the dispersion of InGaAsP semiconductor amplifiers have been done using a pulse-echo technique [1]. In this technique, an optical pulse stream is sent through an optical amplifier. The output of the amplifier is cross-correlated with the original pulse stream. Since the facets of the amplifier cause reflections, a train of echo pulses is produced when a single pulse is sent through the diode. The time between the echo pulses is the round trip time for the pulse in the amplifier. Hence, if the length of the amplifier is known, one can calculate the group velocity of the pulse. By measuring the group velocity at various wavelengths, the GVD may be measured. These measurements were made on a bulk amplfier and a

Diode	L	$-\lambda\frac{d^2n}{d\lambda^2}\|_{TE}$	$-\lambda\frac{d^2n}{d\lambda^2}\|_{TM}$
Bulk	475μm	-0.63 μm^{-1}	-0.95 μm^{-1}
MQW	900μm	-0.71 μm^{-1}	-0.74 μm^{-1}

Table 3.2: Group velocity dispersion measurements in InGaAsP semiconductor amplifiers as reported by [1].

quantum well device. Table 3.2 summarizes these results, for TE and TM polarized pulses.

These measured parameters were found to be in close agreement with the theoretically predicted dispersion. It is interesting to note that the dominant contributing factor to the dispersion was the material dispersion GVD_{mat}. The remainder term, GVD_r was negligible. The waveguide and composite profile terms, GVD_{wg} and GVD_{cpd} were comparable in size and opposite in sign, so their sum effect was negligible. The dominance of the material dispersion term indicates that the dispersion values measured in these devices should provide a good estimation of the dispersion encountered in other InGaAsP devices.

3.6 Discussion

Semiconductor waveguides are attractive for use in all-optical switching devices because of their potentially large nonlinear index of refraction. Typically, the value of n_2 in semiconductors is on the order of 10^{-12} cm^2/W. This is very large compared to other nonlinear materials that have been considered. As we have discussed in Chapter 1, a large n_2 reduces the interaction length and optical powers required to achieve a desired phase shift. By comparison, optical fibers typically have $n_2 \approx 10^{-16}$ cm^2/W. Typically, hundreds of meters of optical fiber are necessary to obtain the same phase shift that can be obtained in a semiconductor waveguide a few millimeters in length.

The small group velocity dispersion that is characteristic of semiconductors is also attractive for switching. This, together with the short device length, allows switching with very short pulses at high bit rates without concern for pulse distortion. The

long interaction lengths required in optical fiber, on the other hand, lead to pulse distortion for widths much smaller than $\sim$ 1ps.

Optical fibers have the advantage of a nonlinear response composed solely of an instantaneous, bound-electron effect, however. In semiconductors, the nonlinear response may be long-lived due to the carrier population dynamics discussed above. The balanced design of the UNI helps to reduce the effects of long-lived refractive index changes. However, as we saw in Chapter 2, at high data rates, long-lived gain changes cause pattern-dependent amplitude modulation of the output pulses. These effects are undesirable and limit the switching operation of the UNI.

There are a number of ways that these effects can be reduced. For instance, the carrier lifetime may be reduced using high bias currents. An $I^{-2/3}$ dependance of the carrier lifetime in semiconductors has been observed [38]. This effect is attributed to nonradiative recombination such as Auger recombination in the diode. Alternatively, the upper state lifetime may be reduced using an optical holding beam in the device [39]. However, the best recovery times that have been observed using these techiniques are on the order of 10 ps. This would limit switching rates to $<$ 100 Gbits/s.

Here, we consider ways to reduce the effects of long-lived carrier population density by reducing the carrier population changes induced by optical pulses in the UNI. To this end, we may employ passive semiconductor waveguides or semiconductor optical amplifiers biased at transparency as nonlinear materials in the UNI.

3.6.1 Passive Devices

In a passive semiconductor waveguide, the signal and control pulses are below the bandgap of the semiconductor. As a result, there are no changes in the carrier populations due to linear absorption or stimulated emission. Hence, the long-lived gain and refractive index changes due to carrier population density changes are reduced. Nonlinear index changes in these devices are generally attributed to the optical Stark effect [40] and to carrier heating arising from free carrier absorption and two-photon absorption. Since the signals are below band, however, they do not experience gain changes due to the carrier heating.

Third order nonlinearities in passive InGaAsP waveguides have been studied for wavelength conversion via four-wave mixing [41, 42, 14, 43, 44]. These experiments have demonstrated high conversion efficiencies indicating the presence of a large third-order nonlinear susceptibility, $|\chi^{(3)}|$. Taking into account the nonlinear loss coefficient, these measurements indicate a nonlinear refractive index on the order of $10^{-14}\text{cm}^2/\text{W}$ for below-band signals.

Rauschenbach and LePage have demonstrated the potential use of passive waveguides for all-optical switching [45]. They demonstrated a 0.8π phase shift in a SAI using near bandgap nonlinearities in a passive AlGaAs waveguide. Their experiments reveal a switching window of about 1.4 ps in the passive waveguide. This is consistent with the recovery time expected for nonlinearities due to carrier heating.

It should be noted that two-photon absorption can have detrimental effects in passive waveguides. Because the nonlinearity in these devices is fairly small, high optical intensities are required for optical switching. At high intensities, TPA can cause significant losses and limit the nonlinear interaction length. This limits the conversion efficiency in FWM experiments [43]. Two-photon absorption limits switching performance by increasing the carrier population density. These carriers recombine due to spontaneous emission on a time scale of $\sim$ 1ns. Hence, TPA can cause long-lived index changes which limit the data rate in optical switches. This spontaneous emission time in passive semiconductor waveguides may be reduced by introducing defects in the active region through proton bombardment [44].

3.6.2 Transparency Point

Alternatively, one can reduce the carrier population density changes by using a semiconductor optical waveguide biased at the transparency point. Recall from section 3.2 that the gain in a semiconductor is dependent on the energy of the incident photons. When the photon energy is equal to the difference in the quasi-Fermi energies for the conduction and valence bands, there is no net stimulated emission or absorption. This is referred to as the transparency point. In Figure 3-4, we saw that the quasi-Fermi energies of electrons and holes vary with the injected carrier population.

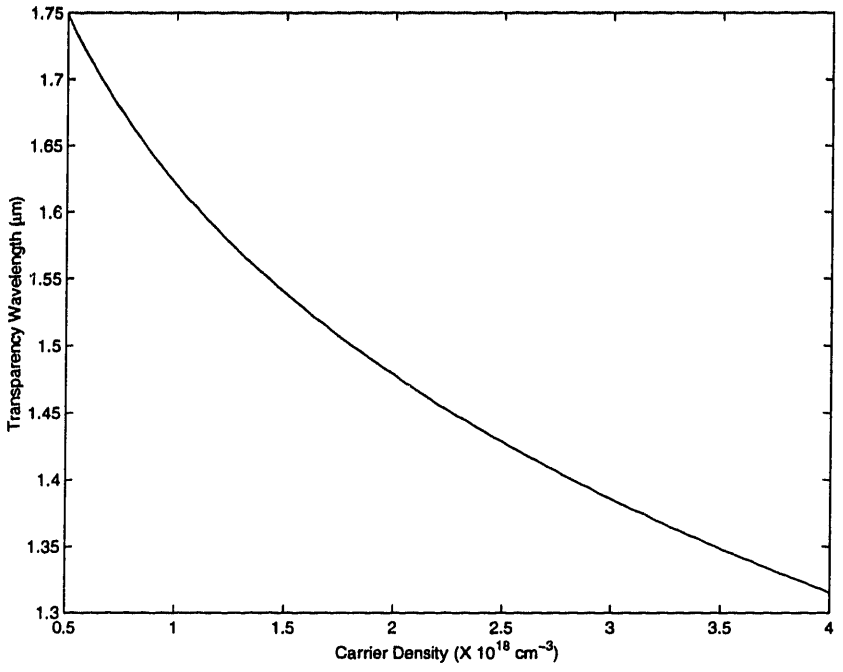

Figure 3-11: Transparency wavelength as a function of the injected carrier population density.

The separation in the quasi-Fermi energies determines the wavelength of photons at the transparency point. Figure 3-11 shows the relationship between the injected carrier population density and the transparency wavelength. Since the injected carrier population density is determined by the current through the diode, we can vary the transparency wavelength by changing the bias on the diode.

When the SOA is biased for transparency at a particular wavelength, pulses at that wavelength travelling through the device cause no net changes in the carrier population density. K. L. Hall has verified that the nonlinear index and gain changes occuring at the transparency point are solely due to ultrafast effects such as carrier heating and two-photon absorption [12]. These effects are fully recovered after a few picoseconds. In an all-optical switch, one might consider placing the control pulses at the transparency wavelength to ensure that the nonlinear effects of these pulses have recovered within one bit period.

Measurements of InGaAsP diodes biased at the transparency point indicate the presence of a large nonlinear refractive index. K. L. Hall has measured an instanta-

neous nonlinear refractive index of $n_2 = -1.5 \times 10^{-12}\text{cm}^2/\text{W}$ for copolarized pump and probe pulses using heterodyne pump-probe technique [12]. Observing self-phase modulation in the frequency domain have also been used to measure the nonlinear refractive index at the transparency point [46, 47].

Semiconductors biased at the transparency point have recently demonstrated potential for all-optical switching applications. All-optical switching using an MQW SOA biased at transparency has been reported in a terahertz optical asymmetric demultiplexer (TOAD) [13]. They demonstrate a 2 ps switching window when the amplifier is biased at the transparency current, indicating that the long-lived refractive index changes due to changes in the carrier population density are negligible.

Thus, we see that semiconductors may be useful as nonlinear materials in all-optical switches. Their low dispersion reduces pulse broadening and walkoff. The high nonlinear refractive index of semiconductors allows switching at low powers with compact waveguides. While the long-lived refractive index changes that accompany carrier population density changes can inhibit switching, these effects can be reduced by using passive waveguides or biasing a semiconductor at the transparency point.

Chapter 4

Device Characterization

As discussed in Chapter 2, there are several characteristics of a nonlinear material which determine its suitability for use in the ultrafast nonlinear interferometer (UNI). Since signal pulses in the UNI are divided into two orthogonally-polarized pulses for propagation through the nonlinear material, birefringence in the material is detrimental to device operation. Large nonlinearities allow for switching with low control pulse powers. Additionally, although the effects of long-lived nonlinear responses are reduced by the single-arm interferometer design of the UNI, a fast nonlinear response is desired to minimize the effects of long-lived gain changes. Materials with small dispersion are needed to reduce distortion of short pulses travelling through the UNI, allowing for cascadability.

In this chapter we discuss techniques for analyzing each of these properties in semiconductor waveguides. We begin with a description of the apparatus used for measuring the transparency current in a semiconductor optical amplifier (SOA). This is used to ensure that the SOA's used in subsequent tests are biased at transparency. Next we present a spectral-interferometric technique that is currently being employed for optical characterization of materials [48]. We describe how spectral interferometry (SI) may be used to measure nonlinear phase changes, dispersion and modal dispersion in semiconductor waveguides. We present the results of SI measurements of a nonlinear phase shift in semiconductor waveguides biased at transparency.

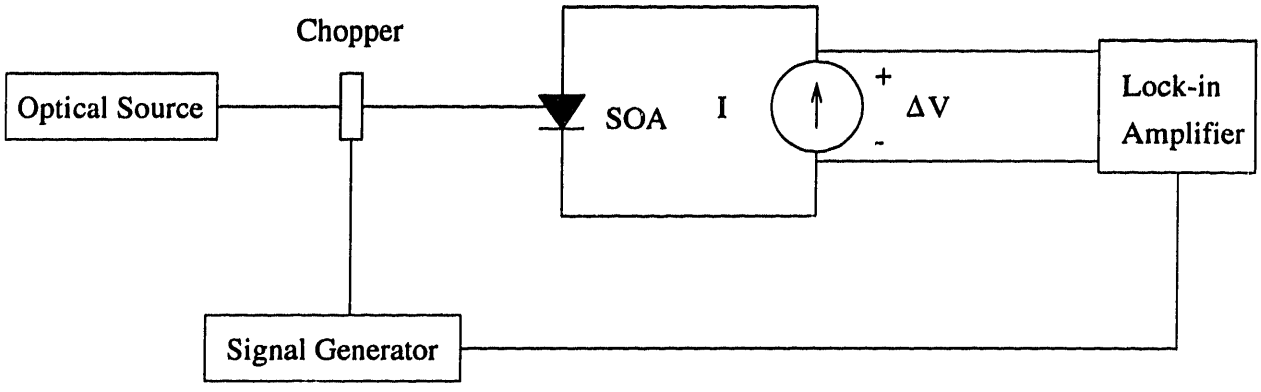

Figure 4-1: Experimental apparatus for measuring transparency current in a semicondcutor laser amplifier.

4.1 Measurement of Transparency Current

To measure the transparency current for a particular signal wavelength in an SOA, we measure the voltage across the diode when the signal is incident on the device [49]. If the signal is in the absorption regime, it generates carriers due to net stimulated absorption as it propagates through the device. If the signal is in the gain regime, it causes a decrease in the carrier population density due to net stimulated emission. These changes in the carrier population densities can be measured by observing the voltage across the diode in response to the incident optical signal. Figure 4-1 shows the experimental apparatus for measuring the transparency current in a SOA. The SOA is biased with a current, I. Light from the optical source is chopped at a frequency, f. Differential voltage changes across the semiconductor at the frequency f are measured by a lock-in amplifier. The bias current may then be adjusted to minimize the detected voltage on the lock-in amplifier. When the differential voltage measured by the lock-in is 0, there are no net carrier population changes due to stimulated emission or absorption and the semiconductor is biased at transparency.

Recently, an intensity dependence of the transparency current has been observed [50]. These variations are attributed to nonlinear absorption processes in the diode. In a switching experiment, we bias the SOA so that the control pulses are at the transparency point (see Chapters 2 and 5 for more information on switching). The intensity of these pulses is varied until a π phase shift is observed in the signal pulses.

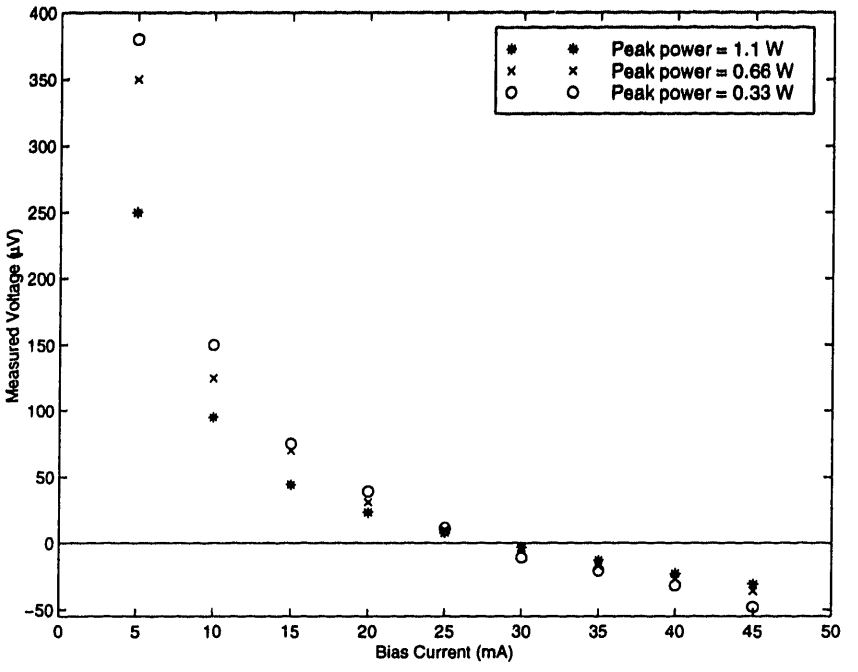

Figure 4-2: Measured differential voltage due to stimulated absorption and emission in a semiconductor optical amplifier as a function of the bias current in the amplifier.

An intensity dependence in the transparency current would therefore have detrimental effects on our switching experiments, as the transparency current would change as the control pulse intensity is varied. To quantify these effects, we have measured the transparency point at intensities which are typical in our switching experiments. The semiconductor optical amplifier used was a commercially available bulk semiconductor fiber-coupled device. Figure 4-2 shows the induced voltage change across the diode as a function of the bias current for control pulses with peak intensities of 1.1 W, 0.66 W, and 0.33 W. Here, the pulses are generated by a gain-switched distributed-feedback laser used as the control source in a switching experiment. We see that the transparency current is nearly identical for all three pulse intensities. Thus, we can assume that the variation in the transparency current as we vary the intensity of the control pulses in our experiments is negligible.

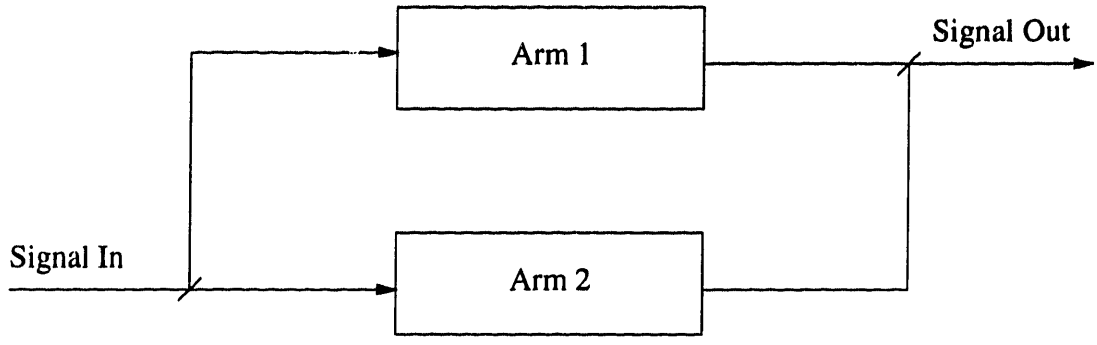

Figure 4-3: Generic Mach-Zehnder Interferometer.

4.2 Spectral Interferometry

Interferometry is an important technique used for studying optical systems. For example, in Chapter 2 we discussed the application of a nonlinear Mach-Zehnder interferometer in an all-optical switch. Figure 4-3 shows a Mach-Zehnder interferometer. Light entering the interferometer on the left is split between the two arms. After propagating through the two arms, the light is recombined, or interfered, at the output. Propagation differences between the two arms may be observed in the interference pattern at the output. If the effective path length differences between the two arms of the interferometer are less than the coherence length of the optical source, interference fringes may be observed in the space-time domain. When the path difference is much greater than the coherence length of the source, these fringes are not observable. However, fringes can be seen in the frequency domain [51, 52]. The interference between two temporally delayed optical fields in the frequency domain is analogous to the beating between two different frequencies in the time domain. This spectral interference may be observed for effective path length differences much longer than the coherence length of the source.

In recent years, spectral interferometry (SI) has attracted much interest. It offers a relatively simple technique for observing a variety of propagation phenomena over a wide range of wavelengths. SI has recently been used for measurements of length and refractive index [53, 54], dispersion [55, 56], birefringence [26], and nonlinearities [57] in optical waveguides. SI has also been used for time-resolved pump-probe

observations of material parameters [58].

In this section, we will discuss the application of spectral interferometry to the study of materials for all-optical switches. First, we describe the short-pulse laser source used in these experiments. Then, we present methods for measuring the nonlinear refractive index, dispersion, and birefringence in semiconductor waveguides using SI techniques. We also present measurements of the nonlinear refractive index in a semiconductor optical amplifier biased at transparency.

4.3 Pulse Source

Spectral interferometry can be used for directly measuring effects such as dispersion over many wavelengths simultaneously. Performing these measurements requires an optical source with broad bandwidth. In the past, many studies have been done using white light sources (for example, [52, 53, 54, 55, 56]). White light sources are attractive because they are relatively inexpensive. However, the advent of additive pulse mode-locked fiber lasers has made short-pulse lasers more available. These lasers have a very large spectral bandwidth. They also have high peak powers, making them useful for studies of nonlinearities.

The laser source for the spectral interferometry experiments performed in this thesis is a stretched-pulse additive-pulse mode-locked erbium-doped fiber laser [59, 60]. This laser is shown in Figure 4-4. The erbium-doped fiber in the ring provides gain for wavelengths around 1.55 μm. The erbium is excited using a MOPA pump laser at 980 nm. This laser provides around 700 mW of coupled power to the laser cavity. The polarization sensitive isolator in the airgap provides unidirectional operation and works with the birefringent plate to provide a band-pass filter for the cavity. The stretched-pulse laser is passively mode-locked. The half-wave plate and quarter-wave plate on the exit end of the open air gap create an elliptical polarization state for pulses entering the fiber. The elliptical polarization is rotated due to third-order nonlinearities in the fiber. The lowest loss in the cavity is obtained when the ellipse is rotated so that the major axis is aligned with the polarizer in the open air gap. Since

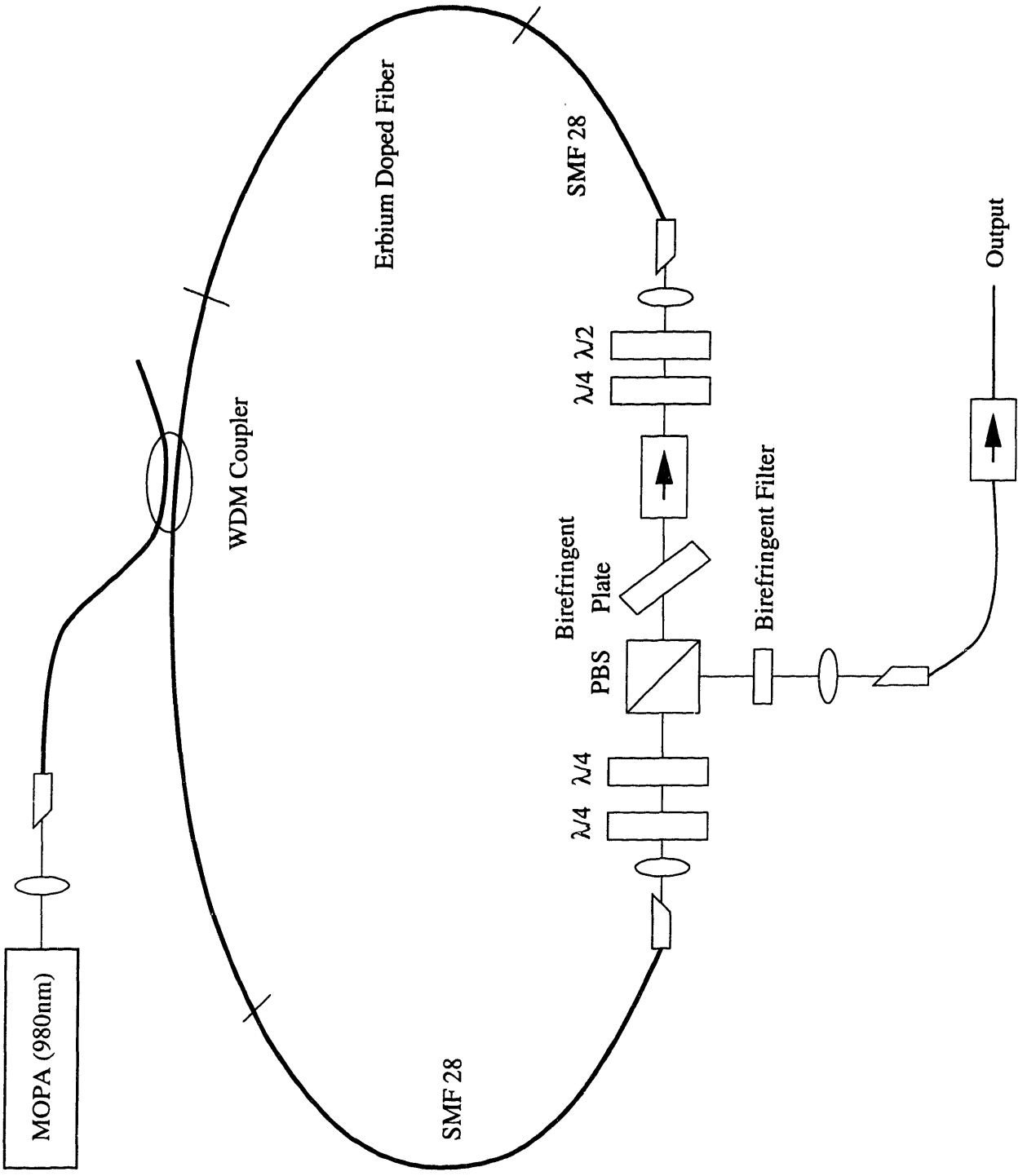

Figure 4-4: Stretched-pulse laser used in spectral interferometry experiments.

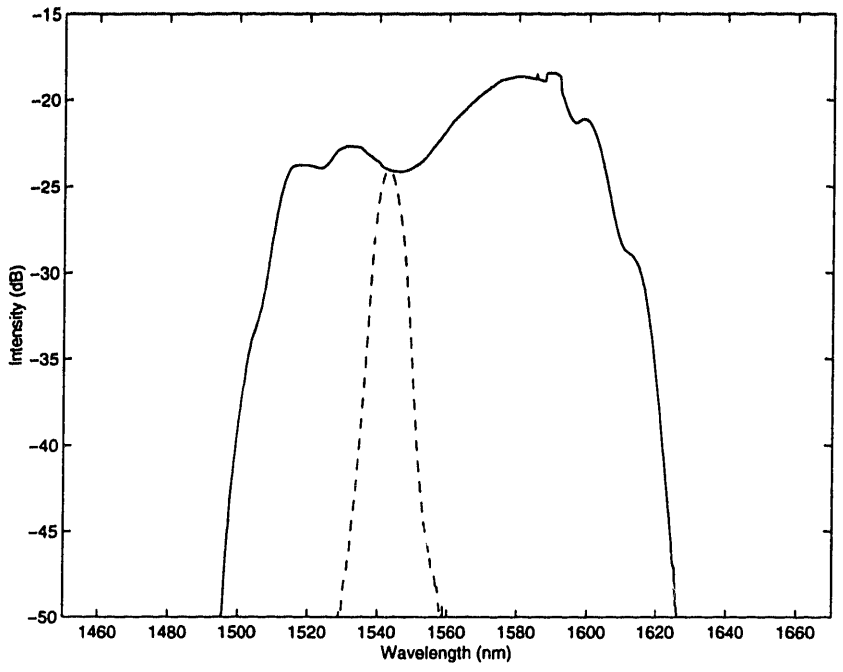

Figure 4-5: Spectrum from output port of stretched pulse laser. The solid line is the unfiltered output spectrum. The dashed line is the output spectrum when a 4.93 nm filter is used.

the polarization rotation is intensity dependent, the waveplates may be adjusted to provide pulsed operation, where the highest intensities occur. In single-pulse operation, the pulse repetition rate is about 38 MHz.

The rejection port of the polarizing beam splitting cube in the air gap is used as an output port. Typically, the average powers from this port is around 40 mW. Pulses exiting from this port have a very broad bandwidth as seen in Figure 4-5 (solid line). When coupled into an optical fiber, the high intensity and large bandwidth of these pulses lead to severe pulse distortion due to the nonlinear and dispersive characteristics of the fiber. To reduce these problems, we use a birefringent filter at the output of the laser. Additionally, dispersion shifted fiber is used when transmission over long distances is required. Figure 4-5 (dashed line) shows an example of the filtered spectrum when a 4.93 nm filter is used. Rotating the filter provides wavelength tunability.

Because of the long lengths of dispersive fiber in the cavity, pulses at the output of the stretched-pulse laser are not typically transform-limited. Figure 4-6 shows an

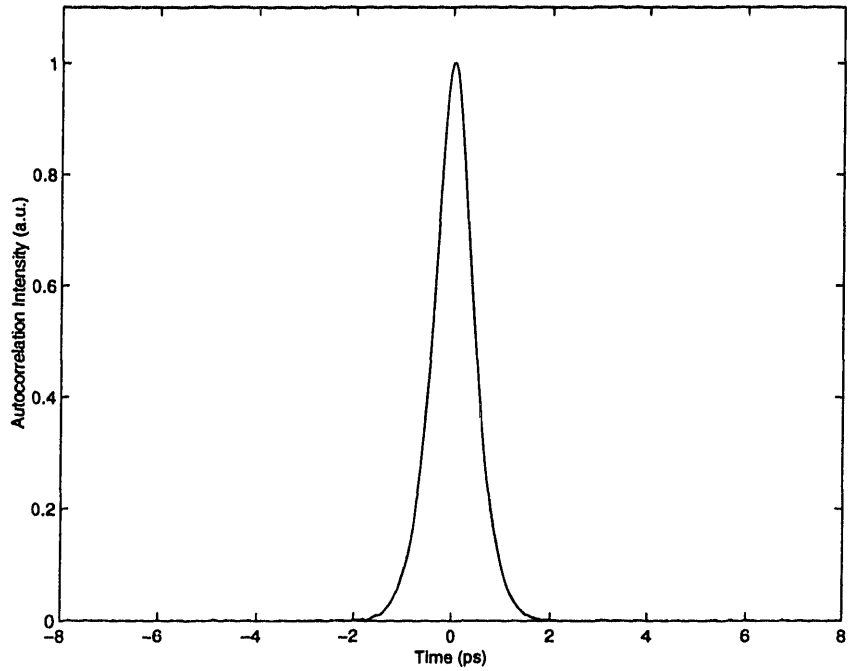

Figure 4-6: Autocorrelation of a 640 fs pulse from the stretched-pulse laser with a 4.93 nm filter at the output.

autocorrelation of a pulse when a 4.93 nm filter is used at the output. Assuming a Gaussian pulse shape, the FWHM of this pulse is 640 fs. Pulse widths in the cavity vary greatly due to the dispersion of the different fiber types [61]. Further pulse compression at the output may be accomplished using dispersion compensating fiber at the output. Pulses as short as 77 fs have been observed from stretched-pulse lasers [62]. However, since the experiments discussed here do not require extremely short pulses or high intensities we do not attempt to compensate for the linear chirp in the pulses.

4.4 Nonlinear Refractive Index

Spectral interferometry may be used to directly measure the nonlinear phase shift associated with an instantaneous nonlinear refractive index, n_2. One method for performing this measurement is diagrammed in Figure 4-7. Observations are made of the spectral interference between two temporally separated optical pulses, a pump pulse and a reference pulse, before and after propagation through a nonlinear material.

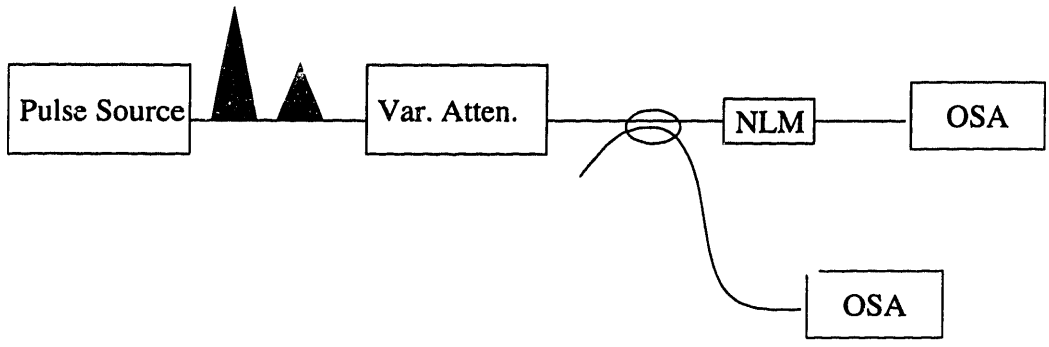

Figure 4-7: Method for measuring the nonlinear refractive index of a material using spectral interferometry.

In the frequency domain, the interference of the two pulses causes a modulation on the pulse spectrum. The reference pulse is low intensity and experiences little phase shift in the nonlinear material. The pump pulse is high intensity and accrues a nonlinear phase shift due to self-phase modulation as it travels through the nonlinear material. As we shall show, this phase shift causes a corresponding phase shift in the modulation of the spectrum of the two pulses. This phase shift may be directly measured by varying the pulse intensities in the nonlinear material. This information may be used to determine the magnitude of the instantaneous nonlinear refractive index in the nonlinear material. This method has recently been used to observe phase shifts due to third-order nonlinearities in optical fiber [57]. Here, we demonstrate its use in characterizing semiconductors.

To better understand how this measurement works let us consider the two pulses before and after propagating through the nonlinear material. Before the nonlinear material, we assume that the reference pulse is identical to the pump pulse and scaled by a factor $\alpha < 1$. The total electric field may be written as:

$$E(t, z = 0) = E(t)e^{j\omega_0 t} + \alpha E(t - T)e^{j\omega_0(t-T)} \tag{4.1}$$

where $E(t)$ is the slowly varying pulse envelope, ω_0 is the center frequency of the pulses, and T is the temporal separation between the two pulses. In the frequency

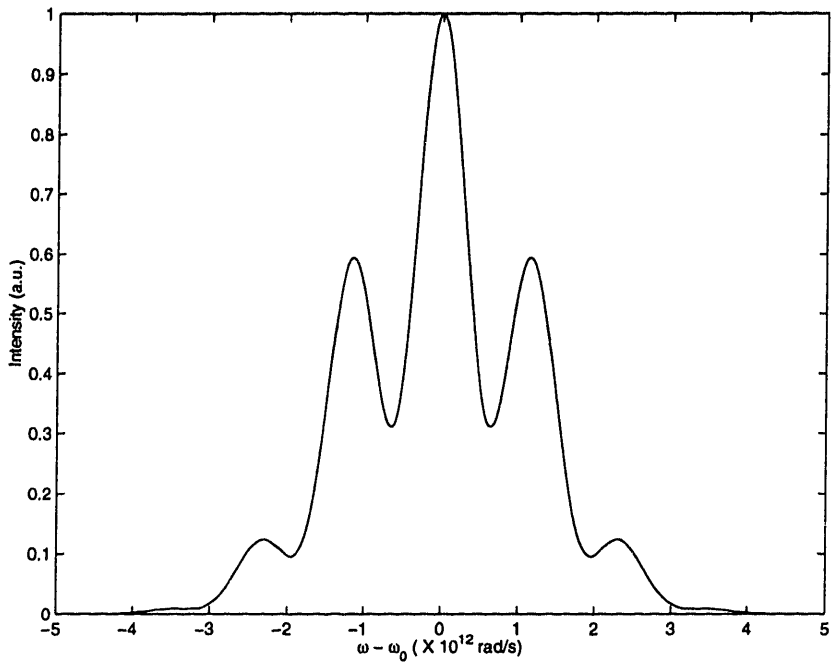

Figure 4-8: Frequency domain interference for two Gaussian pulses. The FWHM for these pulses is 1 ps. The temporal spacing between the pulses is $T = 5$ ps. The scaling factor is $\alpha = 0.25$.

domain,

$$E(\omega, z = 0) = E(\omega - \omega_0)(1 + \alpha e^{-j\omega T}) \tag{4.2}$$

where $E(\omega)$ is the Fourier transform of the pulse envelope, $E(t)$. The detected intensity is then,

$$I(\omega, z = 0) = |E(\omega - \omega_0)|^2[1 + \alpha^2 + 2\alpha\cos(\omega T)]. \tag{4.3}$$

Thus, the observed spectrum of the two pulses has the same shape as the single pulse spectrum, $|E(\omega - \omega_0)|^2$ only there is a cosine modulation on top of the spectrum. The frequency of the modulation in the frequency domain is related to the temporal separation of the two pulses, $\Omega = 2\pi/T$. The depth of the modulation is determined by the scaling factor, α. An example of the calculated interference of two Gaussian pulses in the frequency domain is shown in Figure 4-8.

After travelling through the nonlinear material, the pulses acquire an intensity dependent phase shift. For simplicity, here we assume that the reference pulse has no nonlinear phase shift. So, in the time frequency, we have:

$$E(t', z = L) = [E(\omega - \omega_0) * \Phi_{\rm nl}(\omega, L) + \alpha E(\omega - \omega_0)e^{-j\omega T}]e^{-j\beta(\omega)L}. \tag{4.4}$$

Here, $\beta(\omega)$ is the propagation constant and $\Phi_{\rm nl}(\omega)$ is the Fourier transform of the time dependent nonlinear phase shift in the pump pulse, $e^{-j\phi(t)}$. We have assumed that the nonlinear and dispersive effects of the waveguide may be treated separately. This is only true when the group velocity dispersion and higher order dispersion terms are small.

To gain a better intuition for the effects of the nonlinear phase shift on the output spectrum, let us first consider the effect of a uniform phase shift, ϕ_{nl} in the reference pulse. In this case, the frequency dependent phase shift is a delta function:

$$\Phi_{\rm nl}(\omega) = e^{-j\phi_{\rm nl}}\delta(\omega). \tag{4.5}$$

Then,

$$E(\omega, z = L) = E(\omega - \omega_0)[e^{-j\phi_{\rm nl}} + \alpha e^{-j\omega T}]e^{-j\beta(\omega)L} \tag{4.6}$$

The observed spectral intensity is then:

$$I(\omega, z = L) = |E(\omega - \omega_0)|^2[2 + 2\alpha\cos(\omega T - \phi_{\rm nl})]. \tag{4.7}$$

Thus, we see that there is a corresponding phase shift of $\phi_{\rm nl}$ in the modulation of the observed pulse spectrum. Figure 4-9 show the interference between the two Gaussian pulses considered in Figure 4-8 when the pump pulse has acquired a uniform phase shift of π.

As was discussed in Chapter 2, the nonlinear phase shift due to an instantaneous

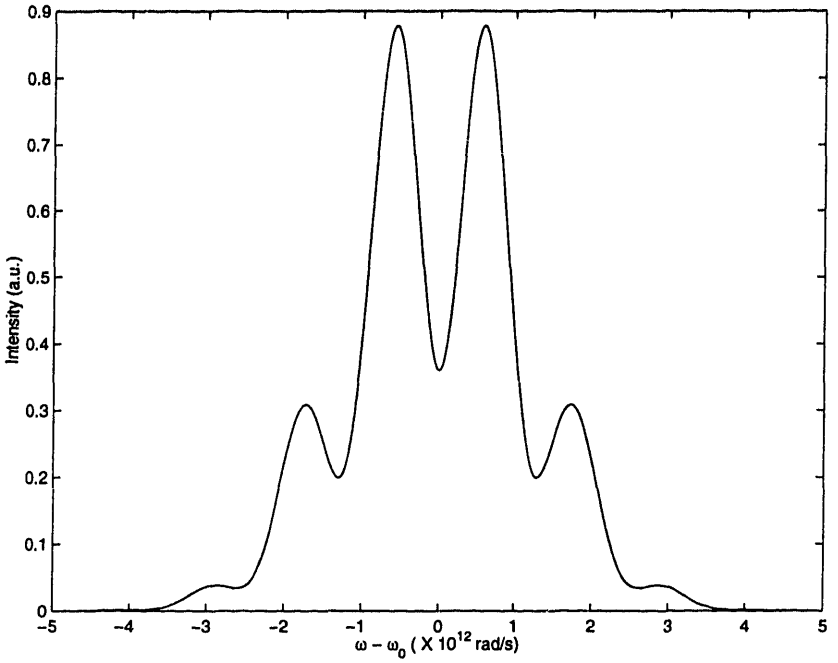

Figure 4-9: Frequency domain interference for two Gaussian pulses. The FWHM for these pulses is 1 ps. The temporal spacing between the pulses is $T = 5$ ps. The scaling factor is $\alpha = 0.25$. The pump pulse has acquired a uniform phase shift of π relative to the reference pulse.

nonlinear refractive index, n_2, is given by:

$$\phi_{\mathrm{nl}} = \frac{2\pi}{\lambda} n_2 I L \tag{4.8}$$

where λ is the signal wavelength, I is the intensity, and L is the effective length of the device, accounting for linear loss. By measuring the phase shift at two different intensities, we can solve for the nonlinear refractive index:

$$n_2 = \frac{\lambda(\Delta\phi_{\mathrm{nl}})}{2\pi(\Delta I)L} \tag{4.9}$$

where $\Delta\phi_{\mathrm{nl}}$ is the differential phase shift measured for a corresponding change in intensity, ΔI.

Figure 4-10 shows the setup used to generate the two temporally separated pulses needed for the nonlinear refractive index measurements. A pulse from the stretched-pulse laser enters from the left. After traveling through a single-polarization fiber

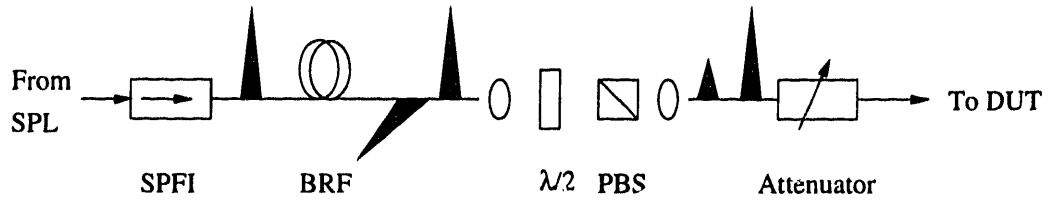

Figure 4-10: Setup for creating two temporally separated pulses used in spectral interferometry experiments.

isolator, the pulse is linearly polarized. The birefringent fiber (BRF) at the output of the polarizer is spliced at 45 degrees to the polarization axis of 18 m of BRF. This fiber is dispersion shifted to reduce pulse distortion. The group velocity difference between the two axes of the BRF leads to a pulse separation of about 1.40 ps/m. Hence, at the output of the BRF, there will be two equal-intensity, orthogonally-polarized pulses separated by 25 ps. These two pulses are then coupled into free space. A half-wave plate allows rotation of the two polarizations before passing through a polarizer. After passing through the polarizer, both pulses are linearly polarized in the same direction. The relative heights of the two pulses may be modified by adjusting the half-wave plate in the air gap. Finally, the two pulses are coupled back into fiber where they pass through a variable attenuator before going to the device-under-test (DUT).

Figure 4-11 shows the spectral interference and autocorrelation of the two pulses from the pulse source. From the autocorrelation, we immediately see that the pulses are separated by $T = 23$ ps. The height of the autocorrelation pulses may be related to α in the following manner:

$$\alpha = \sqrt{\frac{D(0) - \sqrt{D^2(0) - 4D^2(\tau)}}{2D(\tau)}} \tag{4.10}$$

where $D(t)$ is the autocorrelation function and τ is the time between the two pulses. Hence, we find for this measurement, $\alpha = 0.08$. This is clearly small enough that we can ignore the nonlinear phase shift in the reference pulse for small phase shifts in the pump pulse. Note that the measurements of T and α are confirmed by measurement

of the depth and period of the interference in the spectral domain.

The phase shift in the spectral modulation was measured as the intensity of the pump and reference pulses was increased. The results of these measurements are shown in Figure 4-12. Taking into account the pulse width and repetition rate shown above, we find that these measurements correspond to a nonlinear refractive index $|n_2| \approx 4 \times 10^{-12}\text{cm}^2/\text{W}$. This value is consistent with previously reported measurements of n_2 in semiconductors [12, 46].

4.4.1 Other Effects

The analysis above made a number of assumptions which may affect its accuracy. First, we assumed that the phase shift in the pump pulse was uniform over the entire pulse. In general, this is not the case as the phase shift is intensity dependent and the pulse intensity is not uniform across the pulse width. Thus, the phase shift in the pump pulse is actually time dependent. This leads to modifications of the pulse spectrum due to self-phase modulation. These modifications must be considered when measuring the interference of the two pulses in the frequency domain.

Let us consider the effect of self-phase modulation on a Gaussian pulse. Before propagation through the device, the pulse envelope is:

$$E(t) \propto \exp(-\frac{t^2}{2T_0^2}). \tag{4.11}$$

The time-dependent nonlinear phase shift is proportional to the intensity of the pulse,

$$\phi_{\text{nl}}(t) \propto \exp(-\frac{t^2}{T_0^2}) \tag{4.12}$$

This leads to a nonlinear frequency shift across the pulse:

$$\omega_{\text{nl}}(t) \propto -\frac{d\phi_{\text{nl}}}{dt} \propto t\exp(-\frac{t^2}{T_0^2}) \tag{4.13}$$

For large phase shifts, the differential phase shift across the pulse leads to spectral broadening. The pulse spectrum for various values of the peak phase shift is shown

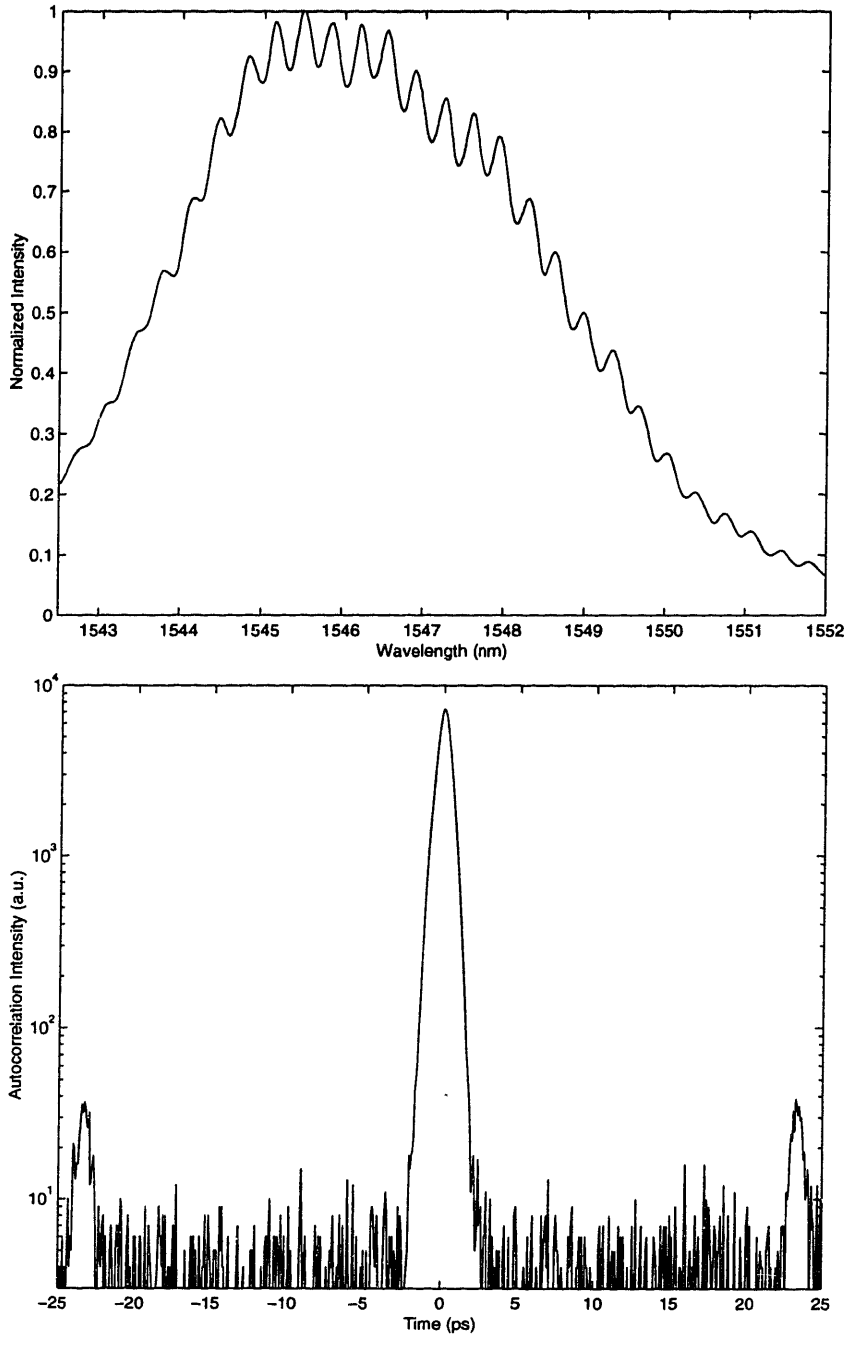

Figure 4-11: Spectral interference and autocorrelation of two pulses used in experiment.

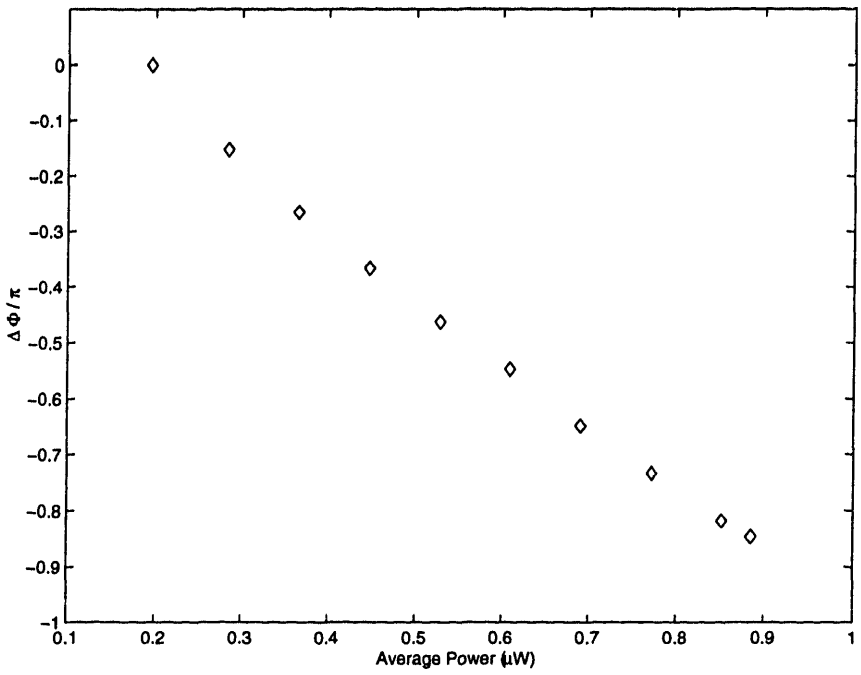

Figure 4-12: Measurements of phase shift in frequency domain versus average power from pulse source

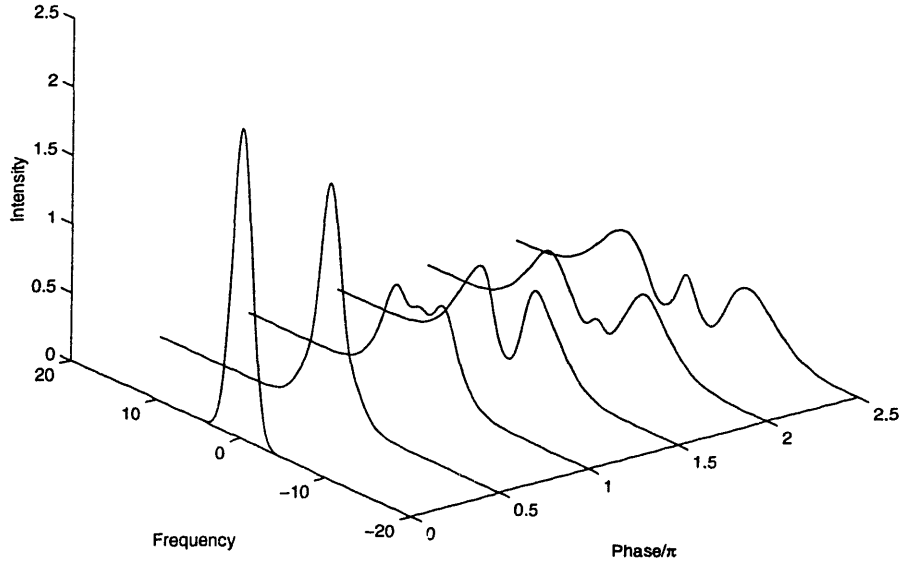

Figure 4-13: Spectral broadening due to self-phase modulation in a Gaussian pulse.

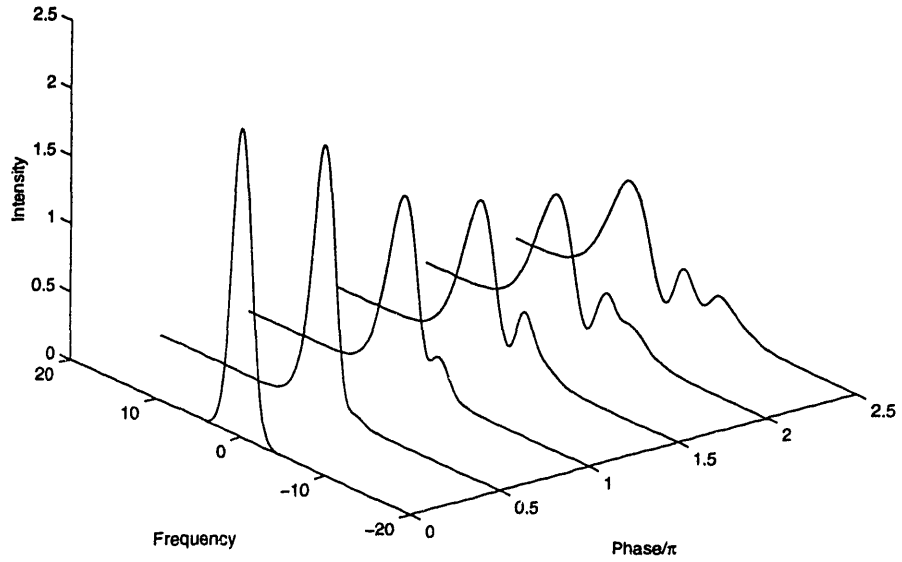

Figure 4-14: Spectral broadening due to self-phase modulation in a Gaussian pulse. Here, the nonlinear refractive index change is assumed to have a recovery time of 600 fs

in Figure 4-13. We should note that the peak phase shift in a Gaussian pulse can be inferred from observations of spectral broadening due to SPM. This has been used to measure the nonlinear refractive index in semiconductors [46, 47], and optical fibers [63]. However, this method is difficult to use when only small peak phase shifts are attainable. Additionally, non-instantaneous refractive index changes lead to asymmetric spectral broadening. Figure 4-14 shows the spectral broadening of a 1 ps pulse when the nonlinear refractive index has a recovery time of 600 fs. We see non-instantaneous refractive index changes make it more difficult to distinguish between the spectra for small phase shifts.

We have done simulations to study the effect that self-phase modulation has on spectral interference measurements of the nonlinear phase shift. Figure 4-15 shows the interference of two Gaussian pulses when the effects of SPM are included. In this simulation, the two pulses have a FWHM of 1 ps. The delay between the pulses is 5 ps. The pump pulse is 100 times more intense than the reference pulse ($\alpha = 0.1$). The graph show the intensity spectrum for peak phase shifts of 0, $\pi/2$, and π, in the pump

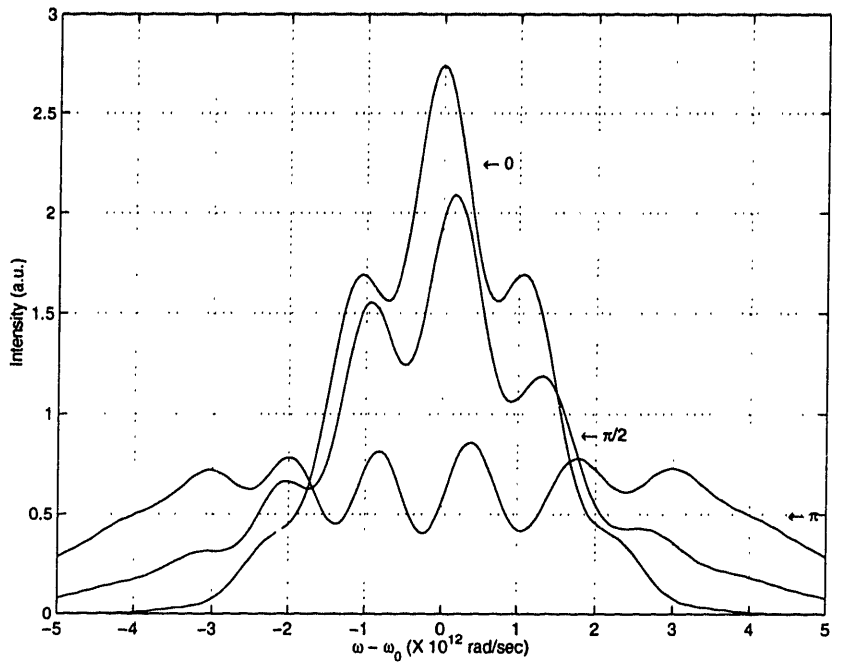

Figure 4-15: Simulation of interference of two Gaussian pulses. The pulse width is 1ps and the temporal separation is 5 ps. The scaling factor is $\alpha = 0.1$. Interference patterns are plotted for peak phase shifts of 0, $pi/2$, and π.

pulse. Clearly, the peak phase shift does not directly correspond to the phase shift in the spectral modulation as it did in the case of a uniform phase shift. Moreover, the modulation on the spectrum may no longer be easily extracted by subtracting the individual spectra of the two pulses before propagation through the nonlinear material.

We have also performed simulations on the correspondance between the observed phase shift in the spectral modulation and the actual peak phase shift in the control pulse. These simulations are shown in Figure 4-16. Again, we have considered the interference between two 1 ps Gaussian pulses that are temporally separated by 5 ps. The scaling factor is $\alpha = 0.1$. The observed phase shift is calculated by following the peak of the central interference fringe in the spectrum as the peak phase shift due to SPM is increased. Initially, the peak is at $\omega = \omega_0$. As the peak phase shift increases, the peak shifts by $\Delta\omega(\phi_{\text{peak}})$. By measuring $\Delta\omega$, we calculate the observed phase

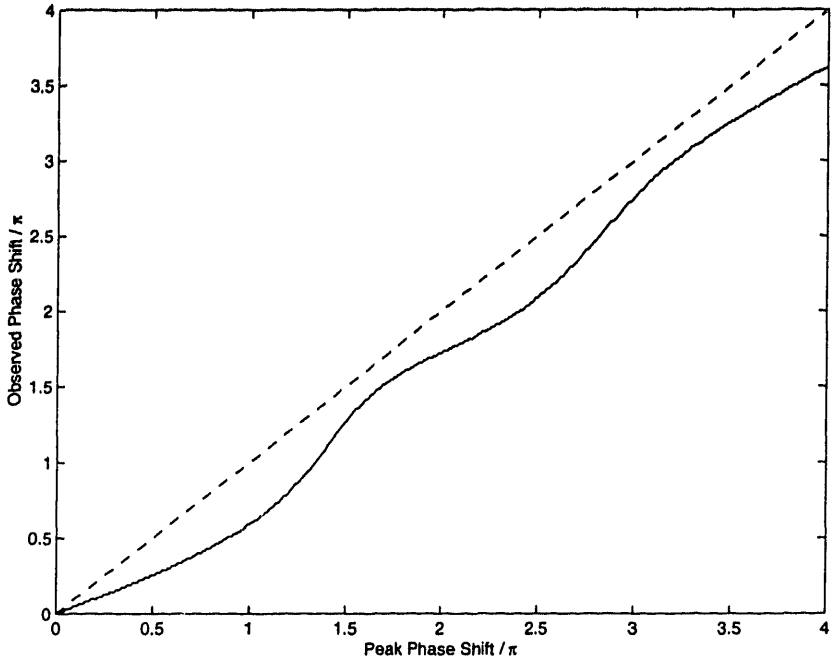

Figure 4-16: Simulation of observed phase shift in spectral modulation versus peak phase shift due to self-phase modulation for two 1 ps Gaussian pulses. The pulses are separated by 5 ps and have scaling factor, $\alpha = 0.1$.

shift in the spectral modulation by

$$\Delta\phi_{\text{obs}} = \Delta\omega T \tag{4.14}$$

In the figure, we have shown $\Delta\phi_{\text{obs}}$ for peak phase shifts between 0 and 4π. The deviation between the actual phase shift and the observed phase shift increases as the actual phase shift increases. This simulation indicates that the observed shift is fairly closely related to the actual phase shift. We are currently exploring other methods for measuring the observed phase shift that may yield more accurate results.

It should also be noted that the placement of the reference pulse relative to the control pulse affects the measured phase shift when materials with non-instantaneous nonlinear responses are studied. In particular, long-lived nonlinear effects will not be as noticeable when the reference pulse trails the pump pulse since both pulses will experience these effects. In our experiments, the reference pulse was behind the control pulse. However, since the amplifier was biased at transparency, there

were no long-lived changes in the refractive index due to interband carrier dynamics due to linear absorption and emission. The 23 picosecond delay between the pump and reference pulses should have allowed plenty of time for the recovery of the various intraband effects. It would be interesting to probe the nonlinear response of the diode using a variable delay between pump and references pulses. Recording the spectral interference between the two pulses for various delays and intensities would provide a wealth of information on the spectral and temporal characteristics of third-order nonlinearities.

4.5 Other Measurements

In Chapter 2, we discussed the effects of dispersion and birefringence on all-optical switching in the UNI. Spectral interferometry may be used to easily measure birefringence [26] and dispersion [55] in waveguides. Measurements of birefringence in a waveguide may be made by observing two temporally separated, orthogonally-polarized pulses before and after the birefringent waveguide. The interference of the two pulses may be observed using a polarizer placed at 45 degrees to the two polarizations. For simplicity, we assume that these pulse have equal intensity. Also, we assume that the intensity is low enough that nonlinear effects such as self-phase modulation are negligible. Before, the waveguide, we may write the electric field as:

$$E(t, z = 0) = \hat{\mathbf{x}}E(t)e^{j\omega_0 t} + \hat{\mathbf{y}}E(t - T)e^{j\omega_0(t-T)}. \tag{4.15}$$

After the waveguide, it is straightforward to show that the detected intensity spectrum for the two interfering pulses is given by:

$$I(\omega, z = L) \propto |E(\omega - \omega_0)|^2[1 + \cos(\Delta\beta(\omega)L + \omega T)], \tag{4.16}$$

where $\Delta\beta$ is the difference in the dispersion constants for the two polarizations. This constant is easily extracted by observing the interference spectrum for the two pulses. Note that we can create the two orthogonally-polarized, equal-intensity pulses by

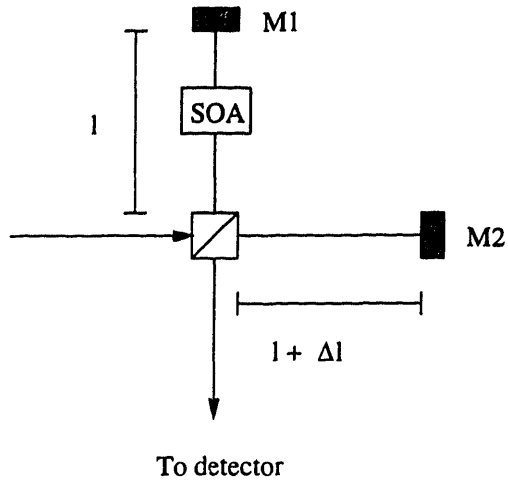

Figure 4-17: Michelson interferometer used for directly observing the propagation constant, $\beta(\omega)$ in a semiconductor optical amplifier.

removing the polarizing beam splitting cube in the nonlinearity measurement setup shown in Figure 4-10.

The birefringence measurements described above can only give information about the difference between the dispersion constants of the two polarization modes. To measure the dispersion in a single mode, the setup must be modified slightly. Figure 4-17 shows how a Michelson interferometer might be used to measure the dispersion in a waveguide. Here, a single pulse entering on the left is split into two separate arms in a polarizing beam splitting cube (PBS). Pulses in the upper arm travel through the SOA and are reflected off of mirror M1. Pulses in the second arm travel through free space and are reflected off of mirror M2. The two pulses are then recombined in the PBS and detected at the output. If the dispersion constant in the SOA is $\beta(\omega)$ and the difference in lengths of the two arms is Δl, then it is straightforward to show that the detected spectrum of the recombined pulses is given by:

$$I(\omega) \propto |E(\omega - \omega_0)|^2[1 + \cos(2\beta(\omega)L + 2\omega\frac{\Delta l}{c})]. \tag{4.17}$$

Hence, the dispersion of the waveguide over the bandwidth of the optical pulses is directly measured by observing the frequency-domain interference pattern at the output.

Chapter 5

Switching Experiments

The device characterization experiments described in Chapter 4 indicate that non-linearities in semiconductor optical amplifiers (SOA) may be useful for all-optical switching. In this chapter we discuss the use of these devices in all-optical switching demonstrations. We begin with a general overview of the experimental setup used. Then we describe the various pulse sources used in the experiments. Finally, we present several switching demonstrations using SOA in the UNI.

5.1 Experimental Setup

The experimental setup for the switching experiments is shown in Figure 5-1. The signal and control pulse repetition rates are determined by two phase-locked RF synthesizers. Note that the repetition rates of the signal and control need not be the same. For example, we can invert a 10 Gbits/s control stream using a 20 Gbits/s signal clock. The signal pulses pass through a variable delay line (a variable length open-air gap), then propagate through the polarization-sensitive delay (PSD) in the UNI to produce two temporally separated orthogonal pulses. The variable delay line is adjusted so that the control pulse overlaps with exactly one of the orthogonal signal pulses.

The data generator is an Anritsu MP1761B Pulse Pattern Generator. It is capable of generating psuedo-random bit strings of up to $2^{31} - 1$ bits at rates up to 12.5 GHz.

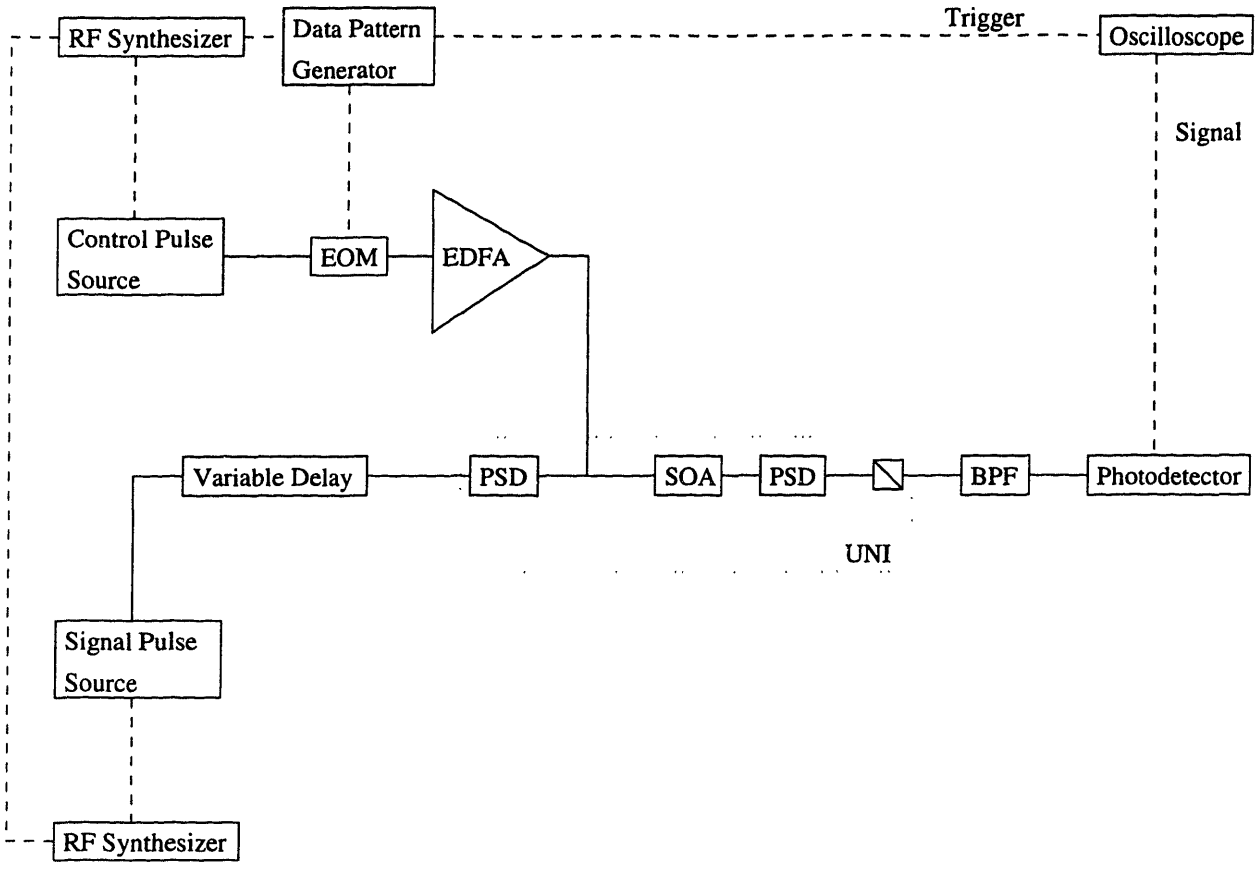

Figure 5-1: Experimental setup for switching demonstrations. Optical paths are indicated by solid lines. Electrical paths are indicated by dashed lines.

The RF output from the data generator is used to modulate the control pulse stream in an electro-optic modulator. The modulated control stream is then amplified in an Erbium-doped fiber amplifier, providing average powers up to 250 mW. The amplified pulses then travel through the SOA in the UNI.

After traveling through the SOA, the orthogonal signal pulses are recombined temporally in a second PSD before being interfered in a polarizer. At the output of the UNI, the control pulses are filtered using a fiber-coupled tunable birefringent filter. The signal pulses are then detected on a 45 GHz photodetector. The output from the photodetector is viewed on a Tektronix 11800 series high-speed digital sampling oscilloscope that is triggered on the pattern repetition signal from the data generator. The oscilloscope has a 50 GHz bandwidth (7 ps rise time).

5.2 Pulse Sources

We used three different pulse sources in the switching experiments reported in this thesis. Gain-switched lasers provided pulses at 10 GHz. A commercial soliton source manufactured by PriTel provided pulses at 12.5 GHz. A soliton-compression source was used for pulses at 100 GHz. The following sections describe each of these sources and provide autocorrelations of the output pulses.

5.2.1 Gain-switched Laser

A gain-switched laser pulse source is made by directly modulating the bias current to a distributed-feedback laser. In our experiments, we used 10 GHz sinusoidal modulation from an RF synthesizer to gain-switch the DFB. The pulses generated by this technique have a significant chirp due to carrier population density changes induced by modulation of the bias current. Consequently, the pulses produced are not transform-limited and have a FWHM of > 30 ps. While the chirp is not entirely linear, significant linear pulse compression can be obtained by propagation through a length of dispersion compensating fiber. We used 400 m of dispersion-compensating fiber to obtain compress the pulses from the gain-switched laser to 12 ps. An auto-

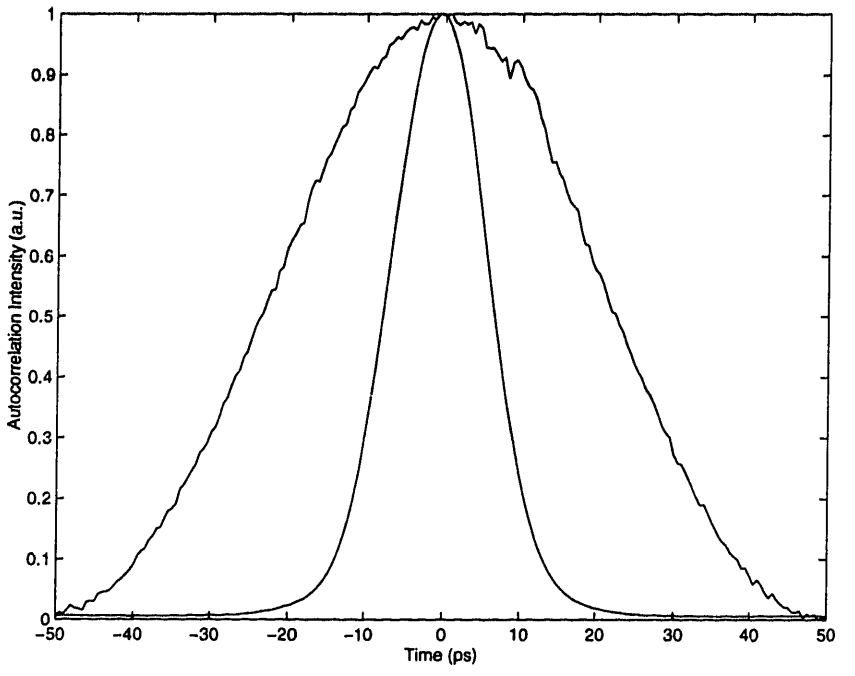

Figure 5-2: Autocorrelation of pulse from DFB laser modulated at 10 GHz before and after compression in 400 m of dispersion compensating fiber. The FWHM is 32 ps before compression and 10 ps after compression

correlation of a pulse from the DFB before and after compression is shown in Figure 5-2.

5.2.2 PriTel Soliton Source

We also used a commercial soliton source produced by PriTel in our experiments. This laser is a single-polarization fiber laser with a sigma configuration [64]. The cavity length in this laser is actively stabilized using a phase-locked loop to align the output pulses with the clock oscillator signal. This source produces pulses at rates up to 20 Gbits/s. The pulses are wavelength-tunable over the entire gain bandwidth of the Erbium-doped fiber. Figure 5-3 shows the autocorrelation of a 3.6 ps pulse produced by the PriTel source operating at 12.5 GHz.

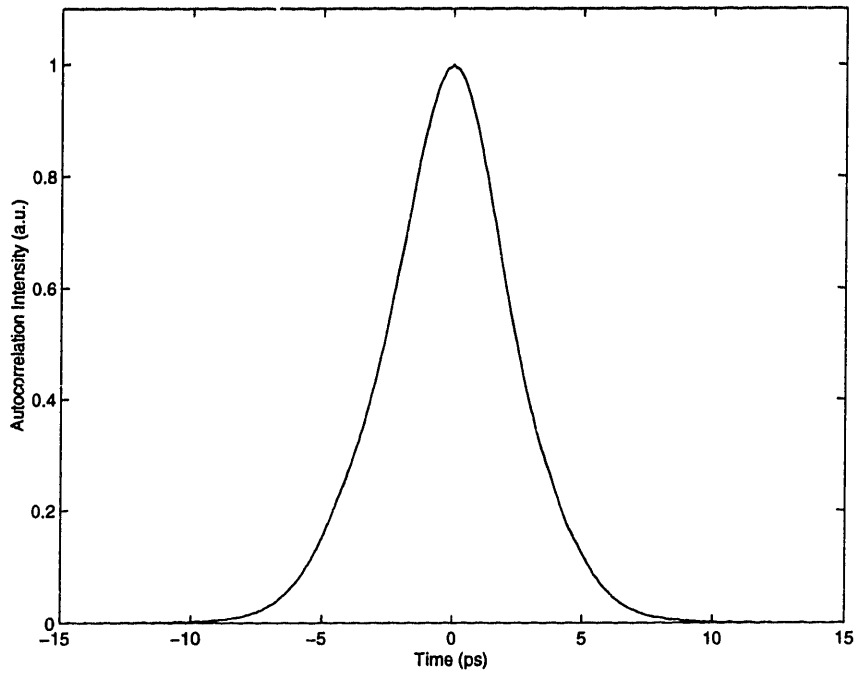

Figure 5-3: Autocorrelation of 3.6 ps pulse from PriTel Soliton source operating at 12.5 GHz.

5.2.3 Soliton Compression Source

The soliton compression source used in these experiments generates a 100 GHz soliton pulse stream by nonlinear compression of the beat signal between two optical carriers [65]. A schematic of the source is shown in Figure 5-4. The source laser is a semiconductor diode with a center wavelength of 1543 nm. The output from this source is modulated by an electro-optic modulator driven by a 50 GHz radio-frequency synthesizer. The modulator bias is set at the transmission null using a bias-control circuit. As a result, for small RF drive signals around this null, the transfer function of the modulator is approximately parabolic. Hence, for a 50 GHz RF drive, the output is modulated at 100 GHz. After the modulator, the 100 GHz modulated signal is amplified and sent through a length of dispersion-tailored fiber (DTF). The DTF consists of alternating lengths of standard fiber and dispersion shifted fiber. This "comb-like" design provides a discrete simulation of an exponentially decreasing dispersion in the fiber and leads to soliton compression of the pulses. To reduce the effects of stimulated Brillouin scattering in the DTF, a small phase modulation is produced in the

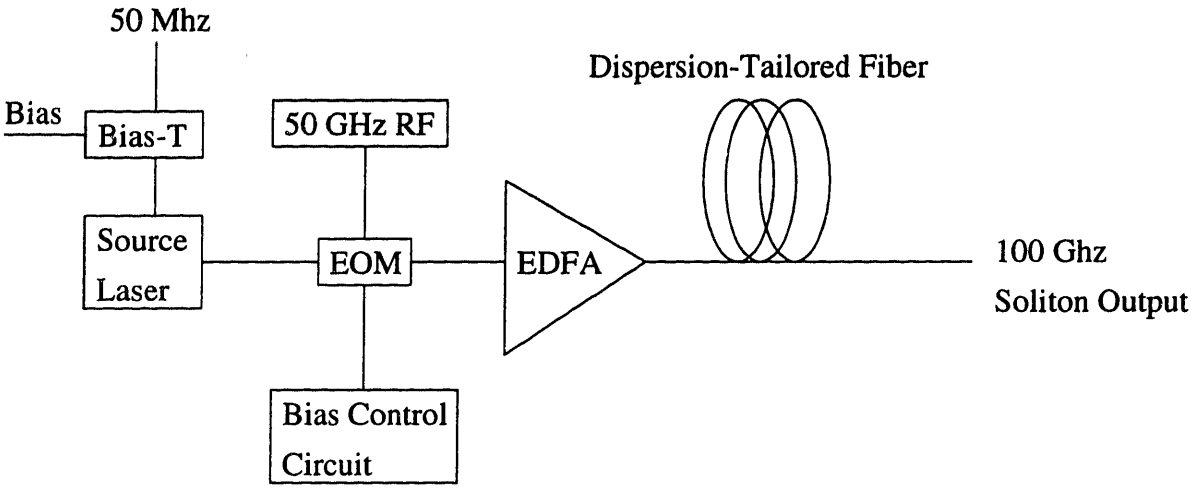

Figure 5-4: Soliton compression source schematic.

signal laser using a 50 MHz RF drive and a bias-T.

The output from the soliton source is a pulse stream at 100 GHz. Figure 5-5 shows the autocorrelation of a pulse from the soliton-compression source. The FWHM for this pulse is 2 ps.

5.3 Switching Results

In this section we discuss three different switching experiments. In the first experiment, we demonstrate the long-lived gain changes caused by changes in the carrier population density when the SOA is biased in the absorption and gain regimes. These results are compared to the operation of the SOA at the transparency point. In the second experiment, we demonstrate the patterning of individual bits that is apparent in the gain regime. In the third experiment, we show the operation of the UNI acting as an AND gate when the SOA is biased at the transparency point.

5.3.1 Interband Effects

The purpose of this experiment is to demonstrate the long-lived effects of the carrier population density changes inherent in the operation of the SOA in the gain or absorption regimes. In this case, the soliton compression source is used for the signal pulses.

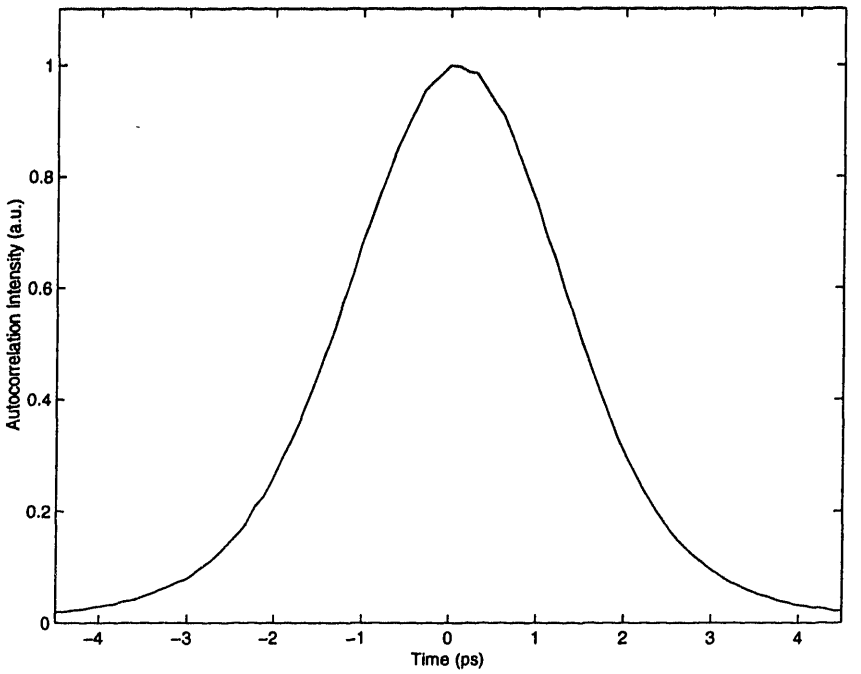

Figure 5-5: Autocorrelation of a 2 ps pulse from the 100 GHz soliton compression source.

These pulses have a center wavelength of 1543 nm. The 100 GHz pulses produced by this source are well beyond the bandwidth of the photodetector and oscilloscope. So, individual pulses are not resolved in the oscilloscope traces. This makes the effect of the lower rate control pulses more clearly resolved. The control pulses are provided by modulating the 12.5 GHz pulses from the PriTel soliton source with a pattern of 10000000. Thus, every eighth control pulse was ON giving an effective control pulse repetition rate of 1.5625 GHz. The control pulses are centered at 1538 nm. Two 2 nm birefringent filters at the output of the UNI reduce the control pulse power to more than 20 dB below the signal power.

The UNI is biased ON. So, in the absence of a control pulse, the signal pulse should propagate through to the output. The presence of a control pulse should induce a phase shift on one of the signal pulse components and switctch off the recombined signal output pulse. These interferometric changes are not visible on the oscilloscope. However, the changes in gain are visible. Figure 5-6 shows the results of this switching demo. The first trace shows the output when the SOA is biased in the absorption regime (15 mA bias current). Here, the control pulses increase the carrier

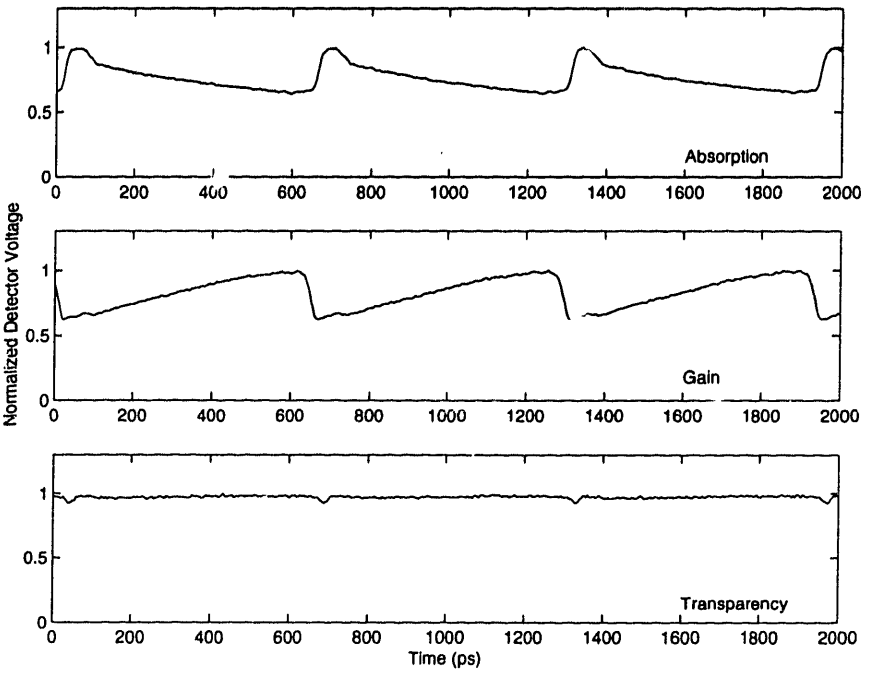

Figure 5-6: Switching demonstration showing effects of carrier population changes in various operation regimes.

population density. As we saw in Chapter 3, increasing the carrier density increases the gain for the signal pulses. The recovery time for this change in gain corresponds to the spontaneous emission time for the semiconductor. In the gain regime (100 mA bias current), the opposite effect occurs. Incident control pulses decrease the carrier population density through stimulated emission. A corresponding decrease in gain is seen in the signal pulse stream. The recovery time for this change in gain is related to the carrier injection rate due to the bias current. The third trace shows the output when the control pulses are at the transparency point for the SOA. Here, the long-lived gain changes are nonexistent. A slight decrease in gain is observed for each control pulse. This is attributed to phase changes leading to destructive interference in a single signal pulse and gain changes due to carrier heating in the SOA. The recovery time for these changes is not clearly resolved by the oscilloscope.

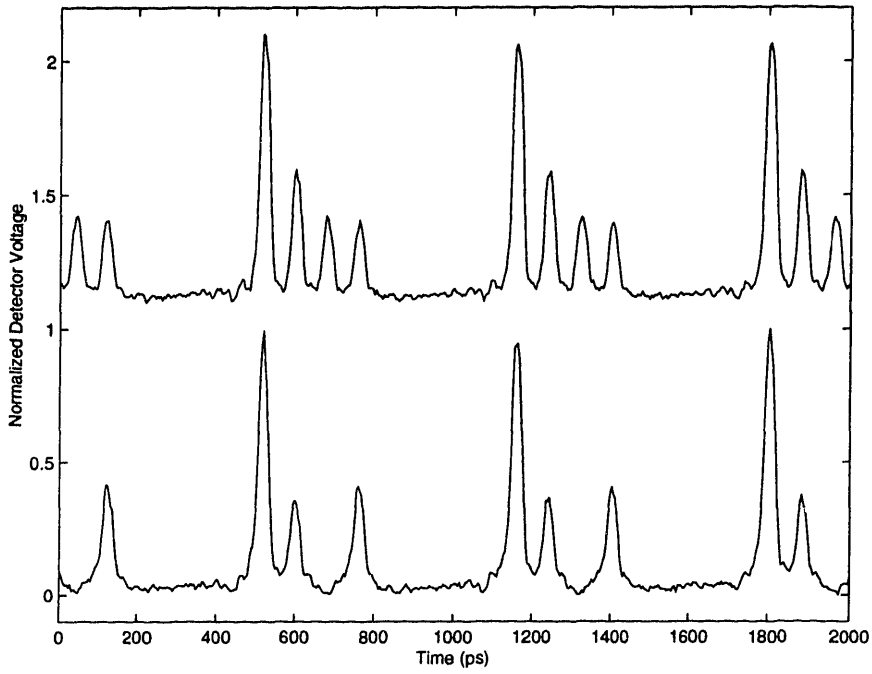

Figure 5-7: Amplitude modulation in the output signal due to gain suppression.

5.3.2 Patterning in Gain Regime

Next, we looked at the effects of gain suppression when the SOA is biased in the gain regime. Again, the signal source was the 100 GHz soliton compression source at 1543 nm. The control source was the 12.5 GHz PriTel soliton source at 1538 nm. The amplifier was biased in the gain regime (100 mA bias current). For this experiment, the UNI was biased OFF. So, in the absence of a control pulse, the signal pulses were not visible at the output. In this configuration, the output is the logical AND of the signal and control inputs. Figure 5-7 shows the results of this experiment. The first trace shows the output signal when the control pattern was 11110000. The output stream shows the effect of gain saturation. Since the bit period is less than the recovery time for the carrier population changes induced by the control pulses, the four consecutive bits at the output are gradually decreasing in height. The second trace shows the output for a control input of 11010000. This time, the absence of a control bit in the 3rd slot allows the gain to recover slightly. So, the fourth pulse is larger than the third.

5.3.3 Transparency

We have also demonstrated all-optical switching at 10 Gbits/s using an SOA biased at the transparency point [66]. The signal and control pulses in this experiment were provided by two synchronized 10 GHz gain-switched DFB lasers. For this experiment the placement of the signal and control pulse wavelengths was an important consideration. The SOA used in this experiment was a commercially available fiber-coupled amplifier. The packaged amplifiers tend to have worse coupling between the fibers than the free space amplifiers. This, together with the losses inherent with operating near the transparency point makes it difficult to observe signal pulses at the output of the UNI. Thus, it is preferable to have a signal wavelength that is longer than the control wavelength. Then, the signal pulses will still experience gain in the amplifier when the control pulses are at the transparency point. For this reason, we chose a signal wavelength of 1551 nm and a control wavelength of 1547 nm. The signal pulse widths were 11.3 ps and the control pulse widths were 10.4 ps. When the amplifier was biased at the transparency point for the control pulses, the total insertion loss for the signal pulses was 11.5 dB.

The signal pulses in this experiment were unmodulated. That is, they were essentially a 10 GHz clock source. The control pulses were modulated with a 10 GHz bit-pattern of length $2^7 - 1$. When the UNI is biased OFF and the control pulses turn the signal pulses ON, the output is the logical AND of the signal and control pulse streams. In this case, since the signal pulse stream is unmodulated, the output pulse pattern is identical to the control pulse pattern and the switch acts as a wavelength converter. On the other hand, if the UNI is biased ON and the control pulses turn the signal pulses OFF, signal pulses will be observed at the output in the absence of control pulses. This is a logical INVERT of the control pulse stream.

Figure 5-8 shows control pulse stream (top trace) and signal pulse stream (bottom trace) for a logical AND operation in the UNI. With the amplifier biased at transparency, we obtained a π phase shift in the signal pulses when the control pulse peak powers were approximately 1 W, corresponding to a switching energy of 10 pJ. We

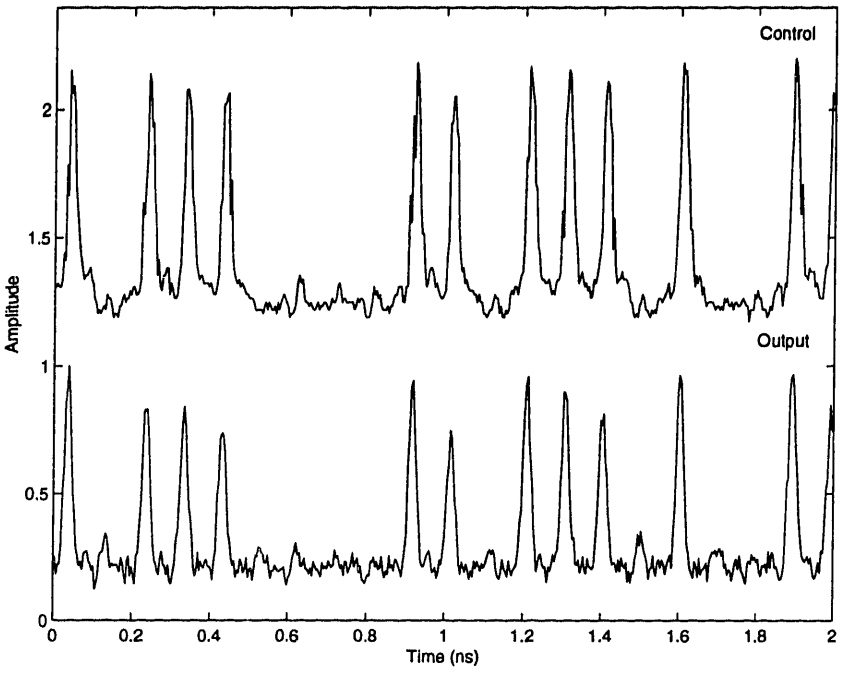

Figure 5-8: Switching demonstration at transparency point.

believe that this is the first demonstration of high-speed all-optical switching in an SOA biased at transparency.

There is still some amplitude modulation in the output signal stream. There are several possible reasons for this. First, note that there is also some modulation in the height of the control pulses. This is due to the fact that the bias on modulator for the control pulses was slowly drifting. Additionally, it was very difficult to maintain the proper polarization bias in the UNI. The switched output was very sensitive to changes in the polarization of the signal pulses. These changes would occur over a period of seconds after the proper bias point was found. We found that it was impossible to maintain the proper bias for periods long enough to perform switching analysis other than a single scope trace. An active stabilization scheme for the various biases in the setup is clearly required in order to further characterize the performance of these devices.

5.4 Discussion

The troubles encountered when trying to switch at the transparency point suggest that gain-effects may be playing an important role in the switching demonstrations that have been done using the UNI. It was very easy to set the polarization controllers to achieve switching when the amplifier was biased in the gain regime. However, at the transparency point, the correct bias point was difficult to find and even harder to maintain. Under these conditions, it was not possible to perform bit-error-rate tests to accurately assess the switching performance of the device.

In fact, it is possible to perform AND and INVERT operations in the UNI using only gain effects. To perform an AND function, the UNI is biased OFF. Here, in the absence of a control pulse, the two orthogonally polarized components of the signal pulse at the output polarizer have a phase difference of π. Hence, the pulses are switched OFF through destructive interference in the polarizer. Intense control pulses can saturate the gain of the SOA, allowing only one of the orthogonal, temporally separated signal components to pass through the device. Now, there will no longer be destructive interference at the output polarizer as only one of the signal pulses will arrive at the output. Since the output polarizer is aligned at 45 degrees to the pulse polarization, half of the pulse power passes through the polarizer and is observed at the output. This will appear to be a switched ON pulse. However, the peak intensity will be only 1/4 of the expected peak intensity when only nonlinear index changes are considered.

Similarly, we can perform a logical INVERT using only gain effects in the UNI. Here, we align the output polarizer so that only one of the signal pulse polarizations passes through. Gain saturation in the SOA can again be used to switch the signal pulse in this polarization OFF. Now, the pulse will not be seen at the output. While this effect does not employ the interferometric properties of the UNI, it is difficult to distinguish from true interferometric switching in the UNI. In fact, since the implementation of the UNI used in these experiments is in fiber, the polarization state of the signal pulses immediately before the output polarizer is unknown. So, it is

entirely possible that the switching results that we have seen in the past are due to the gain effects described above, rather than phase effects.

This explanation seems likely for two reasons. First, as we discussed above, switching was very difficult when the control pulses were at the transparency point. Only with very high control pulse powers, were we able to observe switching of the signal pulses. In the gain regime, on the other hand, good contrast ratios were easily obtained with low control pulse powers. This is consistent with the possibility that the switching may be largely due to gain effects. Additionally, the relative ease with which the proper bias point is found in the gain regime suggests that the effect may not be very polarization dependent. In the methods described above for obtaining AND and INVERT operation, small changes in the polarization state do not significantly affect switching operation. However, at the transparency point, we found that the switching characterization was very sensitive to the bias settings. This is expected when the switching effect is due to a nonlinear phase shift and the pulses must be interfered at the output. Further investigation of the UNI should be performed to determine whether gain effects dominate the switching performance.

Chapter 6

Conclusions

We have discussed the effects of time-dependent nonlinear responses, dispersion, birefringence, and losses on all-optical switches. In particular, we have shown that long-lived refractive index and gain changes can lead to intersymbol interference in interferometric switches. The ultrafast nonlinear interferometer (UNI) offers a solution to the problem of long-lived refractive index changes. However long-lived gain changes remain a problem.

Semiconductors are a popular choice for nonlinear materials in optical switches. The nonlinear response in semiconductor waveguides is typically quite large. However, pump-probe experiments have shown that carrier population dynamics in semiconductors lead to long-lived nonlinear gain and refractive index changes. To reduce these effects, we consider biasing semiconductor optical amplifiers at the transparency point, where control pulses in the UNI induce no net changes in carrier populations.

We have demonstrated the use of a spectral interferometric technique to measure the nonlinear response in semiconductor waveguides. This technique allows direct observation of the nonlinear phase shift due to self-phase modulation (SPM) in a waveguide. We used this technique to measure the nonlinear response in a bulk InGaAsP SOA biased at transparency. The magnitude of n_2 we measure is comparable to previous measurements based on pump-probe experiments and observations of spectral changes due to SPM. We demonstrate that a π phase shift is achievable in these devices, indicating potential for all-optical switching in the UNI.

We have demonstrated the effects of carrier population changes in an SOA. In the UNI, we have observed the effects of gain recovery times in the gain and absorption regimes. These recovery times are much longer than the bit period for switching experiments at rates above 10 Gbits/s. There, long-lived effects result in amplitude modulation on the output pulses from the UNI that is dependent on the control pulse pattern. We have shown that when the SOA is biased at the transparency current for the control wavelength, the long-lived gain changes due to carrier population dynamics are eliminated. At this bias point, the recovery time for gain changes is less than 1 ps. This recovery time suggests potential for switching at rates well beyond 100 Gbits/s.

We have demonstrated all-optical AND and INVERT operation in the UNI at 10 Gbits/s. However, the results of this experiment do not offer conclusive evidence of the possible advantages of operating at the transparency point. The high losses at the transparency point compared to the gain regime are certainly a disadvantage. Additionally, it was observed that maintaining the bias of the signal polarization in the UNI was very difficult near the transparency point. This suggests that gain effects, which are reduced at the transparency point, may be playing a large role in switching demonstrations in the gain regime. Further investigation of the effects of long-lived gain and refractive index changes in the UNI are required before practical application of the switch in a network can be considered.

6.1 Future Work

As we have discussed above, spectral interferometry is a very attractive technique for measuring a wide range of device characteristics. Here, we have demonstrated a method for directly observing a nonlinear phase shift in an optical pulse by observing its interference with a reference pulse in the frequency domain. However, we found that because of the effects of self-phase modulation, the actual peak phase shift of the pulse was not the same as the observed shift in the spectral modulation. Further study of this technique may provide a better method for inferring the actual peak phase

shift in an optical pulse based on the observed shift in the interference spectrum.

Additionally, we have not considered the effects of non-instantaneous nonlinearities on the observed spectral interference between two pulses in our measurements. A long-lived nonlinear response in the semiconductor waveguide due to an intense pump pulse may affect a subsequent reference pulse, reducing the observed phase shift in the pump pulse. Observations of these effects may be made by using a pump-probe spectral interferometry technique where the interference spectrum is observed for various temporal delays between the reference and pump pulses. Such a technique can provide much information about the spectral and temporal characteristics of the material nonlinearities.

We have discussed ways in which spectral interferometry may be used to make direct measurements of the dispersive and birefringent properties of a waveguide. In Chapter 2, we demonstrated that both birefringence and dispersion in a waveguide can have detrimental effects on the operation of the UNI. Hence, it would be useful to characterize these properties of a waveguide before attempting to use it in a switch. Traditional methods for measuring dispersion and birefringence are difficult and time-consuming. Spectral interferometry offers the possibility of developing a single apparatus which can be used to easily measure the dispersive, birefringent, and nonlinear characteristics of a waveguide.

Previous analyses of switching operation in the UNI have neglected the effects of long-lived gain changes in the nonlinear material and assumed that switching was mainly due to nonlinear phase changes in the interferometer. Our results suggest that this may not be the case. Further study of these effects in the UNI is required. For example, high repetition-rate pump-probe experiments may be performed on semiconductor waveguides and the UNI to explore the effects of gain saturation at high bit rates.

We have not had much success with passive devices in the UNI. The small nonlinearity and large losses in these devices make it difficult to achieve a π phase shift in a signal pulse. As the control pulse intensity is increased, nonlinear absorption becomes a considerable problem. To overcome these problems, one may consider a "hybrid"

design where the control pulses have energies above the semiconductor bandgap while the signal pulses are below the bandgap. In this design, the control pulse induced gain changes would not affect the below-band signal pulses. However, the associated refractive index changes extend below the band. Therefore, we can potentially demonstrate interferometric switching that is due solely to refractive index changes.

Bibliography

[1] K. L. Hall, G. Lenz, and E. P. Ippen. Femtosecond time-domain measurements of group velocity dispersion in diode lasers at 1.5μm. *Journal of Lightwave Technology*, 7:39–44, 1989.

[2] M. N. Islam. *Ultrafast Fiber Switching Devices and Systems.* Cambridge University Press, Cambridge, England, 1992.

[3] R. A. Barry, V. W. S. Chan, K. L. Hall, E. S. Kintzer, J. D. Moores, K. A. Rauschenbach, E. A. Swanson, L. E. Adams, C. R. Doerr, S. G. Finn, H. A. Haus, E. P. Ippen, W. S. Wong, and M. Haner. All-optical network consortium– ultrafast TDM networks. *JLT/JSAC Special Issue on Optical Networks*, 14(5):999, 1996.

[4] Agnes Hui Chan and M. Medard. Reconfigurable feedback shift registers. In *Proceedings of the IEEE International Symposium on Information Theory*, pages xxvi+542, 178, June 1997.

[5] J.-M Jeong and M. E. Marhic. All-optical analog-to-digital and digital-to-analog conversion implemented by a nonlinear fiber interferometer. *Optics Communications*, 91(1-2):115, July 1992.

[6] C. Joergensen, S. L. Danielsen, K. E. Stubkjaer, M. Schilling, K. Daub, P. Doussiere, F. Pommerau, P. B. Hansen, H. N. Poulsen, A. Kloch, M. Vaa, B. Mikkelsen, E. Lach, G. Laube, W. Idler, and K. Wunstel. All-optical wavelength conversion at bit rates above 10 Gb/s using semiconductor optical am-

plifiers. *IEEE Journal of Selected Topics in Quantum Electronics*, 3(5):1168, October 1997.

[7] G. I. Stegeman and E. M. Wright. All-optical waveguide switching. *Optical and Quantum Electronics*, 22(2):95–122, March 1990.

[8] M. Nakazawa, K. Suzuki, E. Yoshida, E. Yamada, T. Kitoh, and M. Kawachi. 160 Gbit/s soliton data transmission over 200 km. *Electronics Letters*, 31(7):545, March 1995.

[9] D. Marcuse. RMS width of pulses in nonlinear dispersive fibers. *Journal of Lightwave Technology*, 10(1):17, January 1992.

[10] J. M. Dudley, L. P. Barry, P. G. Bollond, J. D. Harvey, R. Leonhardy, and P. D. Drummond. Direct measurement of pulse distortion near the zero dispersion wavelength in an optical fiber by frequency-resolved optical gating. *Optics Letters*, 22(7):457, April 1997.

[11] K. L. Hall. All-optical switching at 100 Gbps. In *Optical Fiber Communications Conference Proceedings*, pages xxvi+542, 178, June 1997.

[12] K. L. Hall, G. Lenz, A. M. Darwish, and E. P. Ippen. Subpicosecond gain and index nonlinearities in InGaAsP diode lasers. *Optics Communications*, 111(5):589, October 1994.

[13] Y. H. Kao, I. V. Goltser, M. N. Islam, and G. Raybon. Ultrafast optical logic gate using a semiconductor laser amplifier operating at transparency in a loop mirror. In *Proceedings of the Conference on Lasers and Electro-Optics*, page 94, May 1997.

[14] A. M. Darwish, E. P. Ippen, H. Q. Le, J. P. Donnelly, S. H. Groves, and E. A. Swanson. Short-pulse wavelength shifting by four wave mixing in passive InGaAsP/InP waveguides. *Applied Physics Letters*, 68(15):2038, April 1996.

[15] Govind P. Agrawal. *Nonlinear Fiber Optics.* Optics and Photonics. Academic Press, San Diego, 2nd edition, 1995.

[16] N. S. Patel, K. L. Hall, and K. A. Rauschenbach. Interferometric all-optical switches for ultrafast signal processing. *Applied Optics*, 37(14), May 1998.

[17] N. S. Patel. High speed all-optical switching based on a single-arm interferometer. Master's thesis, Massachusetts Institute of Technology, Department of Electrical Engineering and Computer Science, May 1996.

[18] M. Shirasaki, H. A. Haus, and D. L. Wong. Nonlinear fiber interferometer and logic gate. In *Proceedings of the Conference on Lasers and Electro-Optics*, May 1987.

[19] K. K. Anderson, M. J. LaGasse, C. A. Wang, and J. G. Fujimoto. Femtosecond dynamics of the nonlinear index near the band edge in AlGaAs waveguides. *Applied Physics Letters*, 56:1834, 1990.

[20] M. J. LaGasse, D. Liu-Wong, J. G. Fujimoto, and H. A. Haus. Ultrafast switching with a single-fiber interferometer. *Optics Letters*, 14:311, 1989.

[21] Govind P. Agrawal and N. Anders Olsson. Self-phase modulation and spectral broadening of optical pulses in semiconductor laser amplifiers. *IEEE Journal of Quantum Electronics*, 25(11):2297, November 1989.

[22] N. S. Patel, K. L. Hall, and K. A. Rauschenbach. 40-gbit/s cascadable all-optical logic with an ultrafast nonlinear interferometer. *Optics Letters*, 21(18):1466, September 1996.

[23] Victor Mizrahi, K. W. Delong, and G. W. Stegeman. Two-photon absorbtion as a limitation to all-optical switching. *Optics Letters*, 14(20):1140, October 1989.

[24] K. W. DeLong and G. I. Stegeman. Two-photon absorption as a limitation to all-optical waveguide switching in semiconductors. *Applied Physics Letters*, 57(20):2063, November 1990.

[25] Anthony E. Siegman. *Lasers.* University Science Books, Mill Valley, CA, 1986.

[26] X. D. Cao and D. D. Meyerhofer. Frequency-domain interferometer for measurement of the polarization mode dispersion in single-mode optical fibers. *Optics Letters*, 19(22):1837, November 1994.

[27] G. H. B. Thompson. *Physics of Semiconductor Laser Devices.* John Wiley & Sons, New York, 1980.

[28] M. A. Omar. *Elementary Solid State Physics: Principles and Applications.* Series in Solid State Sciences. Addison-Wesley, Reading, Massachusetts, 1975.

[29] G. P. Agrawal and N. K. Dutta. *Long Wavelength Semiconductor Lasers.* Electrical/Computer Science and Engineering Series. Van Nostrand Reinhold Company, New York, 1986.

[30] K. L. Hall. *Femtosecond nonlinearities in InGaAsP diode lasers.* PhD thesis, Massachusetts Institute of Technology, Department of Electrical Engineering and Computer Science, May 1993.

[31] Katherine. L. Hall, Erich P. Ippen, and Erik R. Thoen. Nonlinearities in active media. Book chapter to be published.

[32] K. L. Hall, E. P. Ippen, and G. Eisenstein. Bias-lead monitoring of ultrafast nonlinearities in InGaAsP diode laser amplifiers. *Applied Physics Letters*, 57(2):129, July 1990.

[33] Charles H. Henry. Theory of the linewidth of semiconductor lasers. *IEEE Journal of Quantum Electronics*, QE-18(2):259, February 1982.

[34] Marek Osinski and Jens Buus. Linewidth broadening factor in semiconductor lasers– an overview. *IEEE Journal of Quantum Electronics*, QE-23(1):9, January 1987.

[35] Frederick C. Brown. *The Physics of Solids.* W. A. Benjamin, New York, 1967.

[36] K. L. Hall, A. M. Darwish, E. P. Ippen, U. Koren, and G. Raybon. Femtosecond index nonlinearities in InGaAsP optical amplifiers. *Applied Physics Letters*, 62(12):1320, March 1993.

[37] M. J. Adams. *An Introduction to Optical Waveguides.* John Wiley and Sons, New York, 1981.

[38] J. M. Wiesenfeld, S. Weiss, D. Botkin, and D. S. Chemla. Carrier transport effects and dynamics in multiple quantum well optical amplifiers. *Optical and Quantum Electronics*, 26(7):S731, July 1994.

[39] R. J. Manning, D. A. O. Davies, D. Cotter, and J. K. Lucek. Enhanced recovery rates in semiconductor laser amplifiers using optical pumping. *Electronic Letters*, 30(10):787, May 1994.

[40] Michael J. LaGasse. *Femtosecond Optical Nonlinearities in AlGaAs.* PhD thesis, Massachusetts Institute of Technology, Department of Electrical Engineering and Computer Science, August 1989.

[41] M. N. Islam, E. P. Ippen, E. G. Burkhardt, and T. J. Bridges. Picosecond nonlinear absorption and four-wave mixing in GaInAsP. *Applied Physics Letters*, 47(10):1042, November 1985.

[42] M. N. Islam, E. P. Ippen, E. G. Burkhardt, and T. J. Bridges. Picosecond study of near-band-gap nonlinearities in GaInAsP. *Journal of Applied Physics*, 59(8):2619, April 1986.

[43] A. M. Darwish, E. P. Ippen, H. Q. Le, J. P. Donnelly, and S. H. Groves. Optimization of four-wave mixing conversion efficiency in the presence of nonlinear loss. *Applied Physics Letters*, 69(6):737, August 1996.

[44] Ali M. Darwish. *Wavelength conversion by four wave mixing in passive InGaAsP/InP waveguides.* PhD thesis, Massachusetts Institute of Technology, Department of Electrical Engineering and Computer Science, September 1996.

[45] K. A. Raushenbach and S. LePage. A high-speed all-optical switch using a passive semiconductor waveguide. Unpublished report.

[46] R. S. Grant and W. Sibbett. Observations of ultrafast nonlinear refraction in an InGaAsP optical amplifier. *Applied Physics Letters*, 58(11):1119, March 1991.

[47] M. A. Fisher, H. Wickes, G. T. Kennedy, R. S. Grant, and W. Sibbett. Ultrafast nonlinear refraction in an active mqw waveguide. *Electronics Letters*, 29(13):1185, June 1993.

[48] K. Naganuma, K. Mogi, and H. Yamada. Group-delay measurement using the fourier transform of an interferometric cross correlation generated by white light. *Optics Letters*, 15(7):393, April 1990.

[49] Vu Van Lun, P. G. Eliseev, Margarita A. Manko, and G. T. Mikaelian. Electrical diagnostics of the amplifier operation and a feasibility of signal registration on the basis of the voltage saturation effect in junction laser diodes. *IEEE Journal of Quantum Electronics*, QE-19(6):1080, June 1983.

[50] G. T. Kennedy, P. D. Roberts, W. Sibbett, D. A. O. Davies, M. A. Fisher, and M. J. Adams. Intensity dependance of the transparency current in InGaAsP semiconductor optical amplifiers. In *Proceedings of the Conference on Lasers and Electro-Optics*, page 11, May 1996.

[51] D. Narayana Rao and V. Nirmal Kumar. Experimental demonstration of spectral modification in a mach-zehnder interferometer. *Journal of Modern Optics*, 41(9):1757, 1994.

[52] K. Saxena, D. S. Mehta, H. C. Kandpal, J. S. Vaishya, and K. C. Joshi. Experimental studies of field correlations using spectral interferometric technique. *Optics Communications*, 111(5-6):423, October 1994.

[53] V. Nirmal Kumar and D. Narayana Rau. Using interference in the frequency domain for precise determination of thickness and refractive indices of normal

dispersive materials. *Journal of the Optical Society of America B*, 12(9):1559, September 1995.

[54] A. L. Guerrero, C. Sainz, H. Perrin, R. Castell, and J. Calatroni. Refractive index distribution measurements by means of spectrally-resolved white-light interferometry. *Optics and Laser Technology*, 24(6):333, 1992.

[55] Scott Diddams and Jean-Claude Diels. Dispersion measurements with white-light interferometry. *Journal of the Optical Society of America B*, 13(6):1120, June 1996.

[56] C. Sainz, P. Jourdain, R. Escalona, and J. Calatroni. Real time interferometric measurements of dispersion curves. *Optics Communications*, 110(3-4):381, August 1994.

[57] C. X. Yu, M. Margalit, E. P. Ippen, and H. A. Haus. Direct and accurate measurement of self-phase shift due to fiber nonlinearity. In *CLEO*, June 1998.

[58] Eiji Tokunaga, Akira Terasaki, and Takayoshi Kobayashi. Femtosecond phase spectroscopy by use of frequency-domain interference. *Journal of the Optical Society of America B*, 12(5):753, May 1995.

[59] S. M. LePage, K. L. Hall, G. Lenz, and E. P. Ippen. Widely tunable source generated subpicosecond pulses at 1550 nm. In *SPIE Vol. 2614*, page 35, October 1995.

[60] G. Lenz, K. Tamura, H. A. Haus, and E. P. Ippen. All-solid-state femtosecond source at 1.55 μm. *Optics Letters*, 20(11):1289, June 1995.

[61] K. Tamura, E. P. Ippen, and H. A. Haus. Pulse dynamics in stretched-pulse fiber lasers. *Applied Physics Letters*, 67(2):158, July 1995.

[62] K. Tamura, E. P. Ippen, H. A. Haus, and L. E. Nelson. 77-fs pulse generation from a stretched-pulse mode-locked all-fiber ring laser. *Optics Letters*, 18(13):1080, July 1993.

[63] R. H. Stolen and Chinlon Lin. Self-phase modulation in silica optical fibers. *Physical Review A*, 17(4):1448, 1978.

[64] Thomas F. Carruthers and Irl N. Duling III. 10-GHz, 1.3-ps erbium fiber laser employing soliton pulse shortening. *Optics Letters*, 21(23):1927, December 1996.

[65] Eric A. Swanson and Stephen R. Chinn. 40-GHz pulse train generation using soliton compression of a mach-zehnder modulator output. *IEEE Photonics Technology Letters*, 7(1):114, January 1995.

[66] B. S. Robinson and K. L. Hall. Interferometric all-optical switching using nonlinearities in semiconductor optical amplifiers biased at transparency. To be published in 1998 Conference on Lasers and Electro-optics Proceedings.

THESIS PROCESSING SLIP

FIXED FIELD: ill _____ name _____

index _____ biblio _____

► COPIES: (Archives) Aero Dewey (Eng) Hum

Lindgren Music Rotch Science

TITLE VARIES ► [X] see p. 144 June 1998

Commencement exercises.

NAME VARIES. ► [ ] _____

IMPRINT: (COPYRIGHT) _____

► COLLATION. 106 l

► ADD. DEGREE: _____ ► DEPT.: _____

SUPERVISORS: _____

NOTES:

cat'r: date:

page: 5

► DEPT. E.E. 144

► YEAR: 1998 ► DEGREE: M. Eng

► NAME: ROBINSON, Bryan S.